

GLOBAL FRACTURE ANALYSIS OF LAMINATED COMPOSITE
MATERIALS FOR AEROSPACE STRUCTURES

Thesis by
Luis González Liñero

In Partial Fulfillment of the Requirements
for the Degree of
Doctor of Philosophy

California Institute of Technology
Pasadena, California
2002
(Defended 2002)

© 2002

Luis González Liñero

All Rights Reserved

ACKNOWLEDGMENT

In Catalonia, Spain, a familiar sight in festivals are the *castells*, “human towers,” rising high in the sky, built of men interlacing their arms and standing on the shoulders of one another. And, at this moment, I feel like the little kid that usually crowns the structure; receiving recognition for something that would have been impossible without the help and support of so many, to whom I am greatly indebted.

First of all, I would like to thank the National Aeronautics and Space Administration for providing the financial support and the test specimens under research grant NAG 1-1975. Special thanks to Dr. James Starnes—the initial program monitor—and to Dr. Damodar Ambur—who continued his support—for their thoughtful guidance and cooperation. My deepest gratitude goes to Mr. Allen Waters for his enduring efforts in organizing and ensuring the supply of the test panels.

I want to thank my advisor, Prof. Wolfgang G. Knauss, for his direction, guidance, patience, and unflagging support, even in the most difficult moments.

GALCIT as a whole has been a tremendous asset; there has always been someone with the required knowledge or skills—and the willingness—to help with any particular problem.

I cannot thank enough all my professors, especially my committee members: Profs. Kaushik Bhattacharya, Paul Jennings, Robert Phillips and Ares Rosakis. From this

last one I received most of my classes at Caltech, and his zeal to ensure that his students had understood the course materials will always remain as a model to follow. Thanks also to Prof. Ravichandran, who chaired my candidacy committee. It is unfortunate that his sabbatical year prevented him from being present at my thesis defense.

I am greatly indebted to Joe H., Ali, Brad and Larry from the aeroshop, to whom I owe the fabrication of my loading frame and the preparation of my specimens. I appreciate the quality and intensity of their work, their constant availability and patience, and their thoughtful advice and insights into the design process.

Petros, Dave O. and fellow students David and Shiming were always there to answer my questions and to help me find my way through the Solid Mechanics laboratories. I am also indebted to Ioannis, Eric, Sangwook, Weidong and Allan.

Without Marta K. and her computer assistance I would have floundered more than once. Dimitty, Cynthia, Dana and Denisse, our help has been invaluable.

During my stay at Caltech I met many friends who made it a very enjoyable time, notably Adam, Andy, Claude, Philippe, Piet, Tobias and so many others. It is going to be great when we get together again.

And finally, I dedicate this work and everything it represents to my parents, whose sacrifice and virtues lie at the base of this castell. This is a fitting opportunity to express my love, gratitude and admiration for their constant and unconditional support of every important endeavor I have undertaken in life. *(Finalmente, quiero dedicar este trabajo y todo lo que el representa a mis padres cuyo ejemplo y sacrificio están en los*

cimientos de esta obra. Esta es una buena oportunidad para expresarles mi cariño, mi gratitud y mi admiración por el apoyo constante e incondicional que siempre han prestado a todas las empresas que he comenzado en la vida.)

Pasadena, May 2002

Luis González Liñero

ABSTRACT

The failure process of laminated composite materials originating from precut sharp cracks, as well as their propagation, is studied from a “global” perspective, appropriate for structural analysis. The size effect in the damage development is explored and the question of “scaling” of the results is addressed.

Two globally orthotropic sets of panels with the notches aligned along the axes of orthotropy are studied. The internally evolving damage in the crack tip region is examined through enhanced x-ray radiographic inspection and surface strain fields are measured by means of the Digital Image Correlation method (the applicability and limitations of which are analyzed and discussed). The results obtained from these two experimental techniques are joined to assess the feasibility of identifying internal damage solely from surface measurements.

The shape of the region of influence of the crack is described and its extension measured. A simplified model for damage progression analysis is proposed.

The process of initiation of the damage propagation is described in detail and the different responses for the two different layups are discussed. The maximum stress/strain and the Tsai-Hill failure criteria are compared with the experimental results on the laminates, and their reliability and limitations are addressed.

The effective properties of the two sets of laminates are measured at three different loading rates and compared to theory, and the relevance of the time dependence of the material is studied.

CONTENTS

1	Introduction	3
1-1	Background, Motivation	3
1-2	Composite Materials	7
1-3	Laminated Composites	8
1-4	Global Failure/Fracture Instabilities	14
1-5	Failure Criteria	18
2	Experimental Work	25
2-1	Experimental Work, Description	25
2-2	Digital Image Correlation (DIC)	28
2-3	Enhanced X-Ray Radiography Inspection	33
2-4	The Specimens	35
2-5	The Loading Fixture	39
3	Results and Analysis	44
3-1	Theoretical Laminate Mechanical Properties	44
3-2	Measured Laminate Mechanical Properties	46
3-3	Numerical Simulation and Load-Displacement Behavior	51
3-4	Experimental Load-Displacement Curves	59
3-5	Damage Initiation	63
3-6	Damage Progression	75
3-7	Damage Area Concept	92
3-8	Surface Deformations and Internal Damage (DIC—X-radiography)	97
4	Conclusions and Recommendations	102
	Appendices	107
A.	Review of Failure Criteria	107
B.	Strain Distributions at Damage Initiation	132
C.	X-Ray Inspection of the Internal Damage Progression	139
D.	Surface Strain Fields on X-Ray Images of Internal Damage	162
	Bibliography	175

There are no pages 1 and 2.

INTRODUCTION

1-1 BACKGROUND, MOTIVATION

From the very beginning, the aerospace industry has made use of all the advances that materials science has provided to construct structures that are energy efficient. For an engineer every gram of the structural weight saved is translated into kilograms of increased payload or an extension in range, since lighter structures require smaller engines and smaller lifting surfaces—in the case of airplanes; consequently less fuel is necessary, which in turn requires smaller tanks and leaves more space available for extra payload, and so on. All this should be achieved without compromising the stiffness, strength, or safety of the vehicle. Moreover, in many cases, the new materials have provided not only significant improvements in the weight-to-strength ratio but also in stiffness and safety, or have facilitated maintenance, repairs or fabrication and in certain instances, only the utilization of the new material has made it possible for the vehicle to get off the ground. Two examples illustrate this point; one is an existing aircraft and the other one is still in the development stage.

The first one is the technology demonstrator X-29 (Figure 1.1.1). This plane is extremely maneuverable due to its forward swept wing design. Only the stiffness-to-

weight ratio provided by advanced composites made the construction of the X-29's thin supercritical wing possible; state-of-the-art composites allowed aeroelastic tailoring which, in turn, produced limited wing bending and twisting to eliminate structural divergence within the flight envelope. Additionally, composite materials allowed the wing to be sufficiently rigid for safe flight without adding an unacceptable weight penalty.

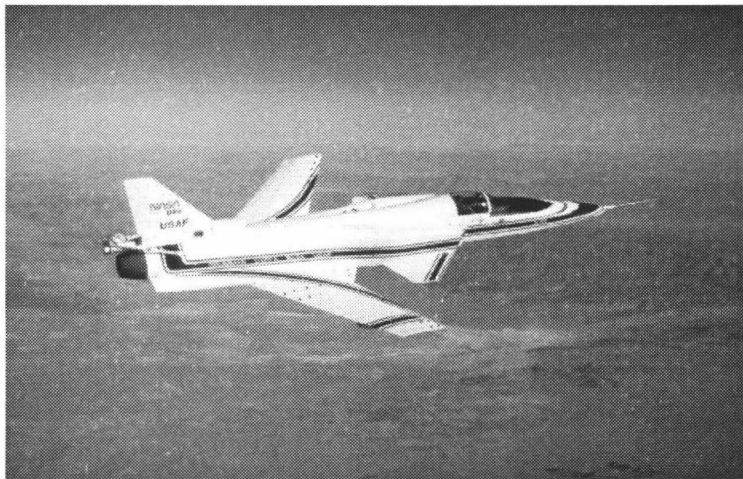


Figure 1.1.1 X-29 technology demonstrator. The use of composite materials made possible the thin forward swept wings that give an extraordinary performance to this aircraft (NASA).

The High Speed Civil Transport (HSCT) is another example. In the 1990s, NASA launched a large scale program—titled High Speed Research (HSR)—to develop the technologies that would make the construction of an affordable, environmentally friendly successor to the Concorde possible. Among its crucial characteristics were a Mach 2.4 cruising speed, 300 passenger capacity, an operational maximal cruise temperature of 350 °F, and a minimum of 60,000 hours, which its materials and structures were expected to endure. Traditional aerospace materials, such as aluminum or titanium, could not serve in this context so that new high-temperature and strong composite materials such as IM-

7/PETI-5 were developed. The HSR program came to an end for financial reasons, but research around the IM-7/PETI-5 has continued because of the great potential that this material holds for many other aerospace applications.

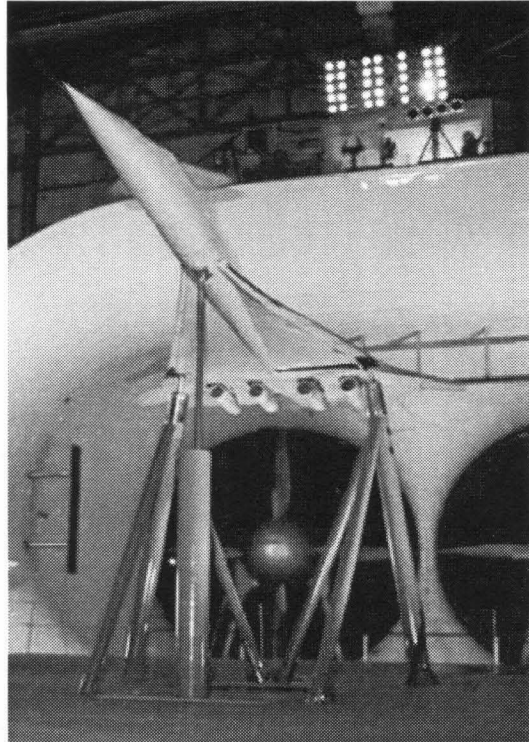


Figure 1.1.2 Wind tunnel model of the HSCT, an aircraft that would make extensive use of advanced composites to withstand extended periods of time at 350 °F temperatures, cruising at Mach 2.4 (NASA).

Since the 1970s, the use of advanced composite materials has constantly increased in aerospace applications. The main benefits of composites over metals technology have been, including high stiffness-to-weight ratio, high strength-to-weight ratio, excellent fatigue resistance, corrosion resistance, low thermal conductivity, acoustical insulation, thermal insulation, and the ability to be tailored to a particular need. If current metal structures were to be substituted by a fully composite one—without changing the manufacturing and the design procedures—weight savings of up to 30% could be

achieved. Furthermore, if the vehicle were to be completely redesigned, making use of the inherent properties and characteristics of the composite materials, further weight savings would be possible (e.g., all the rivets could be replaced by monolithic constructions or by stitching or bonding).

If composite materials present all these advantages, why is it that their application is still somewhat limited? Some of the obstacles for a more expanded composites application in the aerospace industry are the high manufacturing costs compared to traditional materials, maintenance related issues—at least for certain applications in commercial transports, and a general lack of knowledge about how damage is initiated and progresses throughout a structure. In addition to the fact that their failure properties are much less explored and characterized than those of the metallic structures, the anisotropic nature of these materials renders more difficult the analysis, and consequently, the prediction capabilities that can be used in design or modeling are very limited.

1-2 COMPOSITE MATERIALS

A *composite material* is simply a material that is formed by the combination of at least two different materials on a macroscopic scale with the purpose of generating a new “material” that has improved overall properties in comparison to its constituents. Advanced composites are composed of fibers of various forms and a matrix. The overall properties are a function of the constituents, their distribution and the interaction between them. According to the disposition of the constituents, three main categories of advanced composites are distinguished:

- 1) Continuous fiber-reinforced composites, which in turn can be classified as
 - i) Unidirectional fiber-reinforced composites and woven fabric composites
 - ii) Random fiber-reinforced composites
 - iii) Three-dimensional fiber-reinforced composites
- 2) Discontinuous fiber-reinforced composites include
 - i) Particulate fiber-reinforced composites
 - ii) Chopped fiber-reinforced composites
 - iii) Whisker-reinforced composites
- 3) Molecular composites.

1-3 LAMINATED COMPOSITES

Aircraft and aerospace industries mainly use continuous fiber-reinforced composites because, due to the anisotropy of the laminae, their properties can be controlled very effectively; i.e., desired property values in different directions can be easily obtained by altering the material and manufacturing variables. For example, in a unidirectional composite, the ratio of the longitudinal strength (or stiffness) to the transverse strength (or stiffness) can be altered by controlling the volume fraction and orientation distribution of the fibers. The longitudinal properties of unidirectional composites are controlled by fiber properties, whereas the transverse properties are matrix dominated. In most engineering applications the transverse properties of unidirectional composites are found to be inadequate. This apparent limitation is overcome by forming laminates from the unidirectional layers by bonding together two or more laminae so that they act as an integral structural element. The principal material axes of the laminae are oriented to produce a structural element with the desired properties in all directions.

Laminates are fabricated such that they behave as a monolithic material. Thence the simplification, in traditional laminate theory, that the bond between two laminae is perfect, i.e., infinitesimally thin and not shear deformable. Thus the laminae cannot slip relative to each other, and the displacements remain continuous across the bond. Equations have been developed for the stress-strain response of thin composite plates (for example, Tsai/Hahn and Jones). Such analyses provide both the intra-ply and the inter-ply stress components. When failure or a stress raiser is present, because of the sharp stress concentrations in all directions, the analysis of local failure modes is usually

complicated. Typically, multiple intra-ply cracks and inter-ply delamination occur during the course of the applied load.

When a laminate is constructed by stacking a number of orthotropic laminae* in an arbitrary sequence of orientations, the laminate stiffness matrix will generally be fully populated; that is, all the elements are nonzero. However, it is possible, and in many cases desirable, to specify the stacking sequence such that a number of elements in the stiffness matrices are zero. This simplifies the laminate analysis and, more importantly, it sometimes avoids undesirable coupling between bending and stretching or twisting, or between midplane normal forces and shear strains. Surely coupling can induce unwanted stresses into a structure if the deformations are restricted. Thus, it is desirable to construct laminates that possess special characteristics. Some special cases are the *symmetric*, the *unidirectional*, *cross-ply*, and *angle-ply*, and the *quasi-isotropic* laminates.

Symmetric laminates are constructed by placing the laminae symmetrically with respect to the midplane. They represent a common class because, besides ease in their analysis, the bending-stretching coupling is eliminated, which in nonsymmetric laminates causes an undesirable warping due to in-plane loads. Also, temperature changes will cause warping, and thus in the fabrication of a laminate at an elevated temperature warping will result when it is cooled to room temperature.

Three different types of **orthotropic** laminates are normally constructed. These are (i) **unidirectional** laminate with all the laminae oriented in the same direction, (ii) **cross-ply** laminate with laminae oriented at 0° or 90° only, and (iii) **angle-ply** laminate with equal number of laminae oriented at $\pm \theta$ angles. All of these laminae can be

* It should be remembered that for an orthotropic material normal stresses and shear stresses along the axes of symmetry will only produce normal strains and shear strains, respectively.

symmetric also. This class of laminates behaves as an orthotropic layer with respect to in-plane forces and strains, i.e., as a laminate in which there is no coupling between the normal stresses and shear strain.

Finally, in the **quasi-isotropic** laminate the extensional stiffness matrix $[A]$ has isotropic character, i.e., it has two elastic coefficients that are independent of the orientation in the plane. Just as for an isotropic material. A quasi-isotropic laminate can be constructed by meeting the following conditions:

- 1) The total number of layers must be three or more.
- 2) The individual layers must have identical stiffness matrices $[Q]$ and thicknesses.
- 3) The layers must be oriented at equal angles with respect to a reference frame. If the total number of layers is n , the angle between two adjacent layers should be $\pm \pi/n$

A peculiarity of laminated composite materials, which becomes quite relevant for failure analysis purposes, is the well-studied fact that stresses in the vicinity of free edges cannot be considered two-dimensional (Pipes and Pagano, 1970). The out-of-plane stress components, often referred to as the interlaminar stresses, are the result of the ply interface load-transfer mechanisms. Agarwal (1990) summarizes Pagano's work about the importance of interlaminar stresses by the following points:

- 1) The interlaminar shear stress is very high (perhaps even singular) at the free edge of a laminate (as the edges on sides of a laminate, cutouts, holes, etc.).

- 2) The interlaminar normal stress, σ_z , has a very steep gradient near the free edge. A tensile value of σ_z at the free edge may initiate delamination and can thus initiate or at least accelerate the failure process.
- 3) The stacking sequence in a laminate affects the magnitude as well as the nature of the interlaminar stresses. Thus a difference in tensile static and fatigue strengths may be observed when the stacking sequence is altered even though the orientation of each layer does not change.
- 4) The interlaminar stresses can be regarded as an edge effect only since their prominence is confined to a narrow region close to the edges. Predictions of the lamination theory are quite accurate in the regions away (e.g., a distance equal to the laminate thickness) from the edges.

Thus, it is clear that the presence of cutouts, holes and through-cracks (that could be the result of high energy penetration, for example) can change the failure mode of the material under load significantly. Another important issue connected with the free edge effects is that it is a source of “size effect” in the failure mechanisms of composite materials. This refers to the observed fact that the strength of these materials is affected by the size of the specimen. It is of utmost importance to determine the nature of this dependence to be able to design full-scale structures based on the information obtained from laboratory tests.

There have been observed significant effects of specimen size on the strength of fiber reinforced composites (Wisnom, N. R., 2000). This is not a single phenomenon, but depends on the failure mechanism. Studies of fiber direction tensile failure, compressive

failure, and matrix dominated failures have all shown a tendency for the strength to decrease with increasing specimen volume, with matrix failures showing the largest effect.

Size effects in tensile failure have been found in both tensile and flexural tests of differently sized specimens, and from higher strengths in bending than in tension (Kies, 1964; Nuismer and Whitney, 1974, 1975). The size effect in bending is not primarily due to the stress gradient since similar results are obtained in direct tensile tests. The magnitude of the effect is consistent with Weibull statistics involving moduli in the range 13 - 29 for glass and carbon fiber/epoxy materials (Cunningham *et al.*, 1985; Hojo *et al.*, 1994; Wisnom and Maheri, 1994). There are some indications that the size effect diminishes with increasing scale.

A number of studies (for example, Jackson, 1992; Wisnom and Atkinson, 1997; Crowther and Starkey, 1988; Bullock, 1974) have shown a reasonable fit with simple Weibull strength theory, and from a practical point of view, this would seem to be a reasonable way of accounting for the effects of stressed volume on tensile strength. However, other studies have shown discrepancies, and Weibull theory is not consistent with the progressive failure and load redistribution that is sometimes observed in tensile failures (Whitney and Knight, 1980). A model treating the composite as a bundle of fiber bundles is able to account for these discrepancies qualitatively.

Lower compressive strengths have been found in large components than in small test coupons, and attributed to defects such as fiber waviness (Clarke, *et al.*, 1997). This is a form of size effect, but one that is critically dependent on the manufacturing process. Size effects have also been found in compressive failure resulting from bending, which

are believed to be mainly a result of constraint due to the stress gradient through the thickness (Wisnom *et al.*, 1997). There may also be size effects due to intrinsic material variability, but difficulties in compressive testing mean that the experimental evidence is currently inconclusive.

There are large size effects for matrix-dominated failures (O'Brien and Salpekar, 1993; Shivakumar *et al.*, 1994). Strength is controlled by defects, especially voids and machining damage during specimen preparation. Weibull strength theory represents the size effect reasonably well, although there is some indication of a limiting value being reached for small volumes of material. Manufacturing quality, especially the level of voidage, has a significant effect on the magnitude of the size effect.

Because there are so many demonstrations of how specimen size can influence failure behavior, it is essential to address this possibility of the failure mode investigated in the sequel to assess whether one may (conservatively) use strength data derived from small coupons in the design of large structures. It is crucial to assure that the manufacturing quality of test specimens is representative of that likely to be achieved in production.

1-4 GLOBAL FAILURE/FRACTURE INSTABILITIES

It has already been mentioned that the anisotropy of composite materials gives rise to complicated three-dimensional states of stress in the presence of geometrical discontinuities such as cutouts, notches or ruptures (which could have been produced by penetration of a foreign object, for example). Another factor that renders the analysis of the failure of composites more complex than that of traditional materials is precisely their distinctive heterogeneity, i.e., the composite is an aggregate of unidirectional plies which in turn are composed of two very different phases: the matrix and the fibers. Thus when a global failure occurs, the propagation of any damage occurs through a mechanism that is only *similar* to a crack.

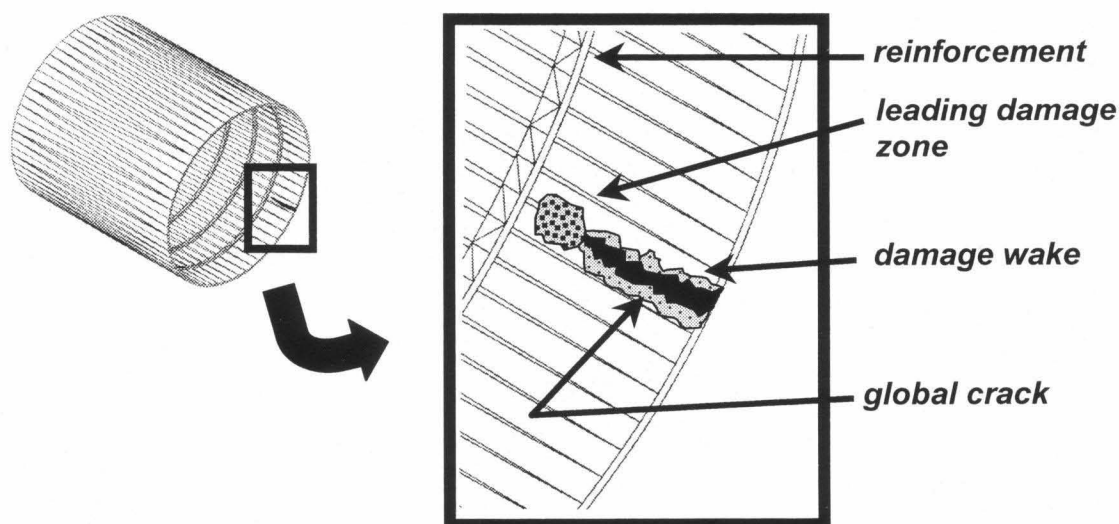


Figure 1.4.1 “Global crack” traversing a built-up structure with damage wake and interaction zone near a reinforcement element.

In detail the failure progression has features of a band or region of damage rather than of a well-defined, classical crack-like geometry, but seen from a properly large or global scale such damage progression may be treatable by a crack analysis. This

situation is represented schematically in Figure 1.4.1, where a “crack” (not sharply defined by flank boundaries) tracks through an extended damage zone which represents a multitude of local or small scale damage phenomena, including matrix cracking, fiber pull-out, delamination, and various forms of fiber fracture.

Such a macrocrack phenomenon has consequences when it interacts with other components of a structure, in that the details of the interaction do become important. Specifically, the issue here is that of the raising of stress levels at skin-structure joints that derive from an approaching macrocrack. This latter feature is likely to have a rather broad “front” with a diffuse but distinct stress concentration capability. Since such a front probably involves ply separations and fractures, this zone could extend on the order of inches. It is, therefore, very important to assess the size of such a zone for computational and design purposes.

It is doubtful that this particular or other structural size parameter (e.g., width of wake, interaction zone near reinforcement) could be established uniquely in the laboratory by using only small (structural) specimens. Rather, (nearly) full-scale simulations would be necessary to be conducted for this purpose to be able to determine, out of the combined results, the scale factors for these failure modes. The test facilities at, and specimen cost to, Caltech impose a limit on the size of the specimens that could be tested but, nevertheless, elements close to working panels fell within these limits.

Specimens of the geometry illustrated in Figure 1.4.2 would allow the understanding of how a macrocrack interacts with a stringer. Clearly, the stiffness of the stringer determines the range over which the forces at the “tip” of the global crack are distributed and abated near the stringer; consequently the failure may stop (temporarily?).

The (possible) stress abatement with approach to the stringer depends on the (tensile and bending) stiffness of the latter, and probably on their relative values compared to those of the fracturing plate. These dependences need to be worked out.

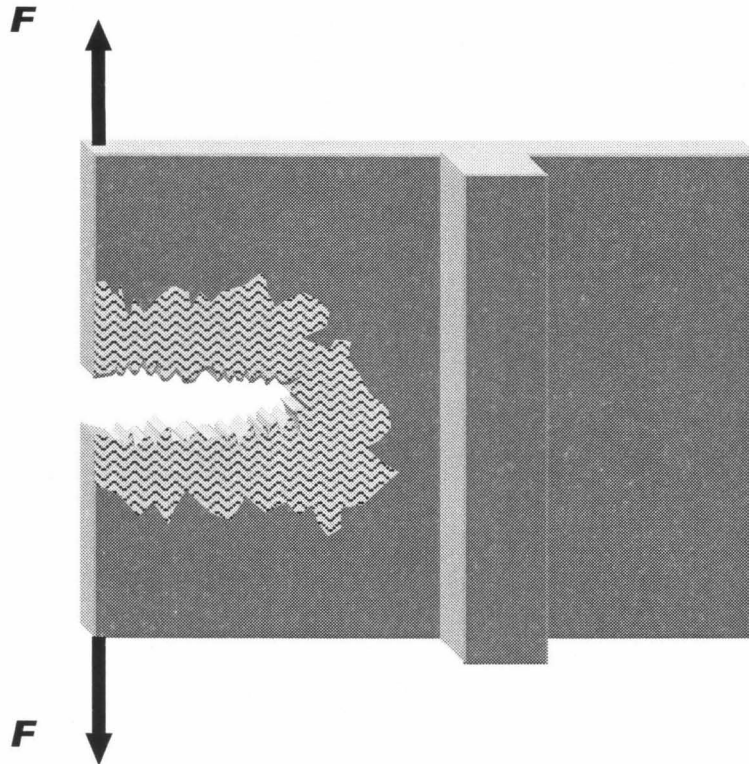


Figure 1.4.2 Exemplar configuration of a global crack traversing a reinforced plate.

A first analysis shows that to understand the crack interaction with a stiffener, the nature of the stress and strain fields (as determined by the internal damage) in a sheet needs to be addressed as a global crack propagates through it. Surprisingly enough, very little work has been done in this area. However, leaving the crack-stiffener interaction for the future, the main topic of this study is the detailed description of the failure process, an assessment of the stress/strain fields in the vicinity of the “crack tip,” the quantification of the extension of the “zone of ‘crack’ influence”; this is to be done for different layups.

To quantify scale effects, it is necessary to conduct tests on differently sized specimens: from the small coupon size to the largest specimens that the testing facilities at Caltech can handle (roughly 18×18 "). The number of ply configurations is nearly limitless; however, a set of typical results could suffice for analysis and design purposes, once extrapolations on such data become better understood (measurements to be made in the future).

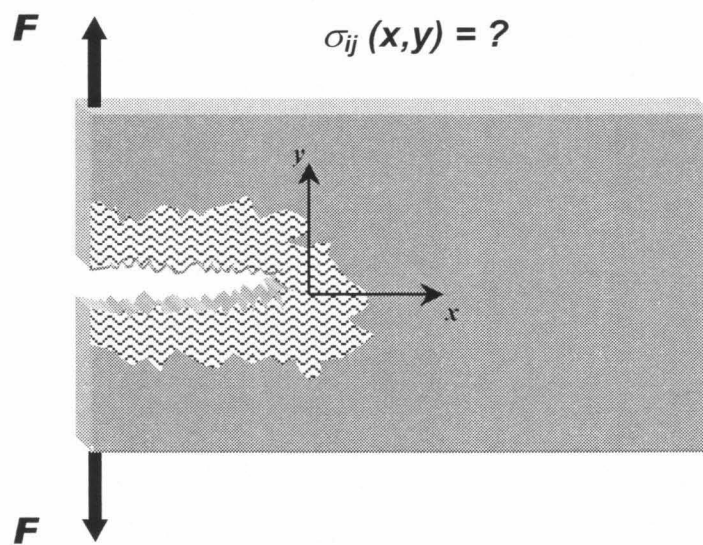


Figure 1.4.3 Examination area at the front of a fracture zone in a composite (unreinforced) plate.

1-5 FAILURE CRITERIA

Throughout the years, different failure criteria for composite materials have been developed. As already discussed, due to the complexity of the process of rupture, and because of the wide range of properties covered under the term “composite material”*, there is no single, universally accepted, failure criterion that can be applied to all possible situations.

Failure criteria typically have been, either stress, strain or energy based, and they have used a micromechanics or a macromechanics analysis. The former can be used for the design of the composite materials themselves or for providing more insight into the failure process but could find only very limited and difficult application in structural design and analysis. The strengths of laminae and laminates with uniform stresses or strain fields were first developed and later on other criteria were proposed for materials in the presence of stress or strain gradients (including cutouts or notches).

The macromechanics approach appears to be more appropriate for engineering applications and many criteria exist in the literature and have been quoted in Appendix A following Tan’s survey (1994). From them, we selected the maximum stress/strain and the Tsai-Hill criteria because they are most widely used, mainly due to their simplicity. Many of the other criteria require the determination of a large number of parameters, some of them difficult to measure or that would require a substantial amount of testing before the accuracy of the particular criterion could be assessed. Other criteria are the result of mere “curve fitting” with—in some cases—little physical basis. These reasons have limited their effectiveness in engineering design and analysis. The two criteria

* For example, some composites are brittle and others more ductile.

mentioned have found widespread application and have even been incorporated in many commercially available finite element analysis programs as failure criteria. In essence, they have become industry's standard for establishing damage initiation. We will first present them and discuss some of their advantages and also their inherent limitations and drawbacks. Then, we will apply them to our experiment and draw some conclusions.

Maximum Stress Criterion

The maximum stress failure criterion assumes that failure occurs when any one of the stress components along the principal material axes reaches, or is greater than, its individual strength value* :

$$\begin{aligned}
 & - X_c \leq \sigma_1 \leq X_t \\
 & - Y_c \leq \sigma_2 \leq Y_t \\
 & | \sigma_6 | \leq S,
 \end{aligned}
 \tag{1.5.1}$$

being X , Y and S the material strengths in the fiber direction, perpendicular to it and in shear, respectively. The compressive strengths are generally different from their tensile counterparts for orthotropic and anisotropic materials (subscripts c and t). Note that shear strengths are the same in + and - directions along the principal material axes.

* Throughout this work, the stresses and strains will be presented indistinctly in the normal tensorial notation (double subscripts $i, j = 1, \dots, 3$) and in the contracted one, i.e., with only the six components of the symmetric tensor. In this case, $\sigma_{\bar{6}} = \tau_{12}$. The case will be obvious from the context.

Maximum Strain Criterion

The maximum strain failure criterion, ubiquitously in use for rapid design estimates, assumes that failure occurs when any one of the strain components along the principal material axes reaches, or exceeds, its individual critical strain value:

$$\begin{aligned}
 -e_{1c} \leq \varepsilon_1 \leq e_{1t} \\
 -e_{2c} \leq \varepsilon_2 \leq e_{2t} \\
 |\varepsilon_6| \geq e_6
 \end{aligned}
 \tag{1.5.2}$$

where e_1 , e_2 and e_6 denote the ultimate strains. They are generally not equal to X_i/E_i ($i = t, c, s$) unless E_i denotes the secant modulus (Jones, 1999). This is because material nonlinearity exists, especially for longitudinal compression and shear. Their strength envelopes would only coincide when Poisson's ratio equals zero.

It is clear that these criteria are suitable for only simple loading conditions since they do not take into account the interaction between the different stress (or strain) components. Furthermore, one can question the validity of producing a “failure envelope” with a curve that connects so different phenomena as fiber cracking with the microbuckling compressive failure.

Mises, Hill and Tsai-Hill Criteria

In 1928 Mises proposed a yield criterion for a crystal or a textured metal of the form

$$A_{ij}\sigma_i\sigma_j = \text{constant}, \tag{1.5.3}$$

where A_{ij} are constants that must be determined experimentally. This criterion was further developed by Hill for orthotropic materials as

$$F(\sigma_2 - \sigma_3)_2 + G(\sigma_3 - \sigma_1)_2 + H(\sigma_1 - \sigma_2)_2 + 2L \sigma_4^2 + 2M\sigma_5^2 + 2N\sigma_6^2 = 1 \quad (1.5.4)$$

In both these equations, the tensile yield strength is assumed to be the same as the compressive yield strength. This is generally not true for fiber-reinforced composites. The difference in tensile and compressive strengths can be considered if these criteria are used to predict one stress quadrant at a time. In this case the strength surface would not be smooth.

The strength coefficients F , G , H , L , M and N were related by Tsai (1968) to the uniaxial strengths. He considered unidirectional specimens and applied σ_1 , σ_2 , σ_3 , and σ_6 one at a time to obtain the strengths X , Y , Z and S . Two additional tests are needed to determine the coefficients L and M by applying σ_4 and σ_5 . In the case of plane stress, Equation (1.5.4) reduces to

$$\frac{\sigma_1^2}{X^2} - \frac{\sigma_1 \sigma_2}{X^2} + \frac{\sigma_2^2}{Y^2} + \frac{\tau_{12}^2}{S^2} = 1 \quad (1.5.5)$$

Equation (1.5.5) is known as the Tsai-Hill criterion. It is an obvious improvement on the maximum stress/strain criterion because it addresses the interaction of the different stress (or strain) components. The nature of that interaction is more questionable. That the transverse (perpendicular to the fibers direction) and the shear stresses (or strains) can couple to produce failure appears reasonable. What is not evident is the influence of the longitudinal (along the fibers direction) components. And, finally, this criterion also suffers from the defect of connecting with the same “enveloping” curve disparate failure modes.

A Procedure for the Strength-Analysis of Laminates

The analysis of stresses in the laminae of a laminate is a straightforward, but usually tedious, task. With the stresses considered a linear function of the applied loads, a single stress analysis suffices to determine the stress field that causes failure of an individual lamina. That is, if all the stresses are known in all the laminae, then they can be compared with a lamina failure criterion and uniformly scaled upward to determine the load at which failure occurs.

The overall procedure of laminate-strength analysis, which simultaneously results in the laminate load-deformation behavior, is shown schematically in Figure 1.5.1 Here, load is taken in the generalized sense to mean both forces and/or moments; similarly, deformations are meant to include both strains and curvatures. The analysis is composed of two different approaches that depend on whether any laminae have failed. If no laminae have failed, the load must be determined at which the first lamina fails (so-called first ply failure). In the process of this determination, the lamina stresses must be found as a function of the unknown magnitude of loads first in the laminate coordinates and then in the principal material directions of each lamina. The proportions of load (i.e., the ratios of N_x to N_y , M_x to M_y , etc.) are, of course, specified locally at the beginning of the failure analysis. The load parameter is increased until some individual lamina fails. The properties of the failed lamina are then degraded in one of two ways: (1) totally to zero if the fibers in the lamina fail or (2) to fiber-direction properties if the failure is by cracking parallel to the fibers (matrix failure). Actually, because of the matrix manipulations involved in the analysis, the failed lamina properties must not be zero, but rather effectively zero values to avoid a singular matrix that could not be inverted in the

structural analysis problem. The laminate strains are calculated from the known load and the stiffnesses prior to the failure of a lamina. The laminate deformations just after failure of a lamina are discussed later.

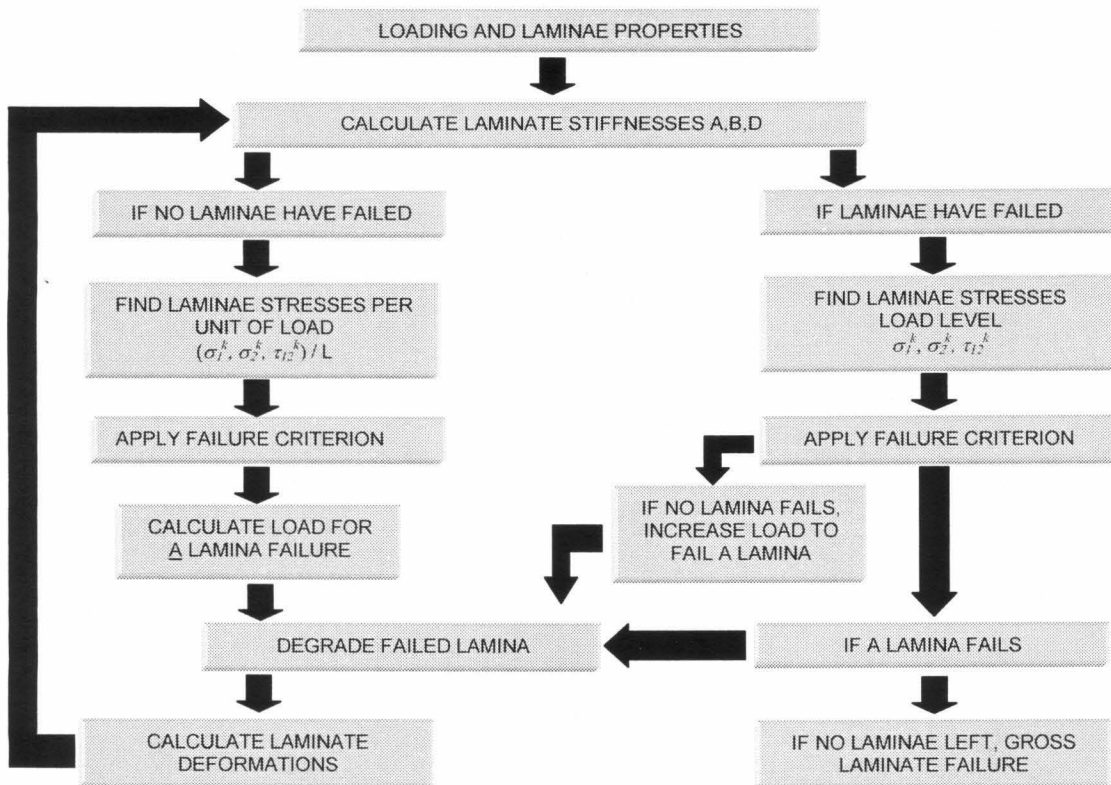


Figure 1.5.1 Analysis of laminae strength and load-deformation behavior (Jones).

Once one or more laminae have failed, new laminate extensional, bending-extension coupling, and bending stiffnesses are calculated. Lamina stresses are recalculated to determine their distribution after a lamina has failed (the stresses in the remaining laminae must increase to maintain equilibrium). Then one must verify that the remaining laminae, at their increased stress levels, do not fail at the same load that caused failure of the lamina in the preceding cycle through the analysis. That is, can the lamina

stresses be successfully redistributed among the unfailed layers? If no more laminae fail, then the load can be increased until another lamina fails, and the cycle is repeated. In each cycle, the increased stresses caused by failure of a lamina must be verified not to cause an instantaneously progressive failure, that is, where the laminae all successively fail at the same load. When such a multiple failures occur, the laminate is said to have suffered gross failure.

Note that the lamina failure criterion was not mentioned explicitly in the discussion of Figure 1.5.1. The entire procedure for strength analysis is independent of the actual lamina failure criterion, but the results of the procedure, the maximum loads and deformations, do depend on the specific lamina failure criterion. Also, the load-deformation behavior is piecewise linear because of the restriction to linear elastic behavior of each lamina. At any rate, the overall behavior of the laminate is nonlinear if one or more laminae fail prior to gross failure of the laminate. This is one of the many models for progressive failure of composites and shares the same problem with all of them, namely, the lack of a constitutive law for the material in the damaged region. Our experiments show the limitations or even the complete inapplicability of some of these criteria that have found a widespread usage.

EXPERIMENTAL WORK

2-1 EXPERIMENTAL WORK, DESCRIPTION

The present study intends to analyze and characterize the failure and “fracture” mechanisms of laminated composite materials in terms of typical structural load descriptions rather than in terms of micromechanics considerations, such that the emphasis on **structural design** dominates the investigation. To understand, predict, avoid, and control these processes, clear and effective criteria need to be developed based on sound physical principles.

To achieve that aim, accurate measurements of the deformation and strain fields are needed during the loading process; particularly, in the region around the “crack tip” or “failure front.” Thus, in summary, this project consists of proposing a failure initiation criterion based on experiment; tracking the damage progression, both qualitatively and quantitatively; assessing the damage zone size as a function of load history and crack propagation; and finally, studying the residual strength after failure. The influence of the stacking order or layup is explored and the time dependence is also addressed.

For determining the strains several methods were considered: strain gages and optical methods, such as the digital image correlation method (DIC), Moiré and Moiré interferometry. These methods provide information about the surface layers but it is not

clear that it can be used to fully characterize the damage state in the interior of the material. Therefore the use of nondestructive evaluation (NDE) techniques was imperative. The options considered were x-radiography, ultrasonic inspection and computerized tomography.

The setup of the experiment limited the choice of measurement methods, eliminating the computerized tomography and the ultrasonic inspection. Besides the fact that the cost of such equipment was beyond the reach of this project, the measurements had to be performed *in situ* while the specimens (in the fixture that limited access to them) were being loaded on an MTS or Instron loading machine. Furthermore, the results of the ultrasonic inspection are of difficult interpretation. The x-radiography was the method that offered the most advantages, which are explained in greater detail in a subsequent section.

The digital image correlation method (DIC) has been chosen to provide “field” measurements of the deformations. The other optical measuring techniques were dismissed because of the complexity of their setup and results interpretation. The strain gages were also dismissed for several reasons. One was that they would obstruct the x-ray imaging and a second one was that to obtain meaningful measurements a large number of very small strain gages would be needed adding too much complexity to the experiment. During the course of the tests it was found that they would have been wasted because, in some cases, early on, the outer layer is lost. This will be discussed in detailed in a subsequent section.

To study the influence of “scaling,” three sets of specimens were utilized; namely, panels of “coupon” size (6×6 in), another of “intermediate” dimension (12×12 in) as

well as a set of panels of roughly “component” size (18×18 in). For a more detailed description of the specimens, see section 2-4. Taking advantage of the fact that the panels are not quasi-isotropic, it was possible to study the influence of the layup by cutting the slits along or perpendicular to the 0° axis of the material.

The tests on the smaller panels were conducted on an Instron screw-driven tension testing machine but it proved to have insufficient load capability for the testing of the medium and larger panels. For that task an MTS servo-hydraulic system rated at 250 kN was used.

2-2 DIGITAL IMAGE CORRELATION (DIC)

The DIC method allows the accurate measurement of displacement fields on a planar deforming solid. Two of its main advantages are that it provides field measurements, as opposed to point values, and that it is nonintrusive.

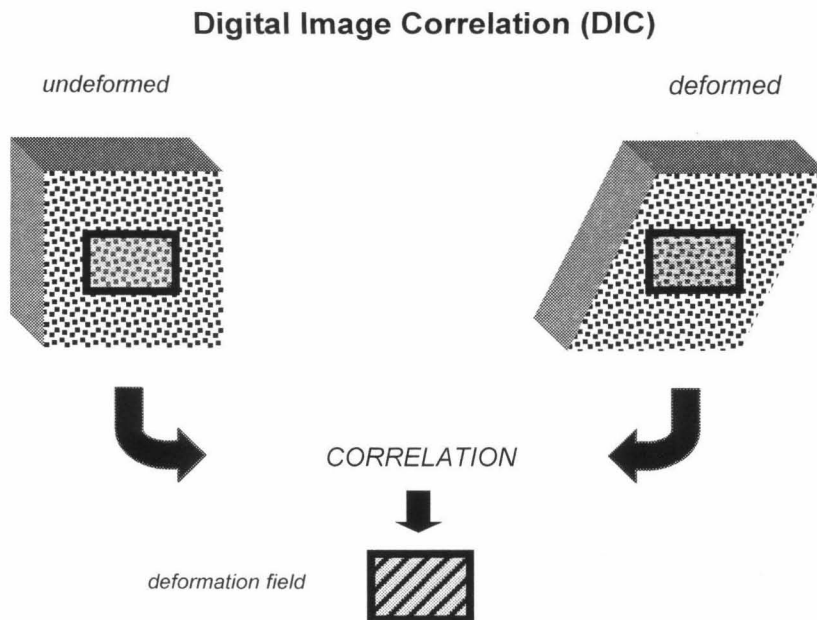


Figure 2.2.1 Schematic description of the DIC method. Two digital photographs of the same area (in the undeformed and in the deformed state) are compared to produce a mapping of the deformation field.

Digital image correlation is a computer vision technique that extracts the whole field displacement data by comparing the features in a pair of digital images of a specimen surface before and after deformation. More specifically, the physical problem of measuring in-plane displacements at grid points on a macroscopically flat surface can be formulated as a correspondence mathematical issue of minimizing a correlation function with respect to six coefficients over a subset image region containing the grid point, namely, the two in-plane displacement components (u and v), and their four derivatives (u_x , u_y , v_x and v_y), all evaluated at the grid point. As the specimen is displaced

during a test, images are taken at prescribed intervals, ultimately reduced to a grayscale and saved as raw data files brightness values. When the test is complete, it is the job of the DIC software to track the brightness values from image to image and extract the in-plane displacements due to translation, rotation, extension, and shear. These, of course, form the two-dimensional whole field displacement and strain maps for the specimen and can be reported cumulatively or incrementally.

Several implementations of the DIC method have been demonstrated in a range of experimental mechanics and materials applications (Sutton et al., 1983; Chu et al., 1985; James et al., 1990; Franke et al. 1991; Vendroux and Knauss, 1994, 1998; Choi and Shah, 1997; Tong, 1998; Li et al., 1998). For the present work, that developed by Vendroux and Knauss has been used.

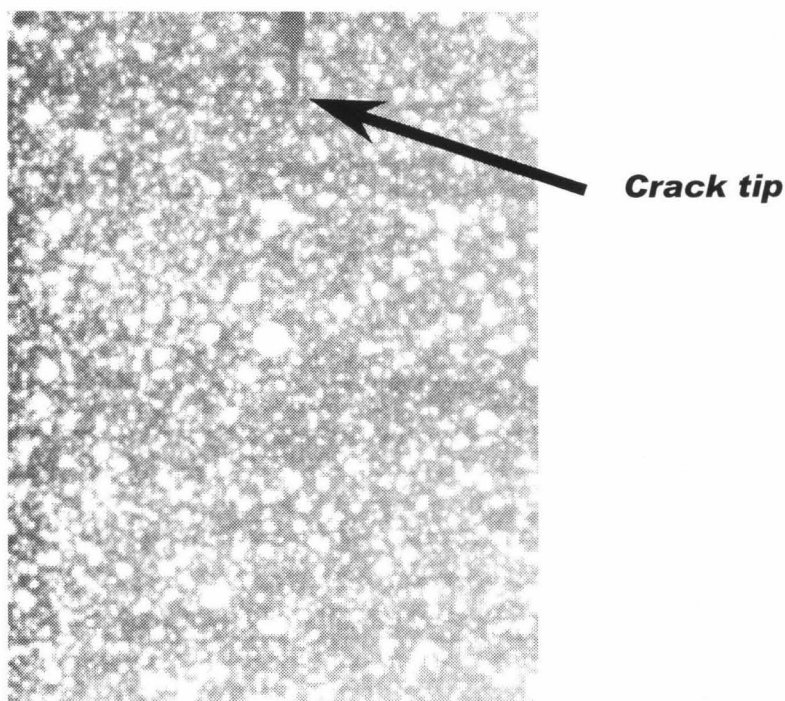


Fig 2.2.2 Photograph of the region around the crack tip with spot pattern used for digital image correlation.

The specimens used in this study did not present surface features that could be used for DIC and thus it was necessary to provide a spot or splatter pattern of white and black paint on the area of interest. An example of this is shown in Figure 2.2.2.

To test the applicability, accuracy and limitations of this method and provide a calibration, a series of tests were performed. All of them consisted in the determination of a known strain field via DIC by subjecting strips 1" wide of polycarbonate and aluminum (5052 alloy) to uniform uniaxial tension, as depicted in Figure 2.2.3. The strains derived with the DIC method were to be compared to those measured with a strain gage. The gage section shows the speckle pattern used for the DIC.

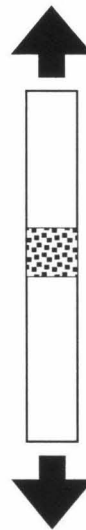


Fig 2.2.3 Tension specimen with speckle pattern at gage section for DIC evaluation.

The aluminum specimens were not of much use quantitatively because they deformed plastically along shear bands and this localized deformation rendered the strain gage measurements troublesome for purposes of method evaluation. Nevertheless,

qualitatively, those tests showed that the method was applicable since the shear bands clearly appeared in the deformation field plots, as can be seen in Figure 2.2.4, which presents the data in the form of a vector plot of displacements.

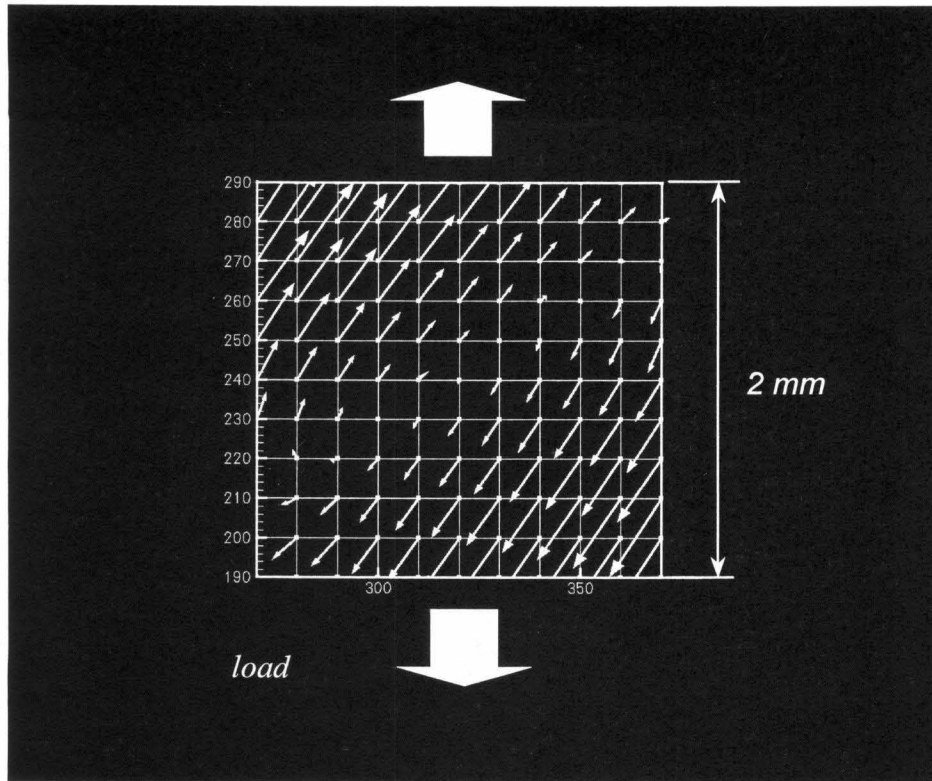


Figure 2.2.4 Deformation field of 5052 Aluminum specimen under uniaxial tension. The shear bands at 45° are clearly distinguishable.

Thus, for calibration purposes, polycarbonate was used instead of aluminum. The test described in Figure 2.2.3 was repeated several times and plots of the deformation field similar to that shown in Figure 2.2.5 were obtained.

Once the deformation field is known, the strains can be computed. The average for the whole region was computed and compared to the measurements obtained with a strain gage. The results of the comparison are presented in Figure 2.2.5. Superimposed is a straight line of unit slope which is where the points would be expected to fall. It can be

seen that the values show reasonable agreement and that the values for the error cited in the literature of 0.1% of strain are correct (for example, Tong, 1998).

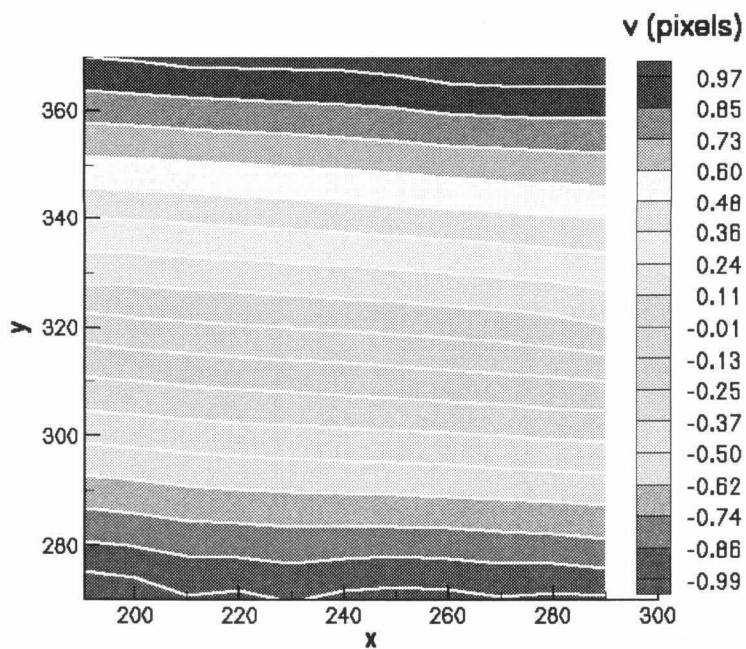


Figure 2.2.5 Deformation field calculated with DIC for a polycarbonate specimen (the area plotted is about $0.045'' \times 0.045''$).

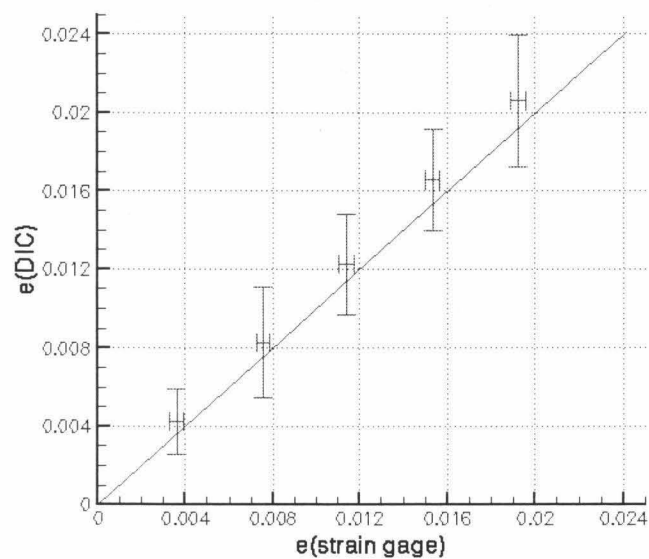


Figure 2.2.6 Comparison between strains calculated via DIC and measured with strain gage for a polycarbonate specimen.

2-3 ENHANCED X-RAY RADIOGRAPHY INSPECTION

X-ray radiography is one of the most common nondestructive evaluation (NDE) techniques in use for composites. Part of the energy in the x-ray beam is absorbed by the constituents in the material as it passes through the part. The transmitted energy is exposes a photographic film placed directly behind the opposite surface (shadow graph). Defects or flaws in the material produce a variation in energy transmission that shows up as shadow images on the photographic film.

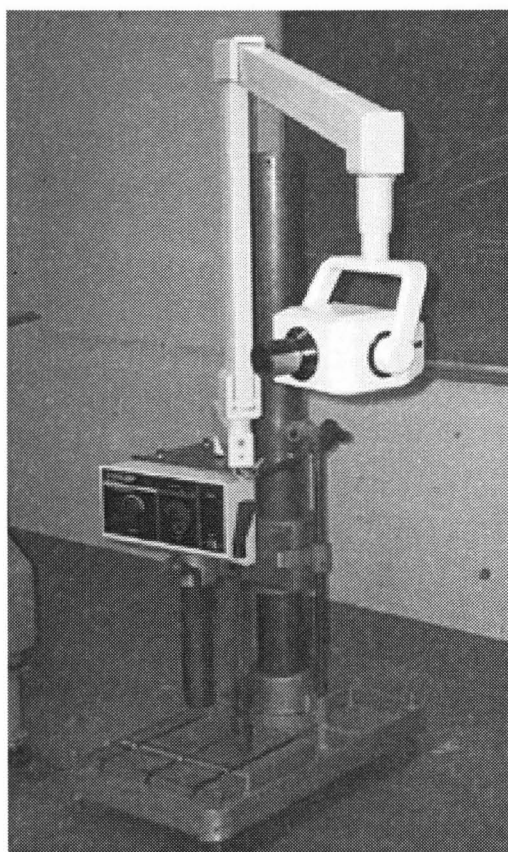


Figure 2.3.1 X-ray equipment for internal characterization of damage.

Planar defects normal to the radiation beam, such as delaminations or interlaminar cracks, are not detected by radiography unless a radio-opaque penetrant is first injected

into these defect areas to improve the contrast. Furthermore, the use of these fluids is necessary to enhance the presence of ruptures because the absorption qualities of the typical composite materials constituents are very close to those of air (Mallick, 1997). This technique, called penetrant-enhanced x-ray radiography (PEXR), is often used to detect delaminations caused by low energy impacts; however, its use requires a way for the penetrant to access the defect areas and is therefore limited to delaminations that are open to the surface through an injection point. Several penetrants, including zinc iodide, silver nitrate, trichloroethylene, diiodomethane (DIM), diiodobutane (DIB), and tetrabromoethane (TBE), have been used for this purpose (Crane, 2000; Chang, 1975). In the present study TBE, DIM and DIB were used. The articles in the literature that deal with PEXR cite them extensively due to their excellent penetrant and x-ray absorption or contrasting capabilities (Chang, *op. cit.*; Mallick, *op. cit.*).

The first tests were performed with TBE but, because of its toxicity and corrosiveness, it was replaced by DIM; the fact that it would dissolve and wash away the paint used for the spot pattern of the DIC method also made its use undesirable. The DIM provides results just as satisfactory without all the inconveniences of TBE.

The x-ray film utilized was in the form of 4×5 in sheets of Kodak Professional TMAX 100. The x-ray machine was a Yoshida X-70 unit, with a 70 kVp source, shown in Figure 2.3.1. Preliminary tests lead to a typical exposure time of 4 seconds to achieve the best contrast.

2-4 THE SPECIMENS

The test samples for the present study were fabricated at the NASA Langley Research Center. The material combination selected was IM7 / PETI-5. This composite has shown great potential for aerospace applications due to its superb heat resistance and high strength. It was a prime candidate for the fuselage material for the HSCT (High Speed Civil Transport). IM7 are carbon fibers manufactured by Hercules and PETI-5 is the abbreviation for the fifth in a NASA-made series of phenylethynyl-terminated imide formulations. Its properties (per lamina) are summarized in Table 2.4.1.

**Table 2.4.1. Properties (per lamina)
of IM7 / PETI-5 as fabricated
(NASA Langley Research Center)**

$$E_1 = 21.8 \text{ msi (in tension)}$$

$$E_2 = 1.24 \text{ msi (in tension)}$$

$$E_1 = 21 \text{ msi (in compression)}$$

$$E_2 = 1.24 \text{ msi (in compression)}$$

$$\nu_{12} = 0.32$$

$$G_{12} = 0.77 \text{ msi}$$

$$\varepsilon_1^{(u)c} = 0.0125 \text{ in/in}$$

$$\varepsilon_1^{(u)t} = 0.0156 \text{ in/in}$$

$$\varepsilon_2^{(u)} = 0.007825 \text{ in/in}$$

$$\gamma_{12}^{(u)} = 0.0305 \text{ in/in}$$

$$\alpha_1 = -0.19 \text{ micro in/in/}^\circ F$$

$$\alpha_2 = 15.5 \text{ micro in/in/}^\circ F$$

$$t = 0.0056 \text{ in}$$

$$\rho = 0.058 \text{ lb/in}^3$$

$$V_f = 60 \%$$

The layup was chosen to represent a generic configuration representative of a typical aerospace application such as an airplane fuselage; this layup was not quasi-isotropic so as to be able to study the influence of the change of orientation on the “fracture properties.” Thus, the panels were fabricated with the following layup, $[90_2, +45_2, 0_2, -45_2, 0_2, +45_2, 0_2, -45_2]_S$, which is presented schematically in Figure 2.4.1. The nominal thickness was 0.179 in.

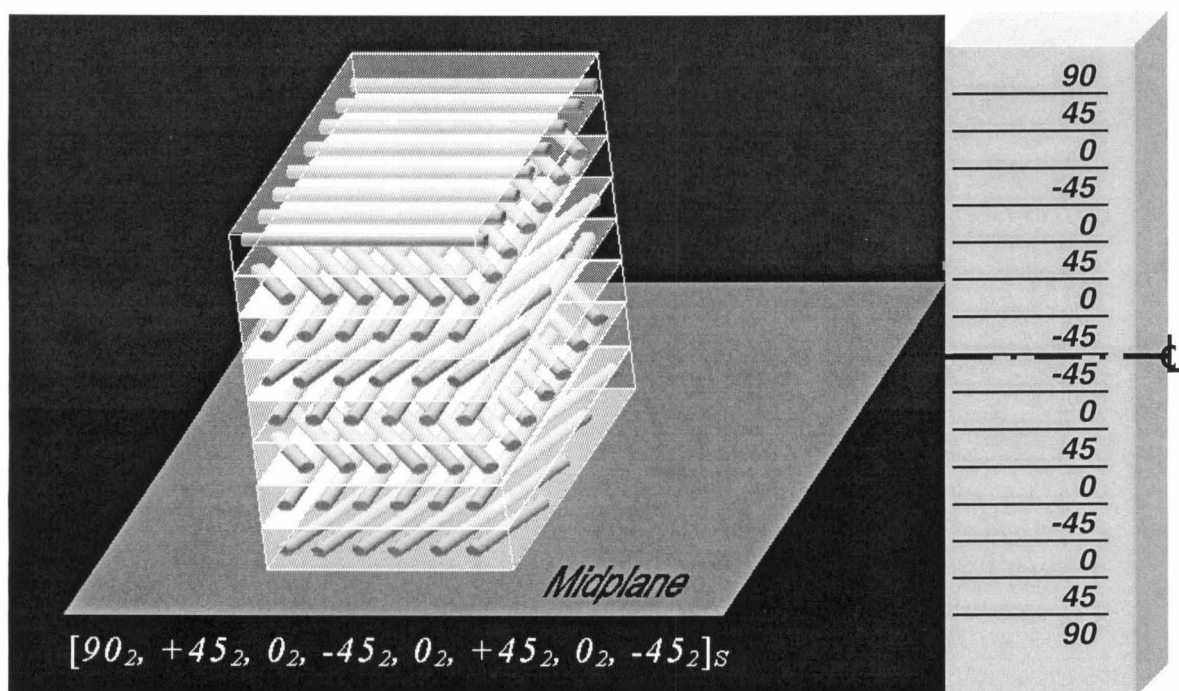


Figure 2.4.1 Specimens layup (each layer is doubled),
 $[90_2, +45_2, 0_2, -45_2, 0_2, +45_2, 0_2, -45_2]_S$.

From these panels compact tension specimens were cut in three different sizes according to the diagram of Figure 2.4.2. Half of the specimens were cut with the notch along the 0° and the rest at a right angle to it. This allowed the testing of two different layups: one with dominance of the 0° plies and, another for which the 90° layers were the most abundant. In the rest of this study, the panels with the notch in the 0° direction will

be identified as the **Parallel** panels and the ones with the crack at 90° as the **Perpendicular** ones.

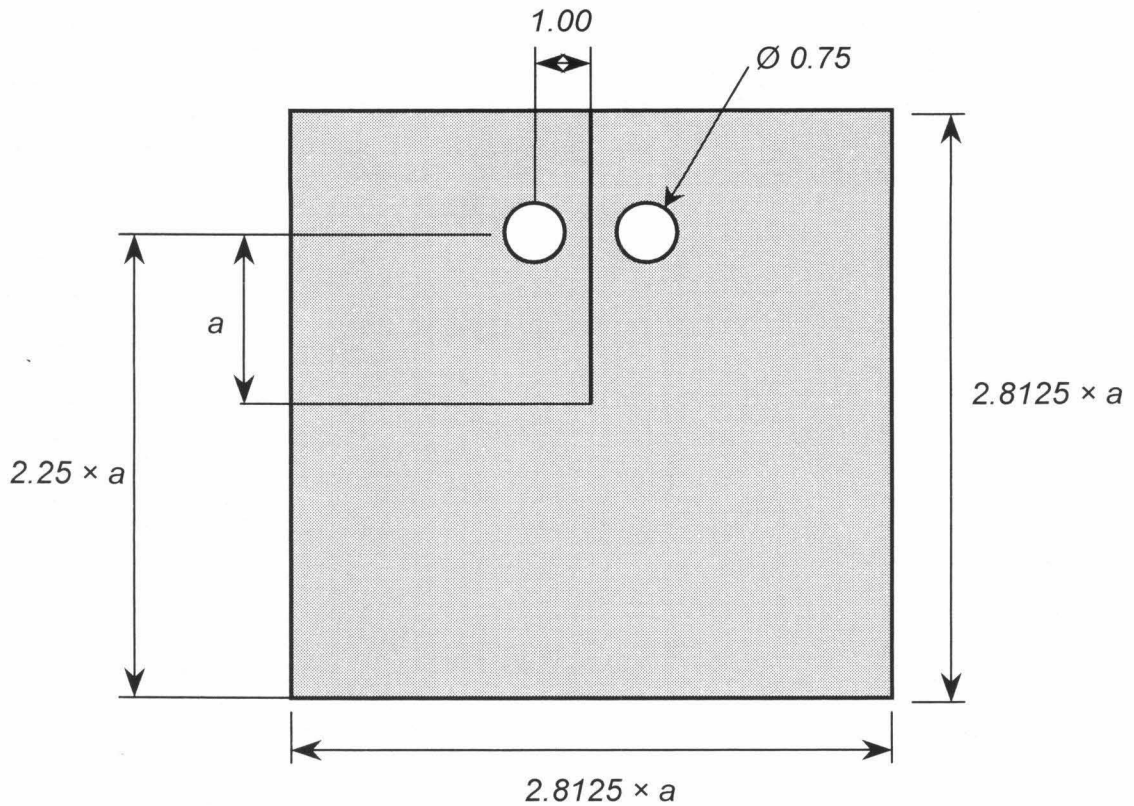


Figure 2.4.2 Specimen geometry. $a = 2.16, 4.32$ and 6.48 in for the small, medium and large specimens, respectively.

The initial notches or slits were needed to be as thin as possible to facilitate the repeatability of the results and the stability of the crack growth. Thus, as can be observed on Figure 2.4.2, they would result in very long cuts, especially for the largest panels. Such long slits cannot be produced with conventional saws since the material is so tough and hard, the tool tends to wobble and cannot produce a straight cut. Besides, the minimum cut thickness that can be obtained by saws would be unacceptably large for our purposes.

Different options were explored. Laser cuts appeared as an attractive solution but after several tests were performed on some scrap material, this method had to be discarded. The high temperature and the high-pressure gas used for the process caused the material to bulge on the exit side and burst. EDM, a technique normally used for producing extremely thin cuts and difficult patterns in metals, was not applicable because of the low conductivity of the composite material.

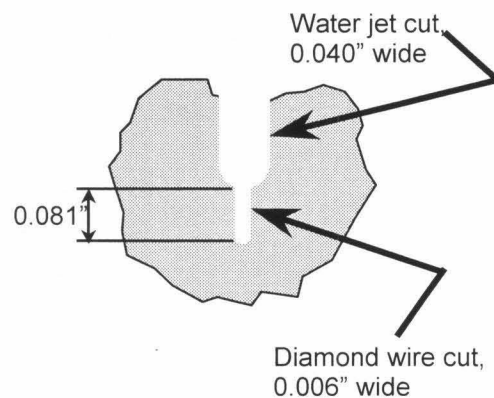


Figure 2.4.3 “Crack” tip detail. The main cut of the slits was produced by water jet process and then extended with diamond-impregnated wire.

Finally, acceptable results were obtained with water jet cutting. The notches and the circular loading holes were produced by a local shop (outside of Caltech). Clean slits were possible but the thinnest cut width that was achieved was 0.040”. Cutting slots with a diamond coated wire would be capable of improving on that, but it was not possible to find a commercial shop that would perform this service. With the aid of a simple scroll saw and commercially available diamond impregnated steel wire, it was possible to extend the notches as shown in Figure 2.4.3. Longer extensions were not possible because the wire would snap or it would simply be impossible to keep the cut straight.

2-5 THE LOADING FIXTURE

To provide stable crack propagation, a loading arrangement under displacement control was preferred over force imposition. The peculiarities of the experimental setup and the techniques that were to be used basically drove the design of the loading fixture; a photograph and a schematic are shown in Figure 2.5.1. In these images, the fixture carries one of the large specimens and is mounted in an Instron testing machine (photograph, left).

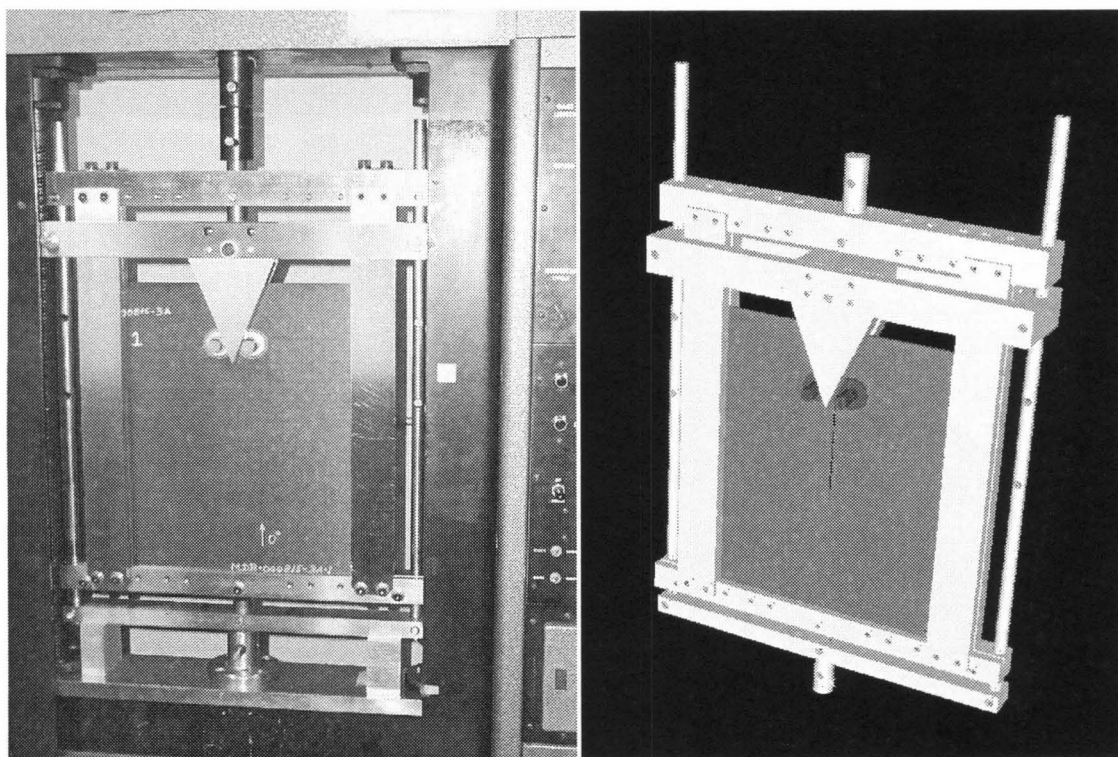


Figure 2.5.1 Loading fixture. Diagram and photograph with a large specimen mounted in an Instron testing machine.

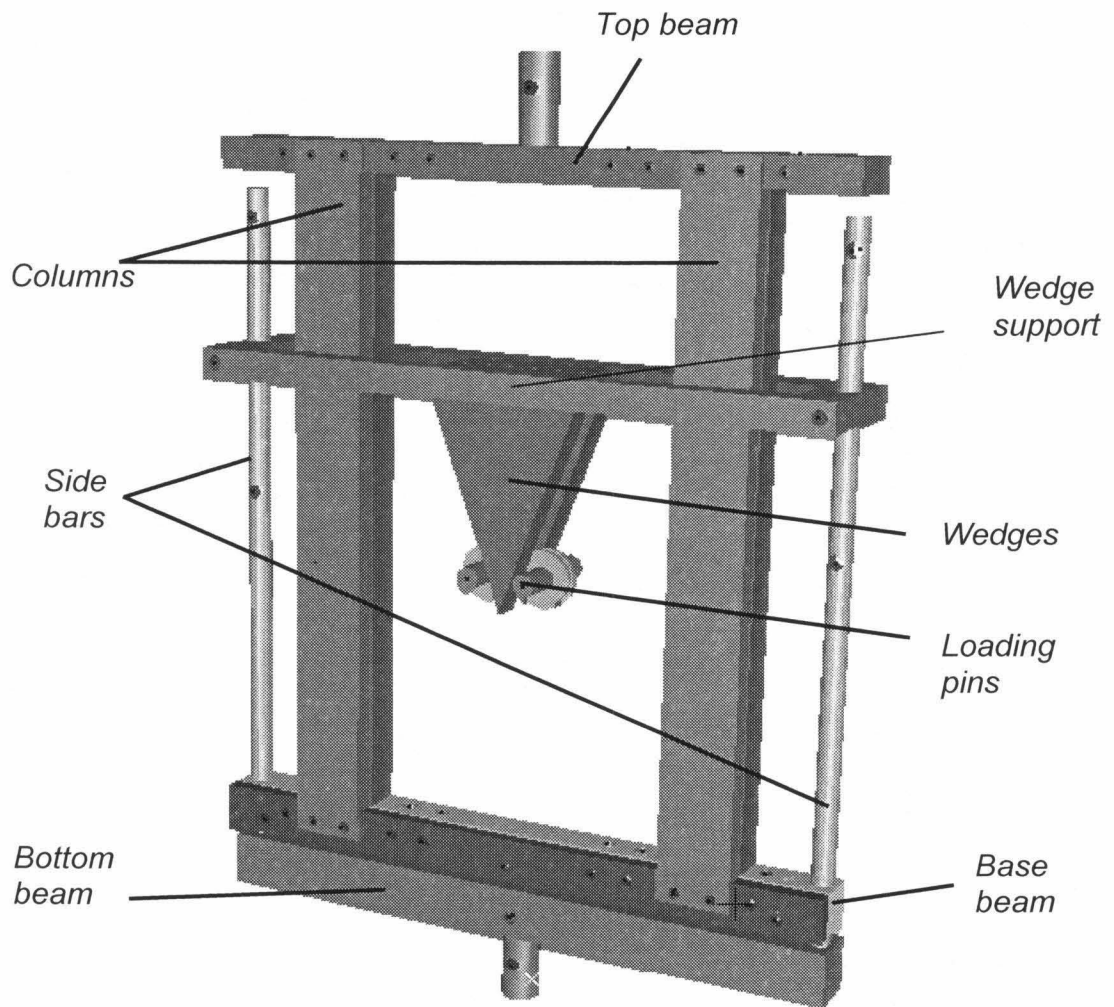


Fig. 2.5.2 Diagram of the loading fixture.

The final configuration of the fixture was determined by the following design constraints (refer to diagram 2.5.2):

- i. The crack is opened under displacement control. Therefore, a wedge and pins with needle roller bearings to minimize friction, was the simplest solution.
- ii. Previous finite element analysis calculations highlighted the probable occurrence of buckling, especially for the larger panels, as shown in Figure 2.5.3. Thus, the specimen is supported along its edges to prevent buckling or out of plane displacements. The columns (Fig. 2.5.2) have a gap where the specimen can only perform the opening motion on the plane.

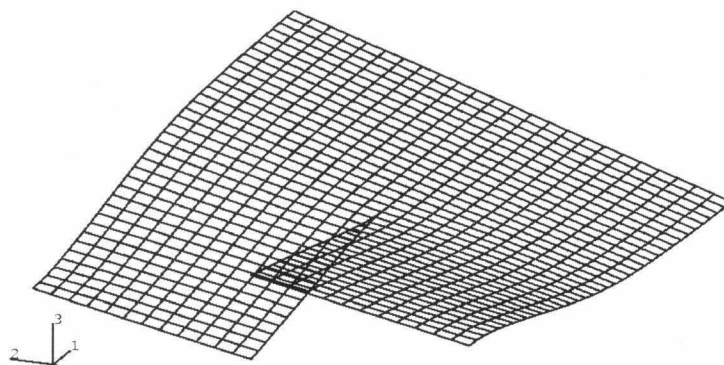


Figure 2.5.3 Finite Element simulation of Mode I crack loading indicated that the specimens would be prone to buckling and would produce out-of-plane displacements.

- iii. The crack has to be located in a vertical direction to facilitate the introduction, penetration and symmetric retention of the opaque x-ray enhancing medium –such as Diiodomethane (DIM)—into the crack. These chemicals allow the

identification of delamination and internal damage through x-ray imaging, as has already been explained in section 2-3.

- iv. The specimen should remain fixed in space during the tests, i.e., rigid body motions and rotations should be minimized or prevented to facilitate the digital image correlation (DIC) process for the determination of the deformations. This presented a challenge since typically all the testing machines (Instron, MTS) are fixed on the top and apply the load from the bottom end. This feature would have suggested driving the specimen into the wedge from the bottom up but, in that case, the DIC measurements would have been much more complicated to perform. To satisfy these two constraints, the specimen sits on a rigid frame formed by the base beam, the columns and the top beam that hangs from the top attachment of the test machine (Figures 2.5.1 and 2.5.2)
- v. The specimen is now fixed in space and the wedge has to be driven into the crack from the top down but the test machine, as has previously been mentioned, has the loading attachment at the bottom. Thus the wedges are mounted on the “wedge support” (Fig. 2.5.2), which in turn are connected by shear pins to the “side bars” that are attached to the “bottom beam,” connected to the test machine.
- vi. The anticipated loads for these tests were expected to be very high (circa 60,000 lb) and the fixture should fit in the space available in the frame of the Instron or MTS testing machines. This limitation made it necessary to use high strength steels for some parts of the loading fixture, e.g., the side bars were made of precipitation hardened 17-4 stainless steel.

vii. And finally, it was very desirable to be able to use only one loading fixture for specimens of different sizes to explore the influence of this variable in the damage process. Thus the fixture was built so that the columns and the side bars could be adjusted to accommodate the three sizes of specimens.

Originally, the first wedge design had an angle of 44° but later on was redesigned to 20° to reduce the compression component as the loads increase for the larger specimens. All small specimens were tested using the 44° -angle wedge.

Other modifications necessary in connection with the larger panels were related to the loading pins, i.e., the pins and bearings against which the wedge runs. It was necessary to harden the surface via heat treatment which, however, embrittled the pins. As a consequence, as the loads increased for the larger panels, some of the pins failed. Thus larger diameter pins were used to better distribute the loads and also to provide a larger cross-section for increased rigidity to better accommodate the bending moments. The original loading pins had a $\frac{3}{4}$ " diameter whereas the latest design called for 2.16".

RESULTS AND ANALYSIS

3-1 THEORETICAL LAMINATE MECHANICAL PROPERTIES

It is always convenient to be able to compare experimental results with well-established theory or sound numerical calculations. This allows assessing the confidence on the measurements and, in many cases, helps identify possible sources of error or other phenomena not anticipated at the beginning of an experiment and, in the end, adds to the better understanding of the problem of study.

We are interested in constructing a computer model of the panels for all the previous reasons and also in using it to evaluate the failure criteria discussed earlier and in studying the size effect. For this purpose, a first simplification that can be done is to consider the panels as monolithic, anisotropic with “average” or “effective” mechanical properties. These can be calculated from the properties of each lamina using classical lamination theory (Jones, 1999).

The mechanical material properties of each lamina, in its reference frame, were introduced in Table 2.4.1. From them the laminate properties were derived and are

summarized in Table 3.1.1. Here we recall the two types of specimens that we worked with (refer to Figure 3.1.1):

- i. **Parallel.** The crack direction coincides with the direction of the 0° ply in the diagram. As appears in Table 3.1.1, for this type of panel the largest elastic modulus is aligned with the crack.
- ii. **Perpendicular.** The crack direction coincides with the direction of the 90° ply in the diagram.

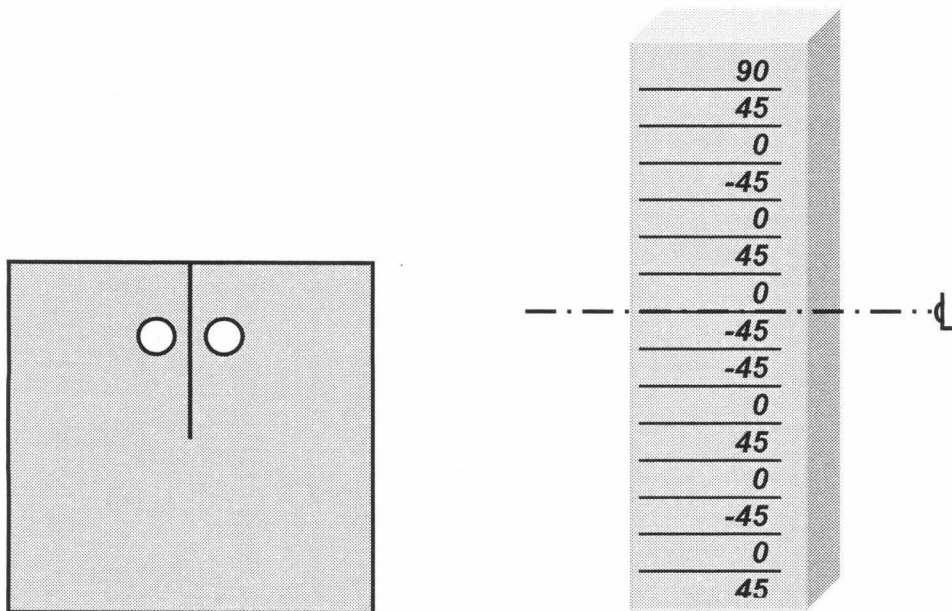


Fig. 3.1.1 Schematic of the panel configuration and the layup of the laminate. By having the crack cut at 90° to the principal direction of this layup, two distinct types of test panels are produced (identified in our experiment as Parallel and Perpendicular)

Table 3.1.1 Calculated Engineering Constants
for the Laminate (all in **msi**)

Type of Panel	E_1	E_2	ν_{12}	G_{12}
Perpendicular	5.92	10.56	0.24	3.18
Parallel	10.56	5.92	0.43	3.18

3-2 MEASURED LAMINATE MECHANICAL PROPERTIES

To verify the results of the previous section, test coupons were cut from some undamaged regions of the panels after the tests had been completed to measure the laminate average properties and also to examine any possible time dependence of the material and its influence on the measurements. It was important to assess this question, often overlooked in the research on composites, materials where close to 50% of their volume is constituted of a polymer.

E_1 , E_2 and ν_{12} were measured in our laboratories by means of the simple tension test of the coupons. Each of them was a $1 \times 10''$ strip, cut from the original panels. The stress was derived from the measurements of the load cell of the MTS machine (the same as used for the fracture tests of the panels) and the strains, both the longitudinal and the transverse ones, were measured by means of strain gages.

The measurements proceeded under displacement control. The coupons were pulled to a certain small displacement (equivalent to approximately 2% strain) and then kept at that load for 5 minutes, after which all load was released. This was performed at three different (ramp) loading rates, a fast (0.2 in/s), a slow (0.002 in/s) and a medium one (0.02 in/s), shown in Figure 3.2.1.

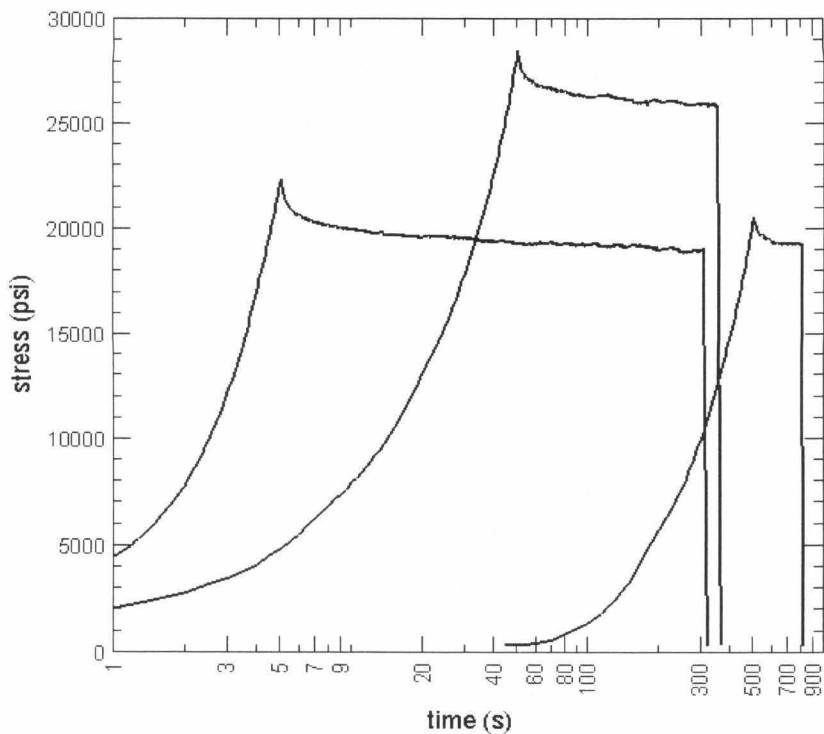
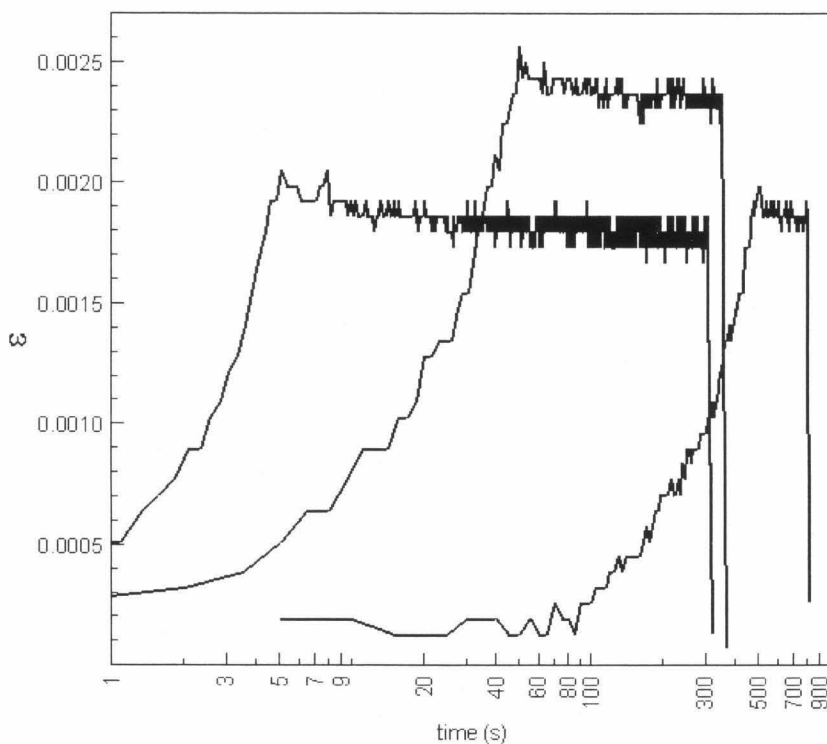


Figure 3.2.1 Stress (above) and strain vs. time curves (in semi-log scale) for tension test on coupons cut from the specimens at three (ramp) loading rates: *0.2*, *0.02*, and *0.002 in/s*.



It is clear from the graphs that there is a small drop in the stress and the strain values after the displacement stops. This drop was observed in both the strain and in the load and because it occurs in a relatively short time, the argument is close at hand that this drop is due to slippage in the grips. After that first moment the value remains fairly constant and no relaxation is apparent in this timeframe (Figure 3.2.2). For the time scale of our experiments (in the order of an hour) we can consider the material as relatively insensitive in its time dependence. More work is indicated to establish whether this assessment holds when one considers longer laboratory tests of around one hour or structures that are to be in service for years.

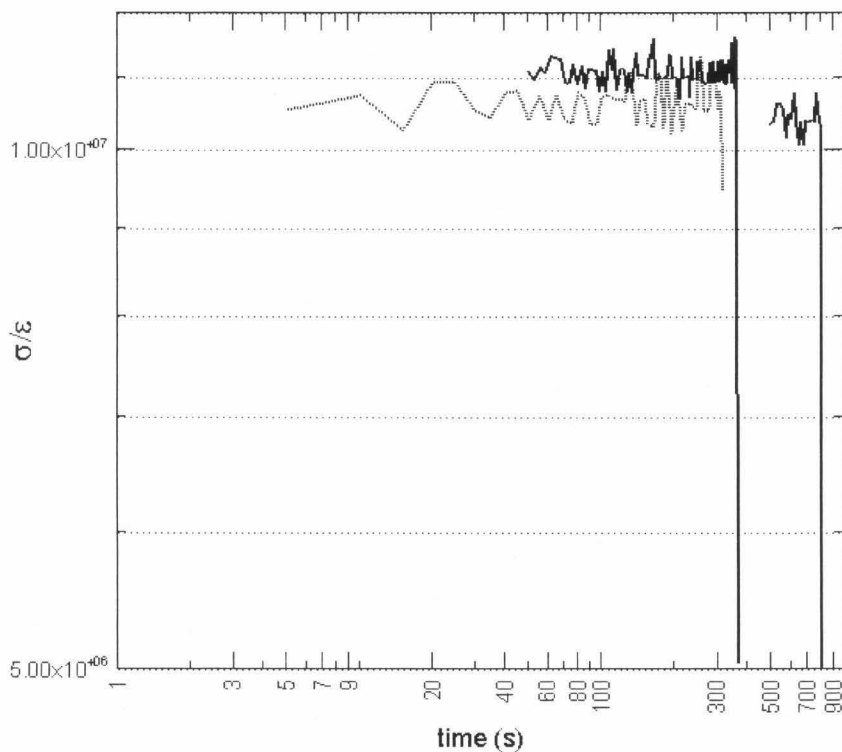


Figure 3.2.2 Log-log plot of the quotient of the results of Figures 3.2.1 for the portion of fixed displacement.

The engineering constants measured in this way are collected in Table 3.2.1. Once again, no systematic variation is observed for the different loading rates and the differences can be said to be statistical. For the remainder of this work the average properties will be used. They provide values close to those calculated in the previous section. To measure G_{12} would have been quite more complicated. Therefore, and since the other values fall very close to their calculated counterparts, we decided to use the theoretical value for this constant.

**Table 3.2.1 Measured Engineering Constants
for the Laminate (all in **msi**)**

Load rate (in/s)	E_1	E_2	ν_{12}
<i>0.2</i>	<i>11.26</i>	<i>5.48</i>	<i>0.48</i>
<i>0.02</i>	<i>11.48</i>	<i>5.81</i>	<i>0.45</i>
<i>0.002</i>	<i>11.27</i>	<i>5.76</i>	<i>0.49</i>
<i>Average values</i>	<i>11.34</i>	<i>5.68</i>	<i>0.47</i>

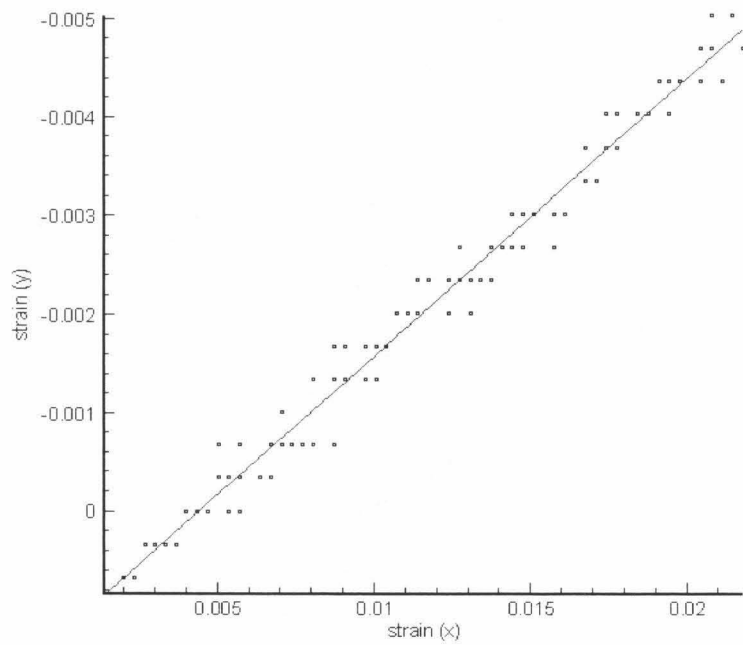
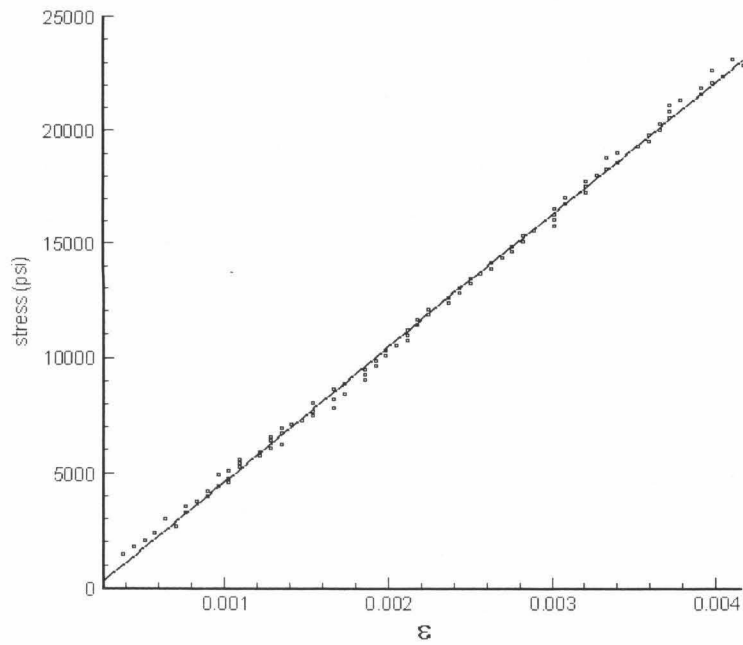


Figure 3.2.2 Measurement of the principal “effective” Young’s modulus (E_I) and the Poisson’s ratio (ν_{I2}) for the laminates.

3-3 NUMERICAL SIMULATION AND LOAD-DISPLACEMENT BEHAVIOR

The engineering constants obtained in the previous two sections were used as input for the numerical simulations with the commercially available finite element program ABAQUS. These served several purposes. They helped to

- i. “validate” the experimental results,
- ii. to determine the compliance of our loading system (MTS machine and loading fixture)—this will be explained in more detail in subsequent sections,
- iii. to obtain values of the J integral that could possibly be used as a normalizing parameter,
- iv. to assess the effect of the change of angle in the wedge of the fixture, and
- v. to determine the strains along the fiber directions* .

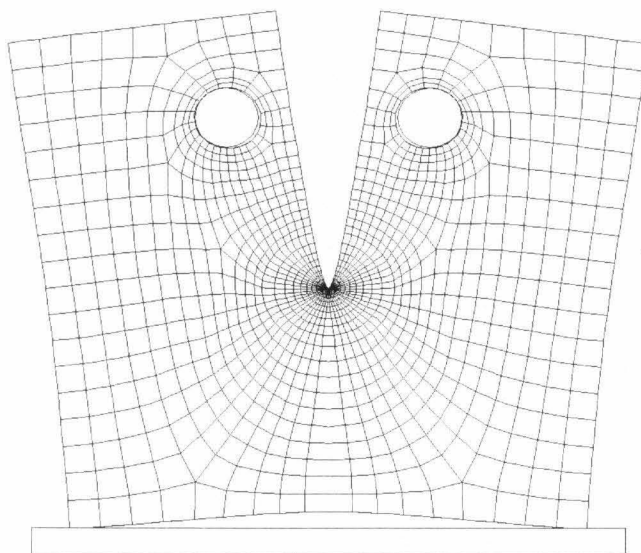


Figure 3.3.1 Schematic diagram of finite element model of one of the panels in the deformed configuration (displacements exaggerated $\sim 25\times$).

* this information can be compared to the strain fields obtained through the digital image correlation method and can also serve as input for a possible failure criterion.

The simulation utilized quadratic, reduced integration elements and included contact between the panel and the base and the loading pins, both of which were modeled as rigid analytical surfaces. Linearly elastic behavior, under plane stress conditions was prescribed. The boundary conditions imposed were zero displacement in the out-of-plane direction and concentrated loads at the reference points of the rigid pins. The concentrated loads, simulating the force produced by the wedge surfaces, had x and y components corresponding to a normal action of the wedge on the pins, i.e., $P_x = P_y \tan \theta / 2$, where P_x is the horizontal opening load and θ is the wedge angle.

The same analysis was performed on isotropic and on anisotropic panels. The load-displacement curves of the former behaved exactly as predicted by Equation 3.3.1. On the contrary, the anisotropic specimens, showed a slight size dependence which, because of its small magnitude, can be considered a second order effect. Figure 3.3.2 shows the load-displacement curves for the three sizes of panels ($6 \times 6''$, $12 \times 12''$ and $18 \times 18''$) and the two layups (parallel and perpendicular, as defined in previous sections). The load is the opening load and the displacement is the pin center displacement, i.e., both are the components in the 1 or horizontal direction in our setting.

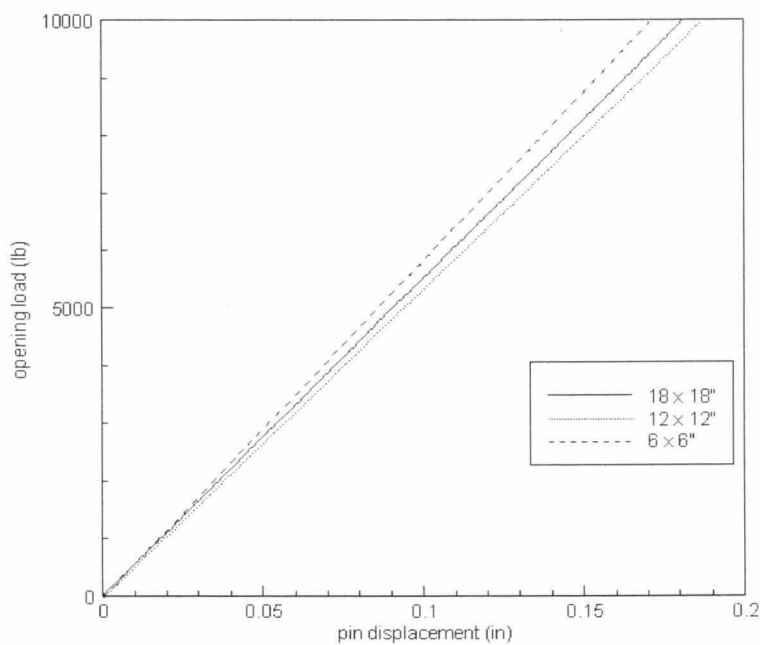
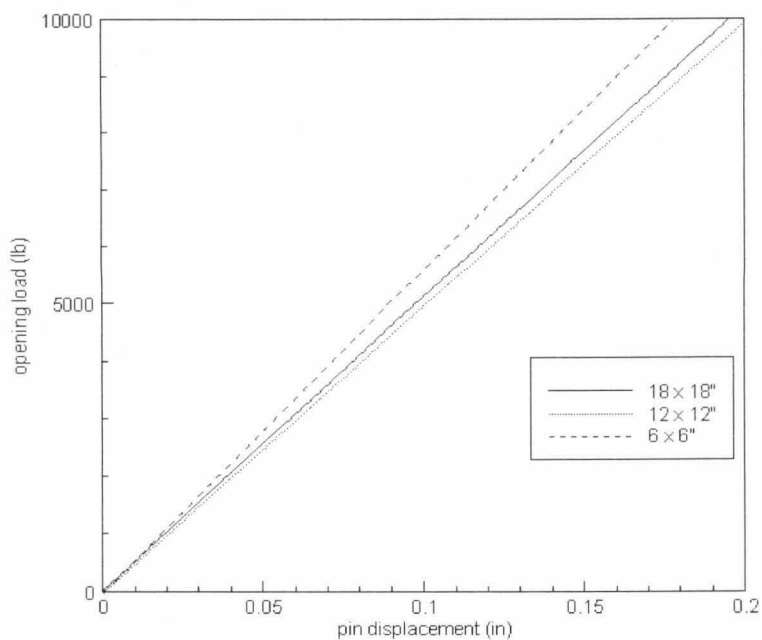


Figure 3.3.2 Load-displacement curves at the center of the pins for the three sizes of panels and for the two layups. On the top, the graph corresponds to the “perpendicular” panels (i.e., those for which E_1 is perpendicular to the crack) whereas that at the bottom refers to the “parallel” panels.

One may draw the following information from Figure 3.3.2. First, as would have been expected, the “perpendicular” panels are stiffer than the “parallel” ones. This is due to the fact the former contain three times as many layers with the fibers oriented at 90° to the crack and, in that sense, could be said to oppose the separation of the pins. Second, the lines for the different panels do not all coincide as is the case for the compact tension specimen made of a homogeneous, isotropic, linearly elastic material according to ASTM Standard E-399-72. The latter may be deduced from the equation given by Tada (Tada et al 2000):

$$\delta = \frac{P}{E'} \left(\frac{1 + a/b}{1 - a/b} \right)^2 [2.1630 + 12.219(a/b) - 20.065(a/b)^2 - 0.9925(a/b)^3 + 20.609(a/b)^4 - 9.9314(a/b)^5], \quad (3.3.1)$$

where δ is the pin displacement, P is the load opening, E' is the elastic constant (E for plane stress and $E/(1-\nu^2)$ for plane strain) and a and b are the dimensions of the panel as shown in Figure 3.3.3.

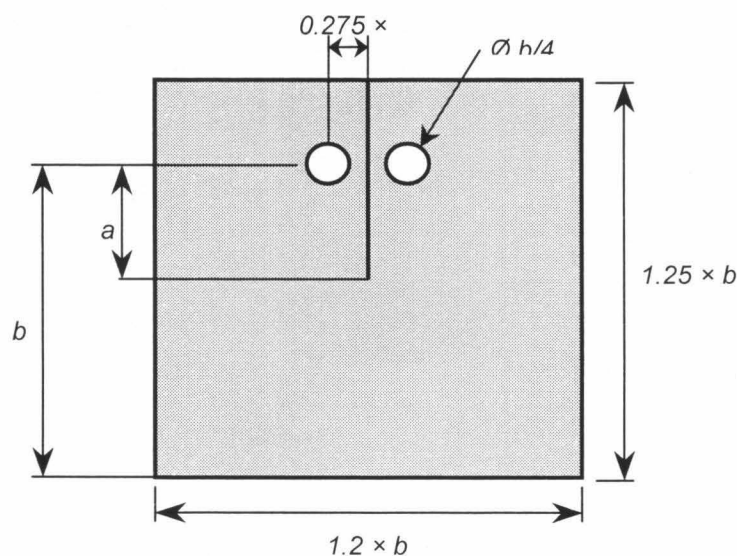


Figure 3.3.3 Standard geometry of the compact tension specimen (ASTM Standard E-399-72).

Since the ratio a/b was kept constant for all the panels in the present investigation, equation 3.3.1 then becomes,

$$\delta = \frac{C}{E'} P \quad (3.3.2)$$

i.e., the displacement is equal to the load times a constant (C/E')

As mentioned before, the size dependence is not evident to identify in the results plotted in Figures 3.3.2 since the differences are small but a trend is observed, small but clear: the stiffness decreases with the dimension of the panel. The response of the small panels presents an anomaly, which is due to the fact that the tests with those panels were conducted using the wider wedge (44°) as opposed to that used for the medium and large panels (20°). The net effect of a less shallow wedge is that the vertical force component is increased which pushes the bottom of the plate flat against the fixture, thus creating a stiffer structure. To verify this assumption, a simulation was executed for the medium/perpendicular panel but now with a 44° wedge. The results were compared to those of the previous simulations and, in effect, the new structure ended up being stiffer than for a 44° wedge angle (Figure 3.3.4). Later on it will be noted that these effects were also observed in the experiments. This justifies the use of a correction factor that would bring the two lines of Figure 3.3.4 into alignment. It was calculated and the value was found to be 1.12.

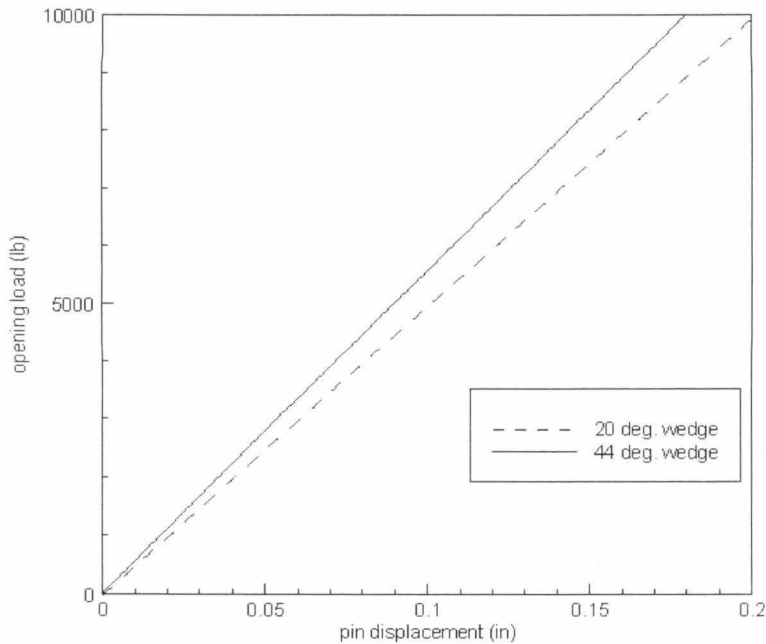


Figure 3.3.4 Load-displacement curve at the center of the pins for the medium sized “perpendicular” panel for two wedge angles. Clearly, a wider wedge renders the plate stiffer.

A very important parameter in fracture mechanics of brittle, homogeneous materials is the stress intensity factor (K_I , K_{II} , K_{III}) since it is the value that controls the stress distribution in the plate. It is a function of the loads and of the geometry of the crack and of the body. For a compact tension specimen made of an isotropic, homogeneous, linearly elastic material K_I is given by (Tada *et al.*, 2000):

$$K_I = \sigma_N \sqrt{b - a} [0.443 + 2.32(a/b) - 6.66(a/b)^2 + 7.36(a/b)^3 - 2.8(a/b)^4], \quad (3.3.3)$$

where σ_N is the far field stress. The value of K_I (or K_{II}) at the initiation of fracture is considered to be a material property.

Unfortunately, for anisotropic materials the stress distribution (in a singular stress field) is not controlled by K_I (or K_{II}) only, but also by functions of the anisotropic material properties and the orientation of the crack relative to the principal material

directions (Wu, 1967) and in some cases the opening and skew-symmetric opening modes are not uncoupled as is the case for homogeneous materials. At any rate, the calculation of these new parameters would be more complicated and commercial finite element analysis programs like ABAQUS do not possess the capability for calculating them for anisotropic materials. For that reason we resorted to the calculation of the J integral, which can be considered as a general representation of the energy release rate and can be readily evaluated with ABAQUS. It should be remembered that for an isotropic, homogeneous, linearly elastic material, the stress intensity factor and J are related by

$$J = \frac{K_I^2}{E'} \quad (3.3.4)$$

In subsequent sections the values of the J integral will be used for normalizing purposes and they will also prove useful in our effort to find a failure criterion and in the reduction of the data on the growth of the damage area.

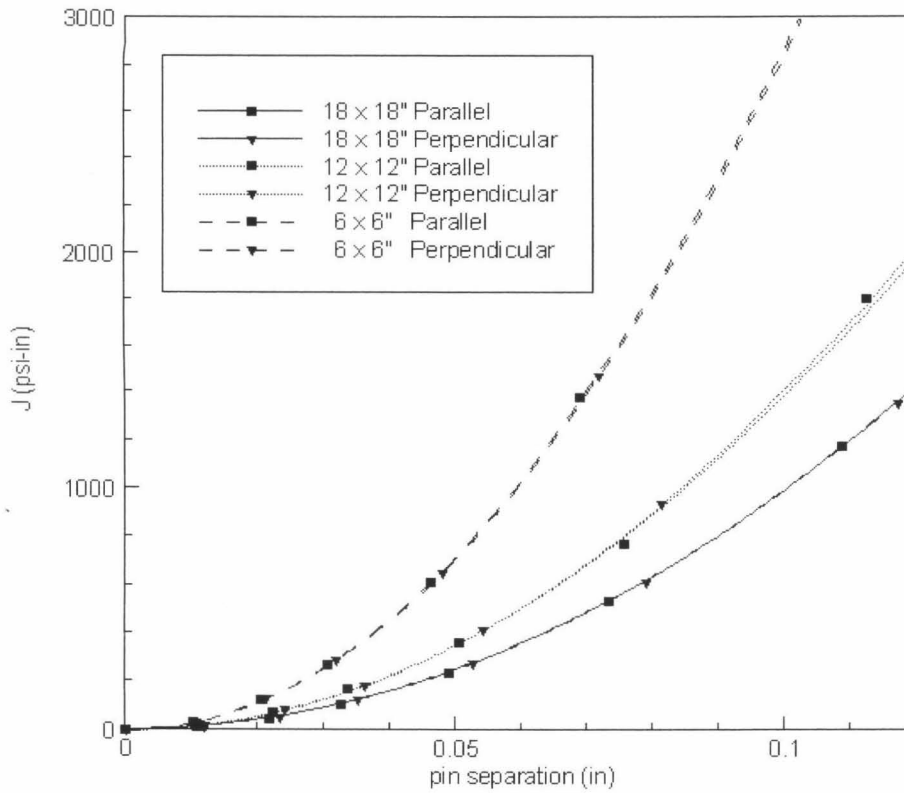


Figure 3.3.5 Numerical calculation of the J integral for the three sizes of panels and the two orientations.

In Figure 3.3.5 it can be observed that the orientation of the crack within the panels has no effect on the J integral because for each size the two curves practically coincide. As for the homogeneous case, the value of the J integral scales linearly with the size of the panels*. This fact is the basis for using J as a normalizing parameter.

* J is proportional to K_I^2 which (from Equation 3.3.3) is proportional to the square root of a linear dimension of the compact tension specimen.

3-4 EXPERIMENTAL LOAD-DISPLACEMENT CURVES

The raw measured load-displacement curves differed by a small amount from the computed ones. This was due the fact that the compliance of the loading system (the MTS machine and more importantly, the fixture) had not been taken into account in the computations. To quantify this contribution, a dummy aluminum specimen (12×12 "") was tested in the load fixture and simulated with ABAQUS; the resulting load-displacement curves were compared (Figure 3.4.1). The planar geometry was the same as that of a medium sized composite panel with the only difference being the thickness, which was chosen to provide a stiffness similar to that of the composite panels. Some iterative finite element simulations were performed to find that thickness, which turned out to be a convenient value (0.125") because in that way a standard aluminum plate could be used and no costly extra machining was needed.

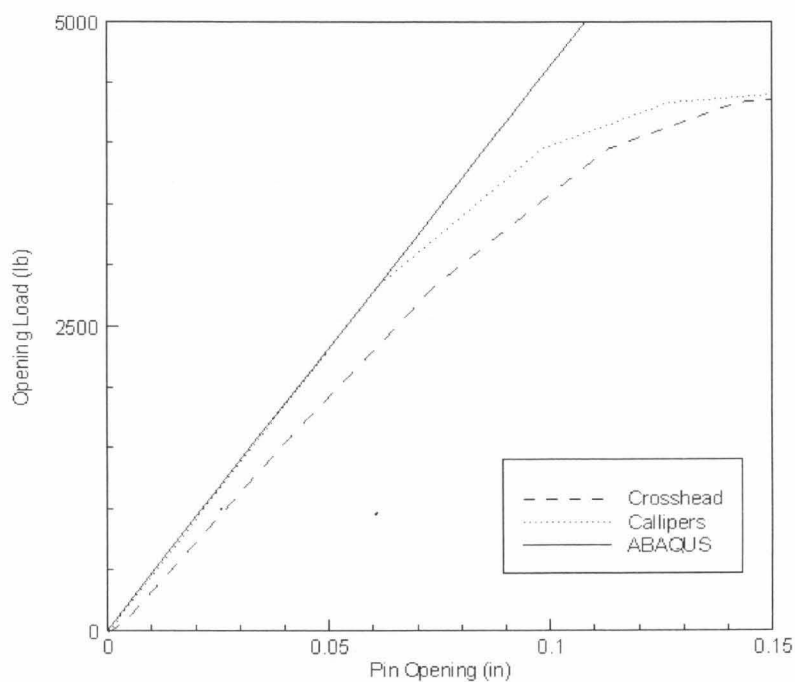


Figure 3.4.1 Load-disp Pin displacement (in) uminum dummy
specimen to measure compnuance or loading system and calibrate
displacement measurements.

Figure 3.4.1 shows the computed curve along with two others. One of the latter corresponds to the pin opening measured directly with calipers on the deforming specimen. The other one represents the pin opening calculated from the crosshead displacement of the MTS machine, which was the primary method employed to obtain the load-displacement curves for all the tests. It can be seen that there is a nearly perfect agreement between the computation and the caliper measurements up to the point where damage appears after which the linear elastic assumption is no longer valid. It can also be observed that the two experimental curves (caliper measurements vs. crosshead motion) differ by a constant, multiplicative factor of 1.2. Once this factor was applied to the experimental data, good agreement was achieved with the numerical curves up to the point where the material starts to degrade; this can be seen in the following graphs. In them, the experimental results appear together with the finite element analysis curves.

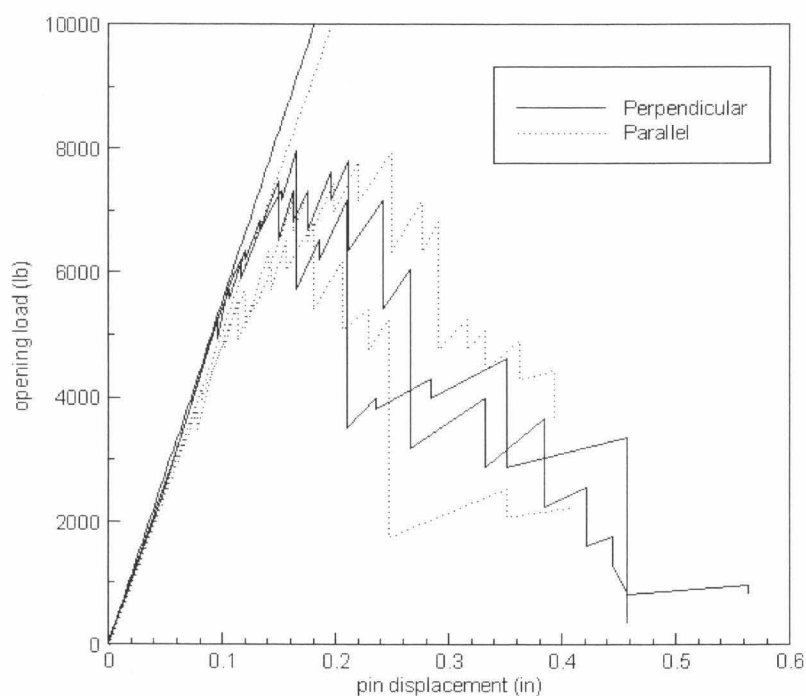


Figure 3.4.2 Load-displacement curves for the Large panels (experimental). The straight lines represent the numerical analysis of the unbroken specimens.

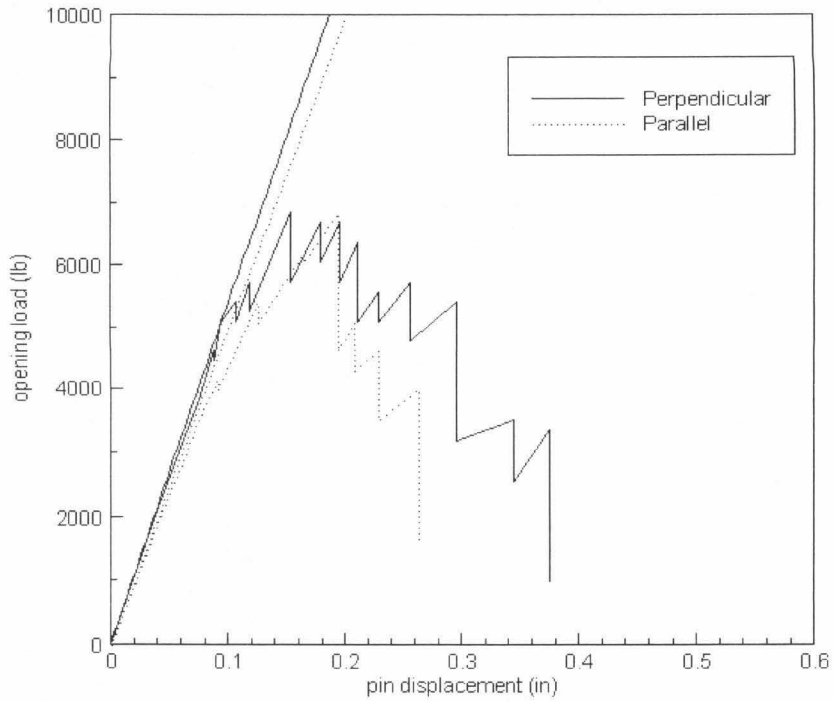


Figure 3.4.3 Load-displacement curves for the Medium panels (experimental). The straight lines represent the numerical analysis of the unbroken specimens.

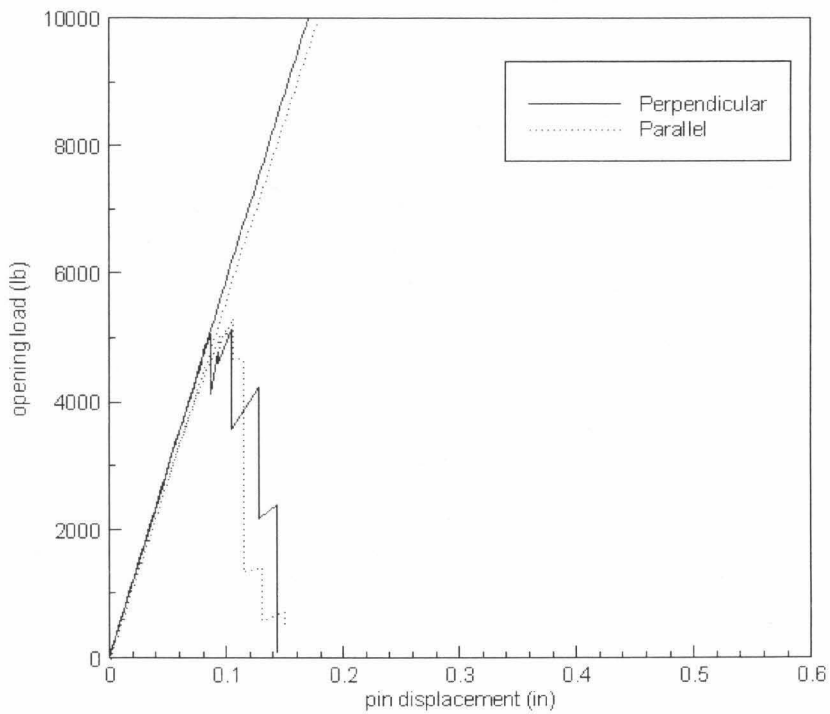


Figure 3.4.4 Load-displacement curves for the Small (experimental). The straight lines represent the numerical analysis of the unbroken specimens.

Figures 3.4.2, 3.4.3 and 3.4.4 suggest there is a scaling parameter that links the three graphs and it turns out to be the square root of the panel length. The large panels are 1.5 times as big as the medium ones, which in turn are twice as big as the small ones. Scaling—both the load and the displacement—for the three sizes of panels with respect to the medium-sized ones (dividing the load and the displacement values of the large panels by the square root of 1.5 and multiplying the small ones times square root of 2) the data can be reduced as in Figure 3.4.3 (here only the experimental data is displayed and not the calculations). It is surprising how well the data scales with size, even in the damage region where one would not expect as much, due to the statistical nature of the failure process.

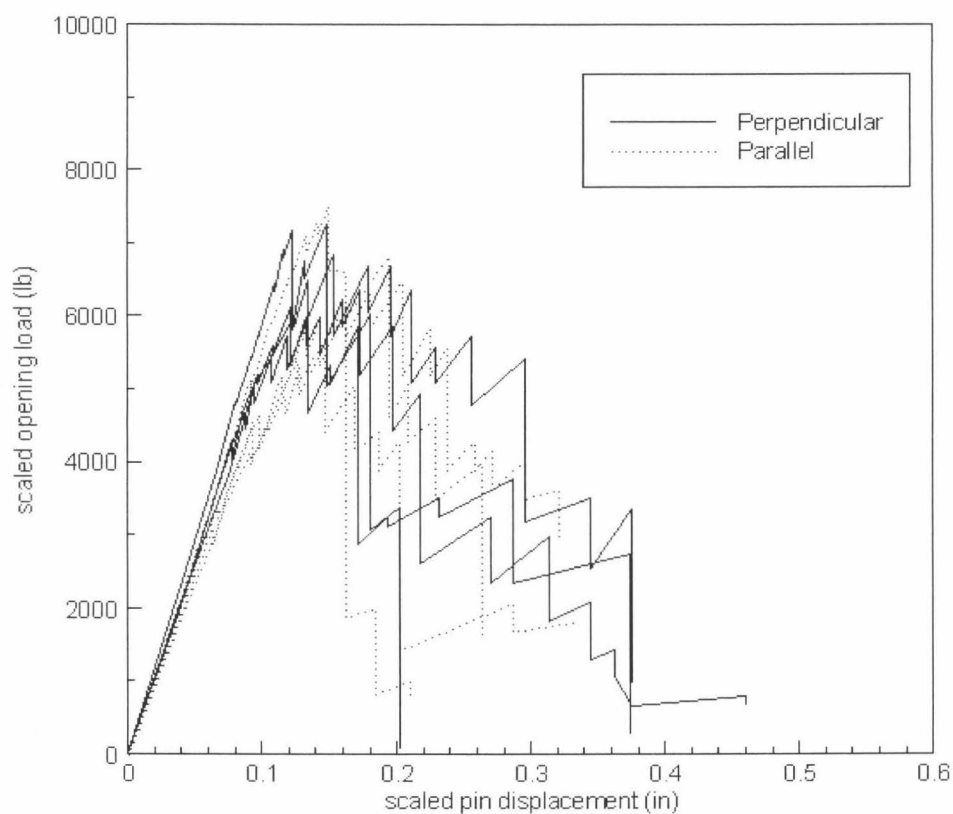


Figure 3.4.3 Reduction of data presented in Figs. 3.4.2. P and δ were multiplied times $2^{1/2}$ and divided by $1.5^{1/2}$ (the size scale parameters) for the Small and Large panels, respectively.

3-5 DAMAGE INITIATION

Throughout the experiment it was observed that damage always started in the inner layers of the cracked plate as lamina cracks extending along the fiber respective directions, with no sign being apparent on the exterior. This is significant because it indicates that for these two layups at least, the delamination was a consequence of the redistribution of stresses after some in-plane failure of one or several laminae occurred—at least in the first instance. There is no indication that failure was locally connected to out-of-plane stresses which are important within a boundary layer on the order of the laminate thickness. Thus it turns out that edge effect correction was not needed here because clearly the in-plane transverse and shear stresses dominate the failure initiation. The other reason why this first statement is very important is because it has become a common practice to rely on visual inspections of composite material components and, as it will be shown, at least in the presence of cutouts, there can exist some significant damage while the exterior looks intact (Figure 3.5.1)

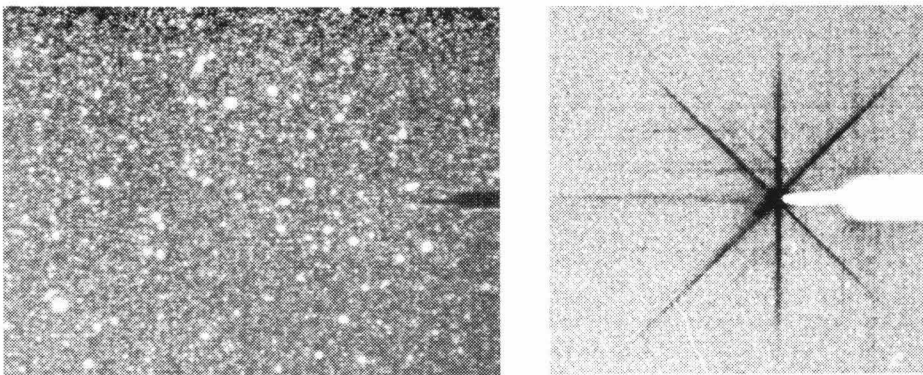


Figure 3.5.1 The image on the left shows the surface of the material with the splatter pattern used for the digital image correlation. No damage is apparent on the outside but the x-ray image of the crack tip shows that some lamina cracks have developed (the dark regions).

Figure 3.5.1 is typical of the damage initiation for the Perpendicular panels. In all the tests of this type of specimens, be it for the Small, Medium or Large ones, the first damage to appear had always this star shape: cracks extending along the direction of the fibers in the different layers with neither any apparent delamination nor fiber breakage. Delamination and fiber breakage would come later in the loading cycle, once the stress distribution had been affected by this early damage. A similar failure initiation pattern was observed for the Parallel panels with the exception that there was no damage along the $\pm 45^\circ$ on the crack side (Figure 3.5.2) which could be explained by the fact that the panel is more compliant in that orientation relative to the crack. This aspect will be explored in more depth when we analyze the differences in the strain distributions for the two panels.

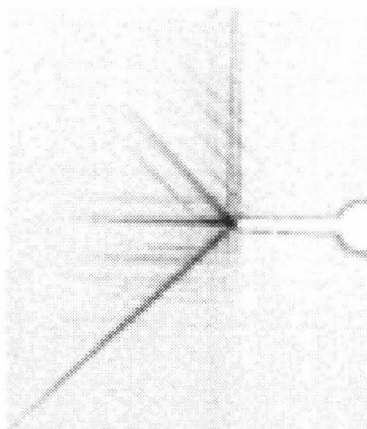
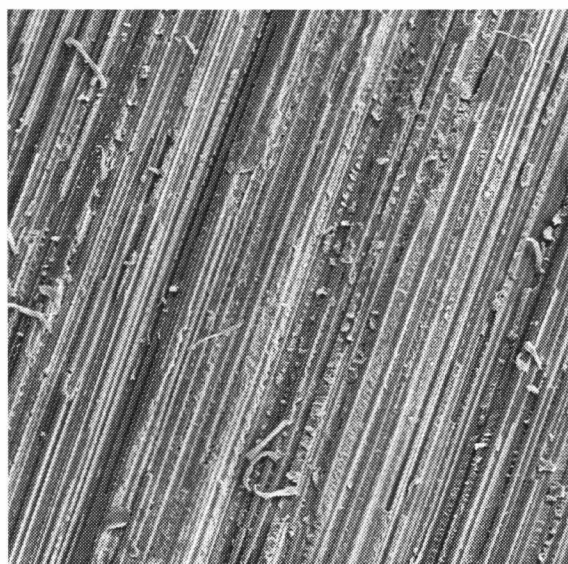


Figure 3.5.2 Initiation of damage in the Parallel panels. Notice that there are no cracks running along the $\pm 45^\circ$ directions on the notch side. This was observed in all the tests of this panel type.

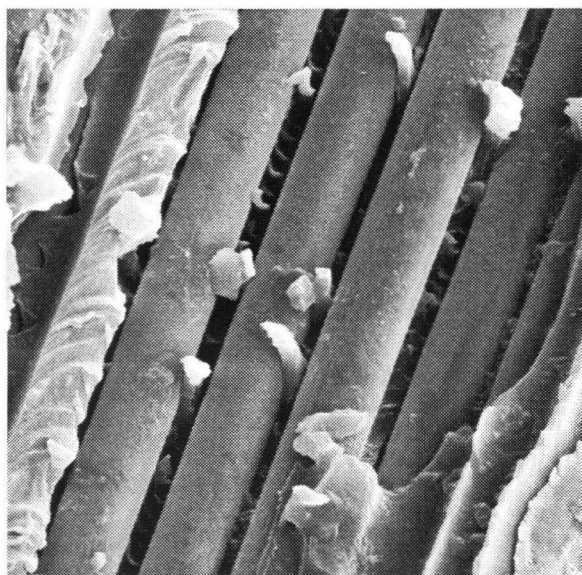
Thus, the damage always started as cracks propagating in the matrix following the fiber directions. More work is needed to determine whether what fails is the matrix or the fiber-matrix bond, something which was beyond the scope of this study. Only a limited exploration of this issue is provided through the following SEM images. They all

proceed from a layer that peeled off by delamination, but it is possible that the mechanism is the same as that which extends the lamina cracks in the interior of the material; after all, the weakest link is that which fails first and the objective is to determine whether separation occurs through the matrix or at the fiber-matrix interface. Only delaminated material was available for examining this issue because the specimens could not be disconnected from the MTS for SEM dissection; there was insufficient material to conduct the experiment in this manner. Figure 3.5.4 shows a detail at a higher magnification. The fibers appear very clearly, almost as if the matrix material had been cleaned off or removed.



100 μ m 250X

Figure 3.5.3 SEM photograph of a layer that peeled off the panel after delamination. It would appear that the material failed at the interface between the fibers and the matrix.

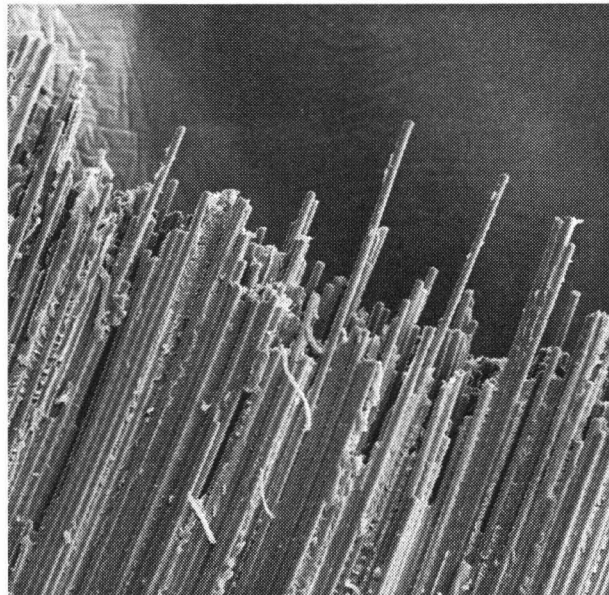


8 μ m 3000X

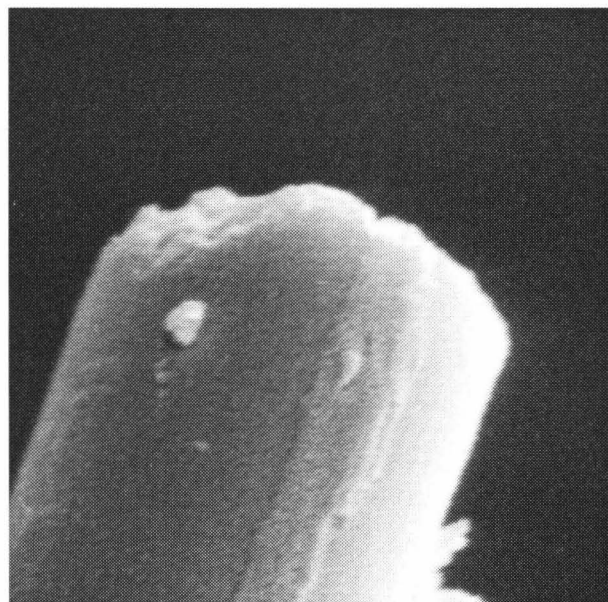
Fig 3.5.4 Detail of delaminated region. Notice how, at least in this region, the fibers are almost stripped of all matrix material.

Since the objective of this study was concerned with the more global rather than micromechanics aspects, this line of detailed investigation was not pursued further. The dominant fact remains that failure starts in the laminae, parallel to the fibers. To assess whether the initial “star-shaped” fracture could be estimated from an intra-lamina strain distribution recourse was taken to the analytical (numerical) evaluation for the strain field in the crack tip region. The specific question raised is then as to whether the strain(s) in the $\pm 45^\circ$, 0° and 90° layers reached critical (combinations of) strains some distance from the common crack tip. Presumably cracking would occur at least between such a location and the common crack tip. In this way a measure of (initial) damage extent might be established. The strain components that appear to be relevant for this problem are the shear and the transverse (in the fiber frame of reference for each ply); the extensional strain would play an important role only if fiber cracking was observed or fiber microbuckling (for the compression case) but neither phenomenon was observed

in the tests. Once again, fiber cracking –and microbuckling for the delamination, most likely—appear later in the failure process, following this initial damage evolution. When the fibers do crack they do it in a brittle fashion as illustrated in Figure 3.5.5.



80 μ m 300X



1 μ m 15000X

Figure 3.5.5 SEM photograph of the edge of a ply that delaminated and where fiber breakage occurred. It is clear that fibers break in brittle fashion. Also, some fiber pull out is evident.

To understand the difference in the behavior of failure initiation between the two layups let us thus turn our attention to the strain profiles around the crack tip, calculated numerically.

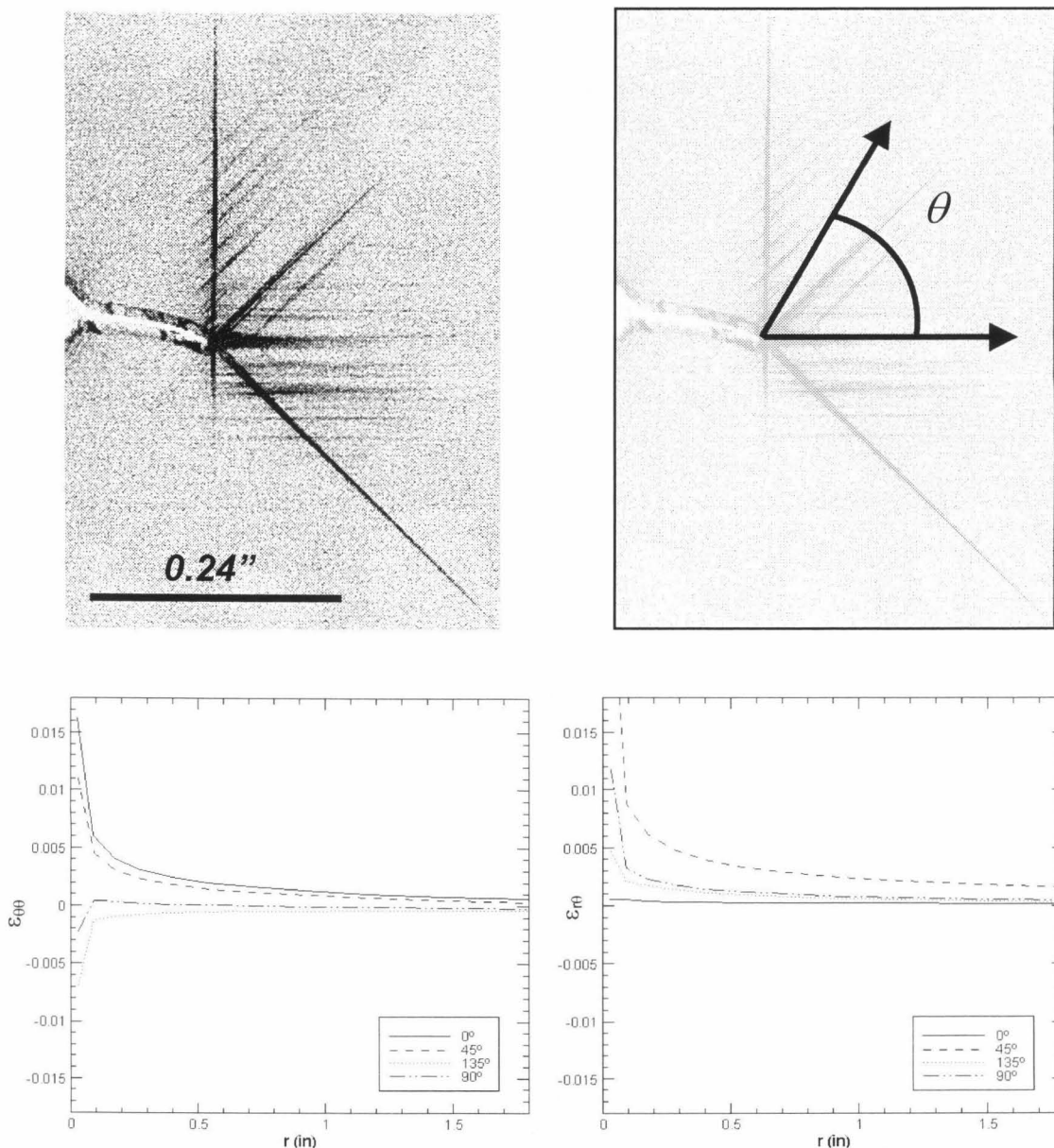


Figure 3.5.6 Analysis for a Large Parallel panel with an opening load of 3,502 lb. On the top, an x-ray image of the internal damage. The bottom graphs show the numerically calculated strain distribution in the different layers. On the left, the transverse strain ($\epsilon_{\theta\theta}$) distribution as a function of distance from the crack tip. To the right, the shear ($\epsilon_{r\theta}$). The values plotted are those at the integration points (4) collapsed to the center of each element.

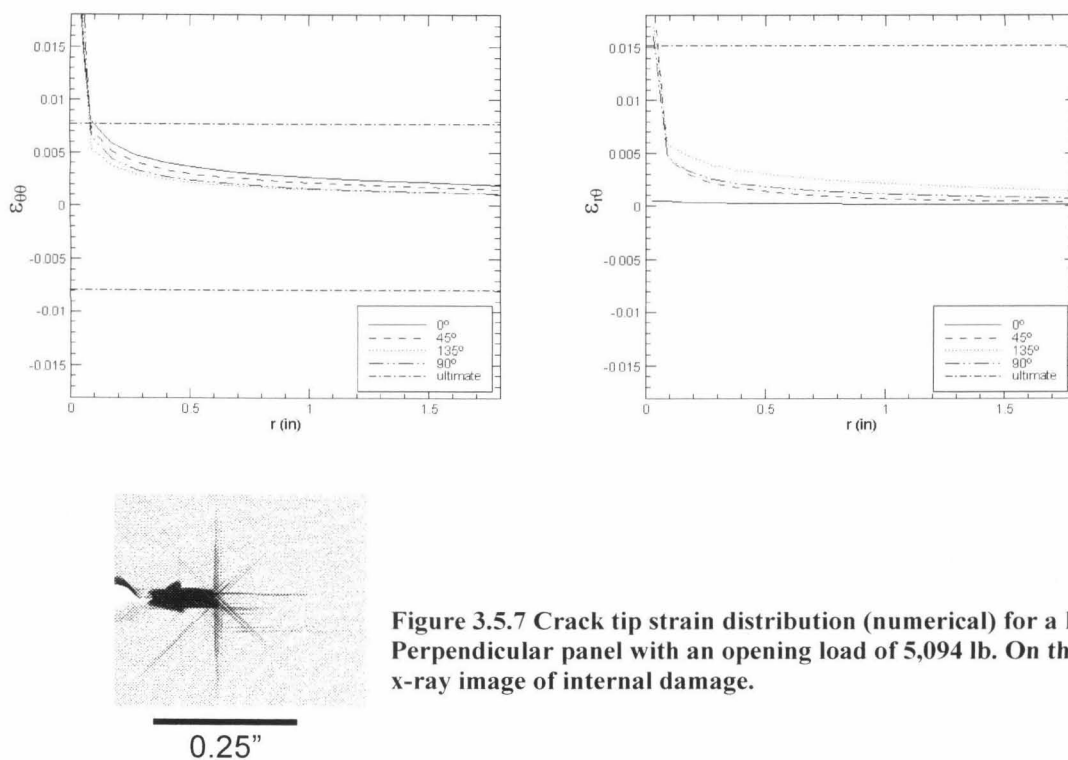


Figure 3.5.7 Crack tip strain distribution (numerical) for a Large Perpendicular panel with an opening load of 5,094 lb. On the left, x-ray image of internal damage.

From these plots it is now evident why the Parallel panels do not show cracks along the $\pm 135^\circ$ rays. For the Parallel panels, the strain there is compressive, whereas for the Perpendicular panels, it is tensile, which, coupled with the shear strain (of the same order of magnitude) produces the failure. The ultimate strain values of the material, for a unidirectional lamina, are also plotted on the previous graphs and it can be observed, in accordance with what has already been mentioned a few pages before, that the cracks on the x-ray images are longer than what a maximum strain criterion would have predicted (i.e., that the material would have failed when any of the strain components would have reached the measured ultimate strains). Thus it is a simple application of a maximum strain criterion for laminates is inadequate, and it is clear that a more elaborate failure criterion is needed.

A criterion that incorporates the coupling of different components of strain is the Tsai-Hill criterion, presented in the previous chapter. This criterion is widely popular and has been utilized as the basis of computational efforts to model the damage progression in composites. It was originally formulated in terms of stress, and, its strain counterpart is

$$\frac{\varepsilon_1^2}{\varepsilon_{1u}^2} + \frac{\varepsilon_2^2}{\varepsilon_{2u}^2} + \frac{\varepsilon_{12}^2}{\varepsilon_{12u}^2} - \frac{\varepsilon_1 \varepsilon_2}{\varepsilon_{1u}^2 (E_1 / E_2)} = 1 \quad (3.5.1)$$

This is a criterion that has the same general form of von Mises' yield criterion but the physical basis to applying it to composite materials is somewhat elusive. It is immediately obvious from our experiments that this criterion includes some terms that do not appear to have any effect on the cross-ply failure process, namely, the extensional contribution in the 1 direction. ε_{22} and ε_{12} can interact—and our calculations show that they do interact—to extend the cracks but there is no reason to believe that ε_{11} would play any significant role, except in the case of fiber damage (breakage or microbuckling –if in compression), which did not occur in any of these tests. Therefore the criterion—any criterion—cannot be applied without first reflecting on the nature of the strains in the structure.

The application of the Tsai-Hill criterion to the strain fields around the laminate crack tip should predict the length of the new cracks emanating from it. Figure 3.5.8 shows the evaluation of the Equation (3.5.1) along the fiber direction for the four ply orientations of the laminates. Figure 3.5.9 shows a comparison of the “predicted” values with the measured ones from the x-ray examination. It is clear that the Tsai-Hill criterion underestimates the extension of the new ply cracks by a factor of 3 to 4. The values are compiled in Table 3.5.1.

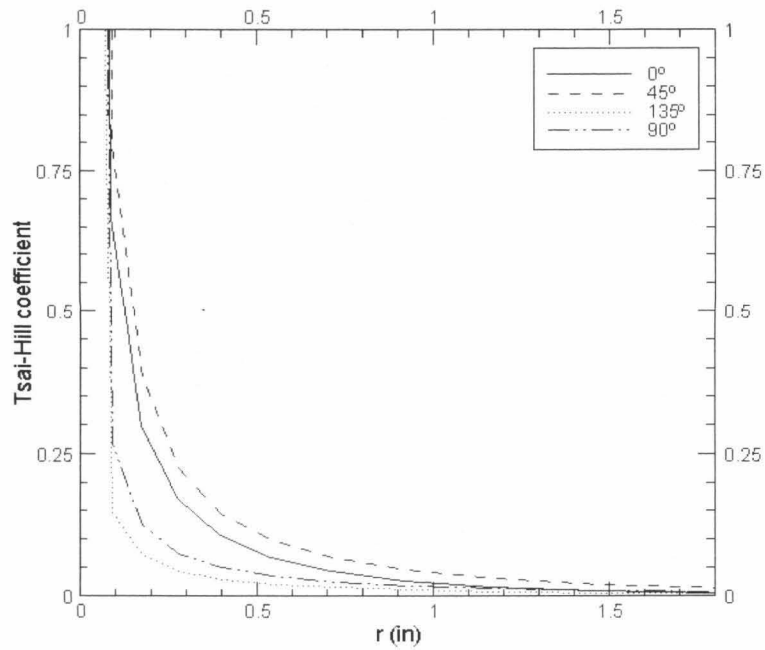


Fig. 3.5.8 Numerical calculation of Tsai-Hill's equation (Eq. 3.5.1) for a Medium Parallel unbroken panel.

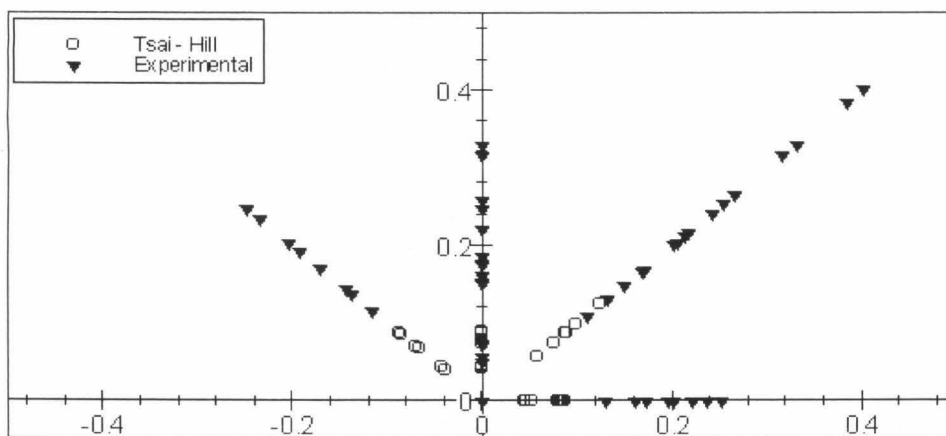


Fig. 3.5.9 Comparison between the crack lengths predicted by the Tsai-Hill criterion and the actual experimental measurements, along the 0, 45, 90 and 135° directions.

Table 3.5.1 Comparison between the crack lengths predicted by the Tsai-Hill criterion and the actual experimental measurements, along the 0, 45, 90 and 135° directions.

	Tsai-Hill				Measured			
	0°	45°	90°	135°	0°	45°	90°	135°
Large Parallel	0.078	0.087	0.075	0.067	0.200	0.383	0.33	0.000
Large Perpendicular	0.083	0.088	0.087	0.086	0.160	0.131	0.162	0.193
Medium Parallel	0.078	0.087	0.075	0.067	0.130	0.315	0.260	0.000
Medium Perpendicular	0.086	0.124	0.089	0.088	0.235	0.265	0.177	0.249
Small Parallel	0.051	0.075	0.042	0.039	0.196	0.401	0.212	0.000
Small Perpendicular	0.044	0.058	0.044	0.044	0.220	0.170	0.187	0.204

Alternatively, one can measure the length of the first damage/ply crack to appear in the x-ray images and assume that those ply cracks were originated because at some point along their length, the ultimate properties of the material were exceeded. That produced a precursor crack that changes the original strain distribution and thus produces further damage. The values of the strains $\varepsilon_{\theta\theta}$ and $\varepsilon_{r\theta}$ in an unbroken panel, calculated numerically, at the locations of the new ply crack tips can be compared to the ultimate values for the lamina and some limits can be deduced. The following figures present that information; first, for the whole set of panels (both layups and the three sizes), and then one plot for each layup.

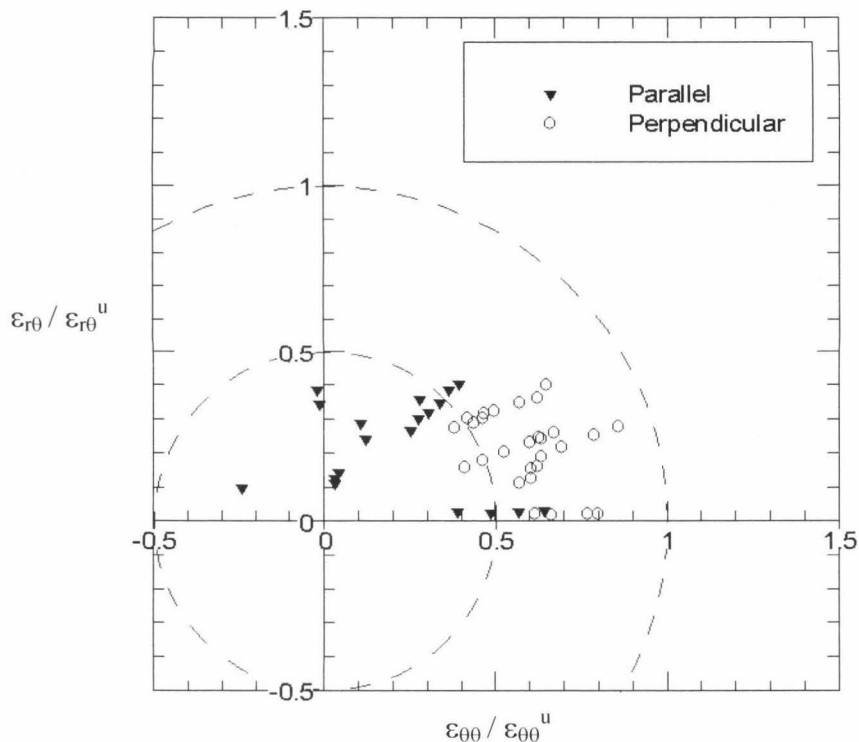


Figure 3.5.10 Normalized failure plot of strains—calculated numerically for unbroken panels—at lengths equivalent to the ply cracks measured from the x-ray images (using the ultimate values for $\varepsilon_{\theta\theta}$ and $\varepsilon_{r\theta}$) for all the panels: three sizes and two layouts.

Several interesting results are contained in Figure 3.5.10. The strains at the locations of the new crack tips are smaller than the expected values of $\varepsilon_{\theta\theta}^u$ and $\varepsilon_{r\theta}^u$. An explanation is that somewhere between those points and the global crack tip the material limits are exceeded and ply cracks are formed. Once this happens, the whole strain distribution is changed and the values are raised because of the new crack tips, producing new asymptotic fields around them. These, in turn, produce strains that exceed the material limits and, in that way, the length of the measured lamina cracks is reached. Of course that one also deals with possible pre-existent flaws and with the constraining effect of the adjacent—and normally unbroken—layers. This last fact can explain the

difference in behavior between the Parallel and the Perpendicular panels, evident in Fig. 3.5.11. We note also that no systematic influence of the panel size is evident.

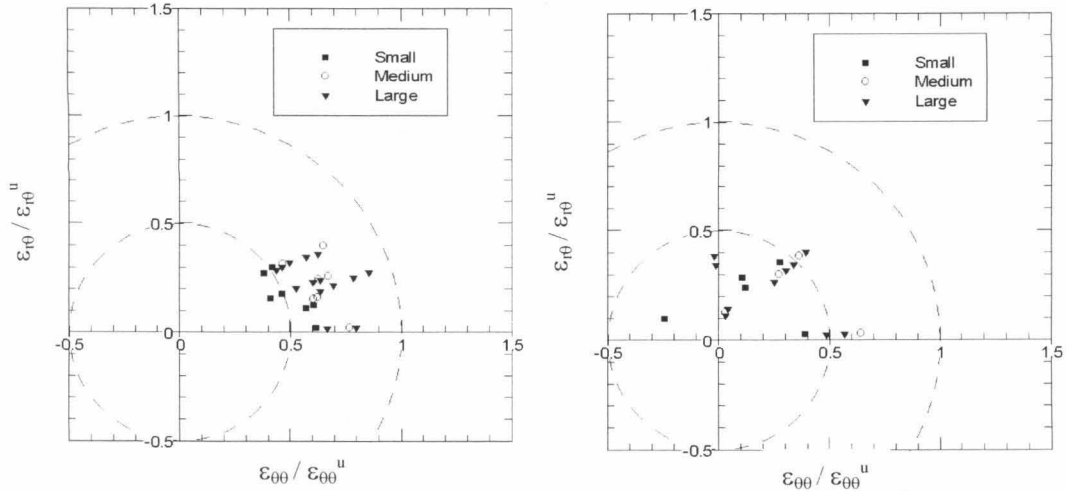


Figure 3.5.11 Normalized plots of strains at ply failure for Perpendicular panels (left) and Parallel panels (right).

Therefore, a conclusion resulting from this examination of initial crack size is that a simplistic application of the Tsai-Hill or equivalent criteria to the strain fields calculated on an unbroken panel will predict cracks 3 to 4 times shorter than what experiments show. This points out the uncertainty existing on failure initiation determination. On the other hand, these first ply cracks propagate but not catastrophically. In fact, they stop and much of the load bearing capacity of the panel remains intact. For all the tests, the load level at which these first cracks were formed was $55.48 \pm 9.45\%$. It is true that the spread is large but one should not forget that failure is statistical in nature and, second, our sample was very limited. Appendix A contains the complete collection of the numerically calculated strain distributions for each of the test panels together with the corresponding x-ray image.

3-6 DAMAGE PROGRESSION

In the previous section, the initiation of crack propagation was addressed. It was recognized that on all occasions these cracks started propagating within their respective laminae, along the direction of the fibers of that ply. As this happens, the states of stress and strain in the panel become complicated as interlaminar shear stresses change and new damage is introduced. Much of that new damage may be in the form of delamination, fiber breakage and intralaminar damage in the same fashion as the initial cracks or a

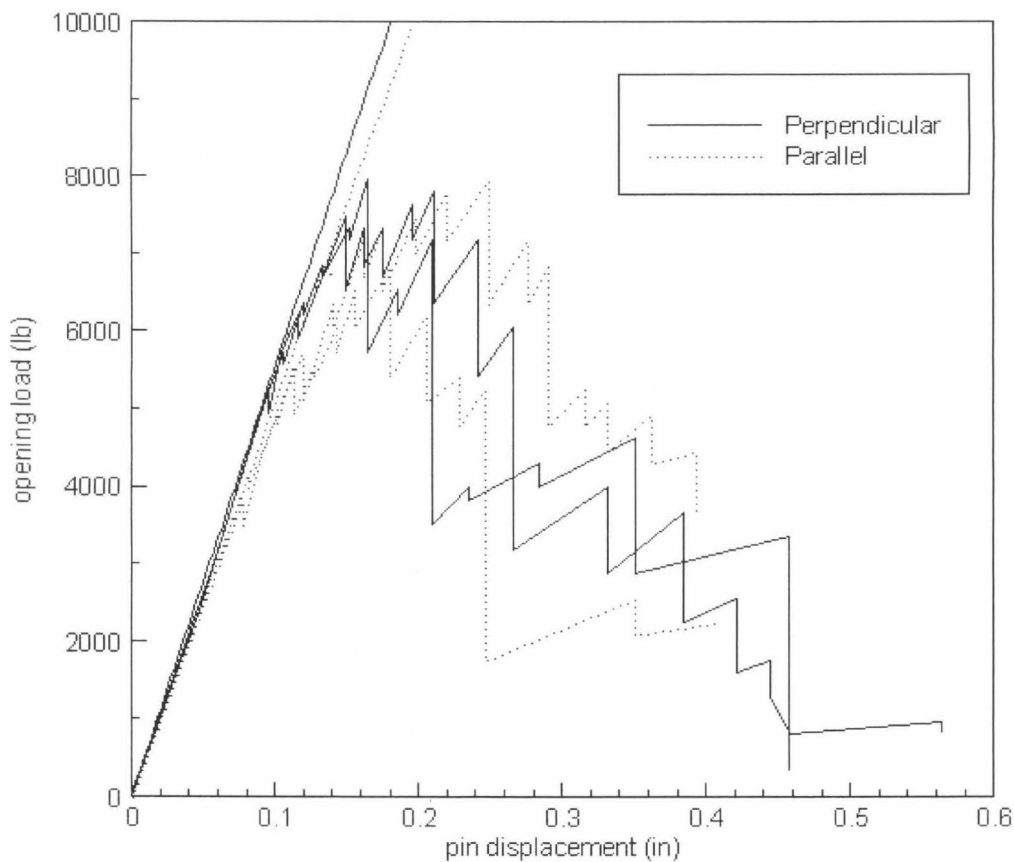


Figure 3.6.1 Opening load vs. pin displacement for four different tests on Large panels (18" × 18"). The straight lines represent the computed panel responses.

combination of all these modes. The process of failure thus continues until no load bearing capacity is left in the structure. Our tests were designed to prevent unstable crack

propagation (performed under displacement control), but from the load displacement curves one can identify certain salient features that assist in understanding the damage propagation process. For illustration purposes we use the P - δ curve for the four large panels (Figure 3.6.1) which represents also the response of the other two panel sizes.

First, the relation is linear up to the appearance of the first damage. In the last section it was found that this first damage occurred close to 50% of the peak load. The peak load is another characteristic to be noted and this maximum load does not occur immediately before the largest drop in load. This significant load drop should correspond to the largest growth of damage, including delamination and additional intralaminar cracks. Thus, in terms of the load-displacement curves the failure process can be described as follows:

- i) The opening load and pin displacement increase linearly up to a certain threshold (approx $0.5P_{max}$) when the first damage appears and the load drops slightly (3.74 ± 2.53 % for all the tests).
- ii) After this initial damage, and accompanied by similarly discrete damage accumulations, the load increases until the peak load, which is immediately followed by a drop in load larger than the previous ones (13.53 ± 6.95 % for all the tests). It is important to note that, in general, this critical point did not correspond to the maximum single load drop reached in the test. We conjecture that under load control unstable crack propagation would follow.
- iii) After the first major drop in the load, and with further separation of the pins, the load also increases incrementally, accompanied by minor drops corresponding to further small scale failure (some matrix cracking, small

delamination, etc.). This process continues until a critical point is reached which, in general, is followed by another major drop in the load measurement (22.31 ± 7.33 % for all tests). This drop is not the largest in magnitude observed throughout the test; as it proceeds the load builds up again but never reaches the maximum again, though larger or more extensive failures take place as evidenced by pronounced load drops until the panel has lost its load bearing capability.

Runaway Delamination

We turn next to the analysis of the physical process that produces the behavior described above. Under superficial examination, the two layups exhibit noticeably different responses. This results from the orientation of the surface layers relative to the crack. For the Perpendicular panels, the outer layer runs parallel to crack and the opposite is the case for the Parallel ones. One first notes that in the Parallel panels the outer layer develops delaminations that reach the panel's edge, regardless of its size. Thus, whole strips would peel off from the Small, Medium or Large panels (Figure 3.6.2). As the test proceeded, more "strips" of the outer layers were shed off. One possible mechanism influencing the response of these layers is their buckling propensity under the generally compressive strains in the regions to either side of the crack ligament of the layer. Being this layer on a stress free surface, it is less constrained against out-of-plane displacement as the interior plies.

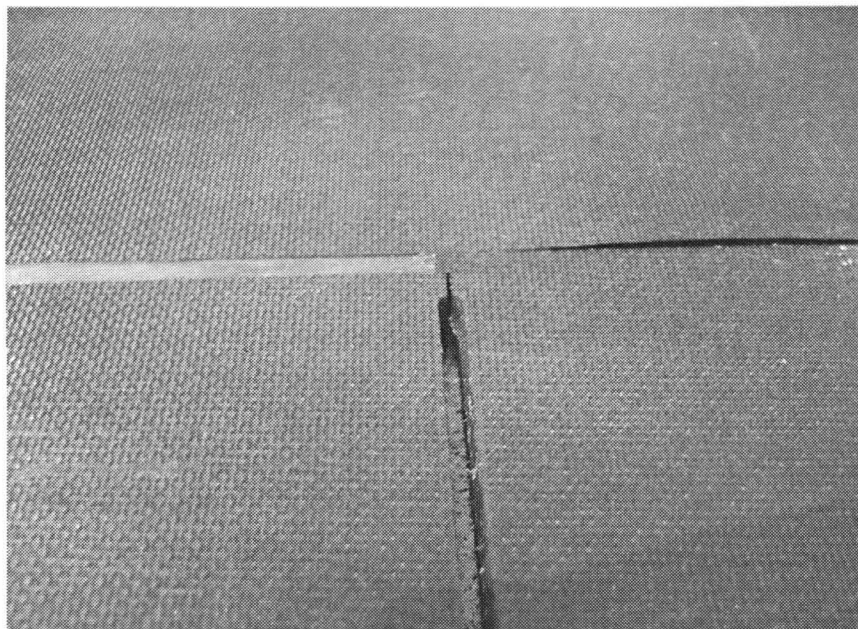


Figure 3.6.2 Delamination in one of the Parallel panels; to the left the strip has completely dropped off, while on the right of the crack tip the layer has not yet detached completely.

This “runaway” delamination of the outer layer is not observed in the case of the Perpendicular panels and would occur repeatedly as the global crack grew. By the end of the test, the specimen would look like the two samples shown in Figure 3.6.3. As the global crack advances, it carries a stress distribution along that, even though is not the same as that of the original sharp crack, it produces incrementally the same effect of delaminating the outside layer. This observation of shedding the surface layer is a significant result with regard to the reinforcement of plates or panels by stiffeners. If the attachment layer is shed off by delamination, the effect of any stiffener is lost. Because this delamination is not a localized effect but rather extends far away, the implication for reinforced structures is serious. Clearly, more work will be needed to address this issue in more detail; to understand its mechanism and to measure the extension of the area affected by it. The question arises immediately, for example, whether the thickness of the

reinforcement could be used to minimize the possibility of the microbuckling of the layer and thus, to increase its peel resistance.

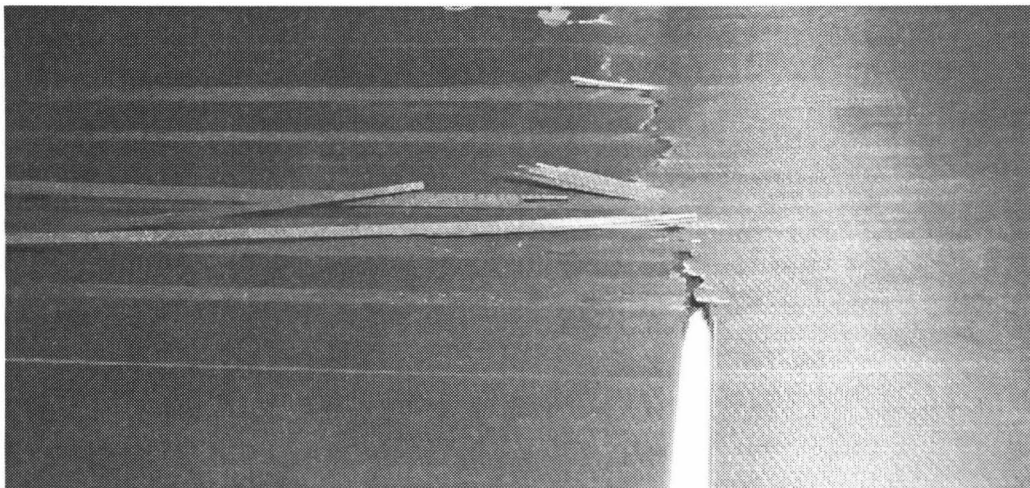
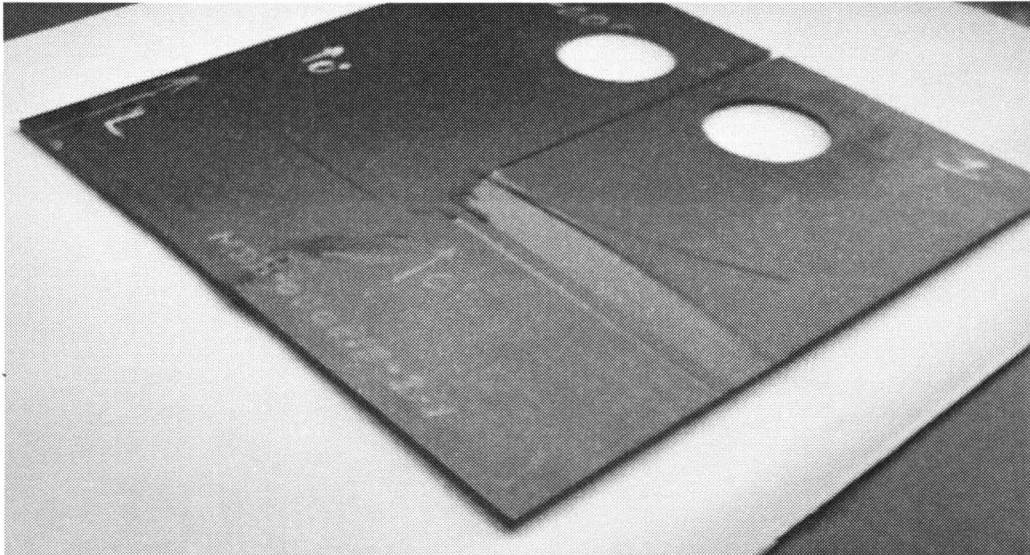


Figure 3.6.3 Views of two different Parallel panels after completion of the test. Note that the delamination in the form of thin strips extends all the way to the edge of the panels (runaway delamination).

In this case of the Perpendicular panels, the outer layer is parallel to the direction or the original sharp crack. For this layup there is no delamination of the external layers. Moreover, the inner plies with a 90° orientation did not delaminate either. Using the same argument as before, one can say that the surrounding layers prevented their buckling off.

On the other hand, since all the layers inside the panel, which are not $\pm 45^\circ$, are precisely 90° , a great amount of the inner damage includes fiber cracking. This will be clearer when we discuss the x-ray examinations. On the outside, the damage of the Perpendicular panels is typified in Figure 3.6.4.

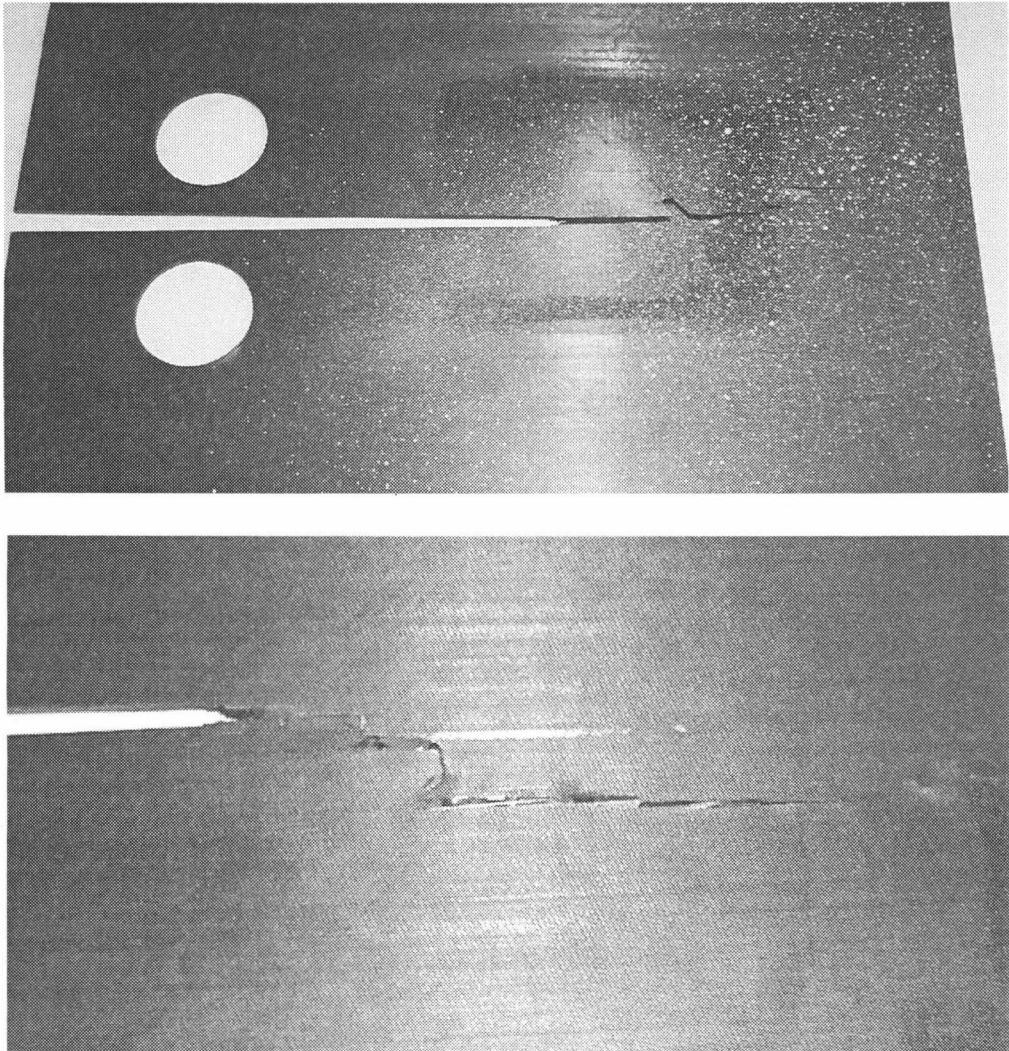


Figure 3.6.4 These images correspond to two different Perpendicular specimens. Note how the exterior damage is more confined than that of the Parallel panels since no long range delamination is present.

Let us turn our attention to the sequence of events in the interior of the panel. We first analyze each layup separately, and then compare the results.

The Perpendicular Panels

It is useful at this point to recall the layup of the specimens, i.e., $[90_2, +45_2, 0_2, -45_2, 0_2, +45_2, 0_2, -45_2]_S$. We obtained the two different sets of panels by having the precursor notches (the global crack) cut along the zero direction or perpendicular to it. Thus, the panels consist mostly of $\pm 45^\circ$ laminae (half of the plies have this orientation). The remainder is constituted as follows: 3/8 are 0° for the “Parallel” type or 90° for the “Perpendicular” one, and 1/8 of the layers (on the two external surfaces) in the direction at right angles to it.

From a global point of view, one can see in Figure 3.6.5 that the damage is bounded by the $\pm 45^\circ$ rays originating at the crack tip while the rest of the panel seems roughly intact. One observes also that the damage is not symmetric with respect to the global crack in that the damage extends more on “the right-hand side.” Figure 3.6.5 is representative for all the Perpendicular panels, regardless of their dimensions. The reader is referred to Appendix C where all the x-ray images are collected and printed to their true scale.

All the images in Figure 3.6.5 have the same scale and are labeled with the load level that was reached before the x-ray image was recorded. That is, the panels were loaded monotonically until a failure event occurred—the load drops that appear in Figure 3.6.1—and at that moment the displacement of the loading fixture was stopped and held at that state when the x-ray images and the photographs for DIC were recorded. After this the increase in load was resumed.

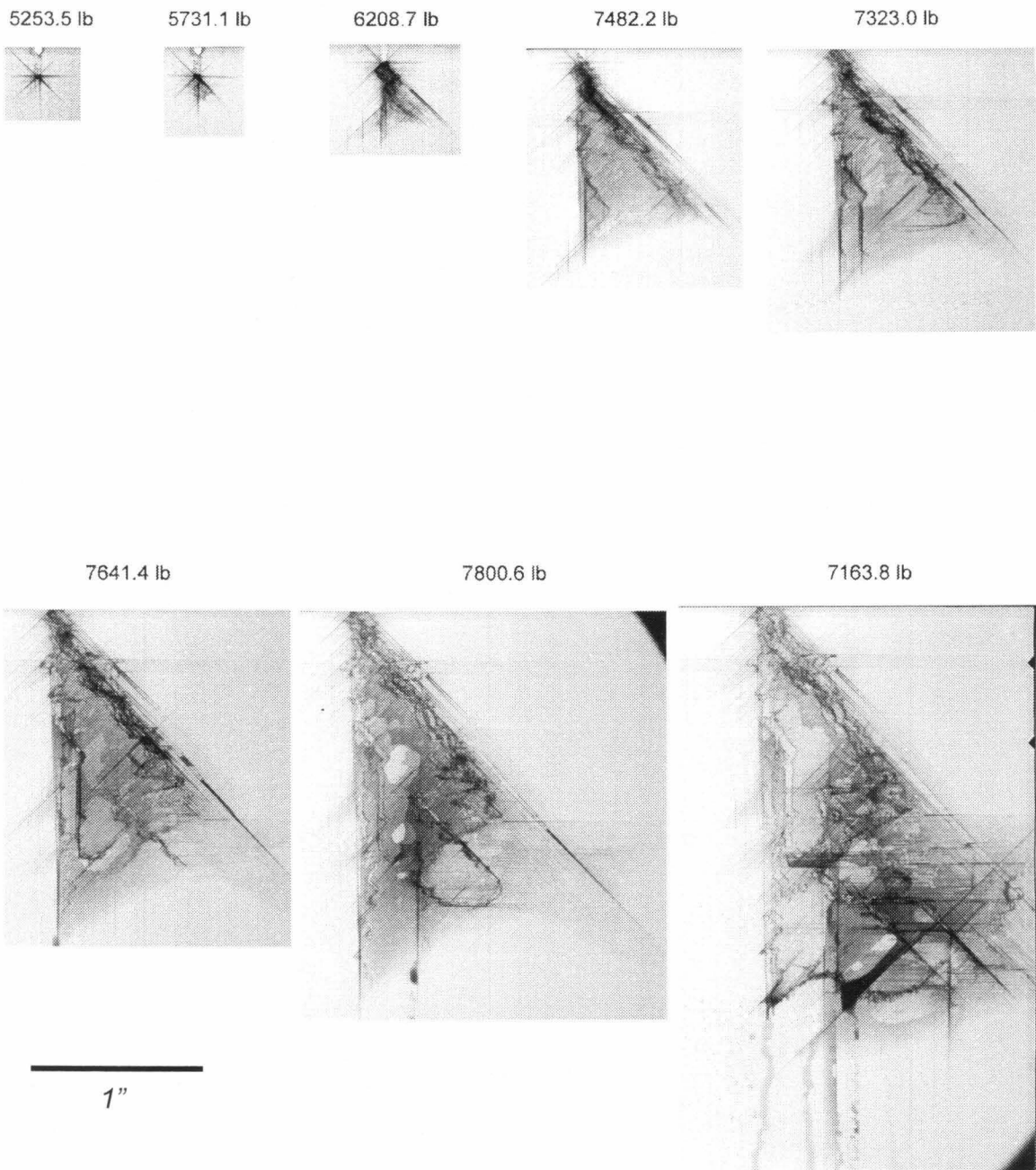
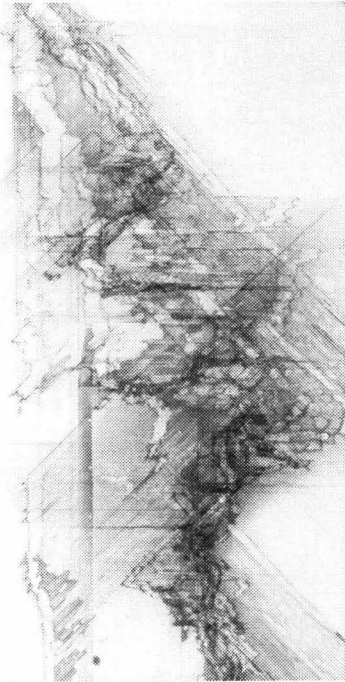


Figure 3.6.5 A sequence of x-ray images following the damage progression in a Large Perpendicular panel. The specimen was loaded to the indicated level where it underwent some stable “crack extension.” The loading fixture was held at that opening displacement while the x-ray images and the photographs for DIC were recorded and then the load increase was resumed.

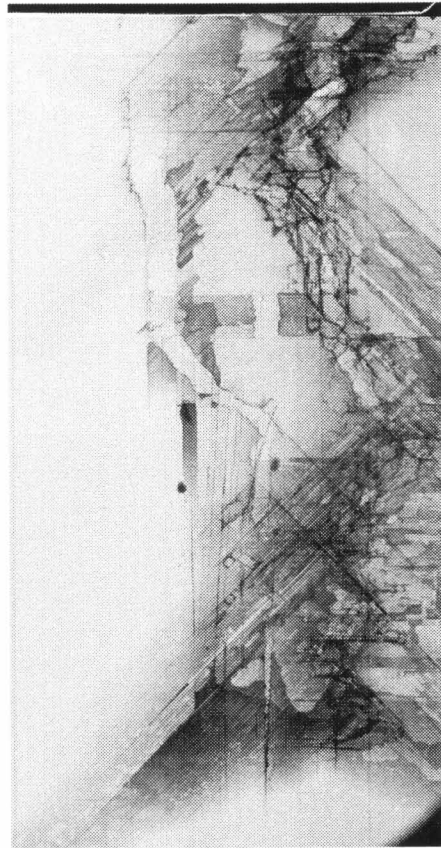
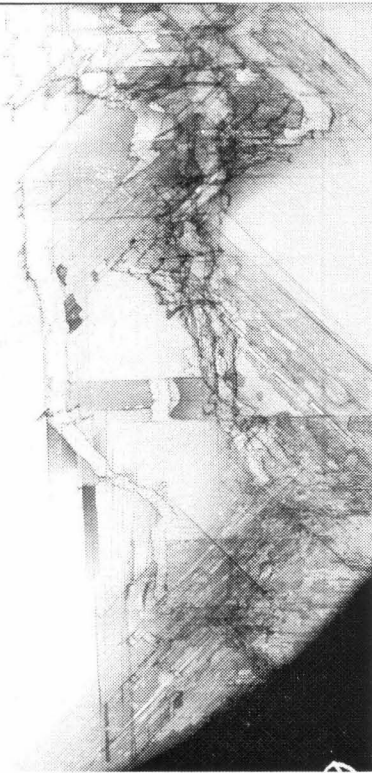


6049.5 lb



3979.9 lb

2547.1 lb



955.2 lb

1"

Figure 3.6.5 Continued.

From the Figures it is clear that trying to describe—much less model—the fracture processes taking place inside the “damage” region is a formidable task. On the one hand, it is beyond our current computational or analysis capabilities to describe this damage and, on the other hand, such a description does not seem to be altogether useful for engineering design purposes. What is significant is, that there is an area of damage possessing a relatively simple geometry that could lead to an approach to the fracture analysis of composites in a way analogous to Irwin’s plasticity correction of linearly elastic fracture descriptions.

The Parallel Panels

Comparison of Figures 3.6.5 and 3.6.6 shows the exact same behavior, namely the development of the damage region bounded by cracks in the 45° and 0° layers and roughly with the same length, except for the delamination of the outer layer. If one were to ignore the horizontal swaths of Figure 3.6.6, the two layups would be undistinguishable from the global point of view. On the other hand, a detailed analysis of the damage region would show that what in one set of panels is fiber breakage corresponds to matrix cracking in the other. This is the reason why the Parallel panels are more compliant than their counterparts, even though the effect is mitigated by the stress redistribution enforced by the large amount of $\pm 45^\circ$ plies.

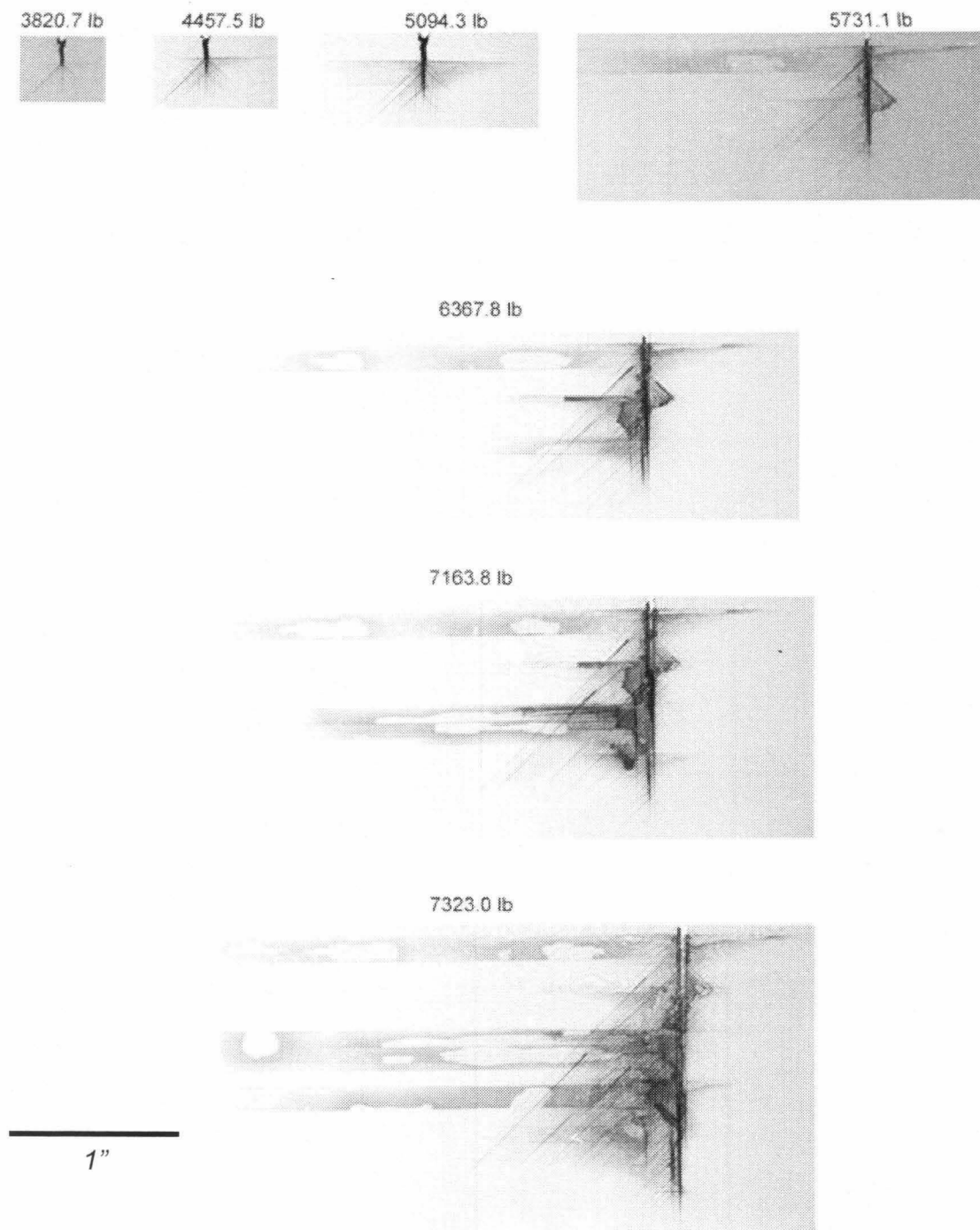
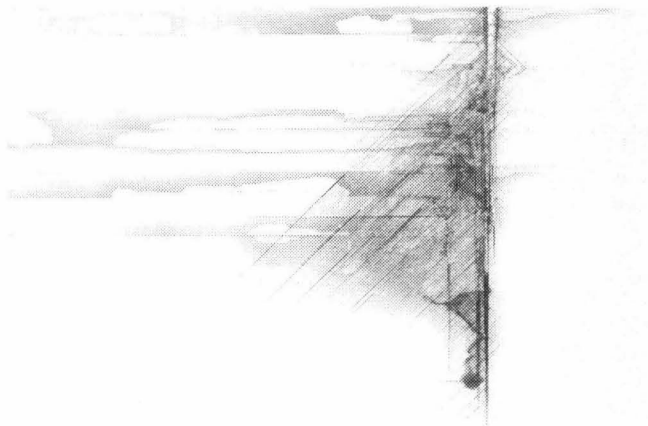
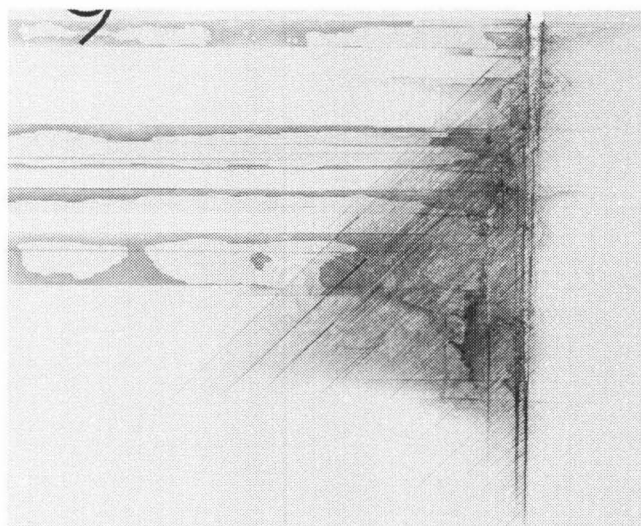


Figure 3.6.6 A sequence of x-ray images following the damage progression in a Large Parallel panel. The specimen was loaded to the indicated after which it underwent some stable “crack extension”.

7482.2 lb



7800.6 lb



1"

Figure 3.6.6 *Continued*

Therefore, the previous results suggest that the panel response, from a global point of view, could be modeled with a correction analogous to Irwin's. This thesis will be explored further in the following section. For the Parallel panels, it could be argued that the loss of the outer layers is a second order effect because they are so thin with respect to the laminate thickness and, furthermore, the load bearing capacity in that direction is not affected significantly because of the presence of the $\pm 45^\circ$ plies. In that sense, one could replace the real panel with an equivalent one as shown in Figure 3.6.7. Obviously, a constitutive relation has to be developed for the damage region but that exceeds the scope of the present work, at the same time opening new avenues for research in composite materials.

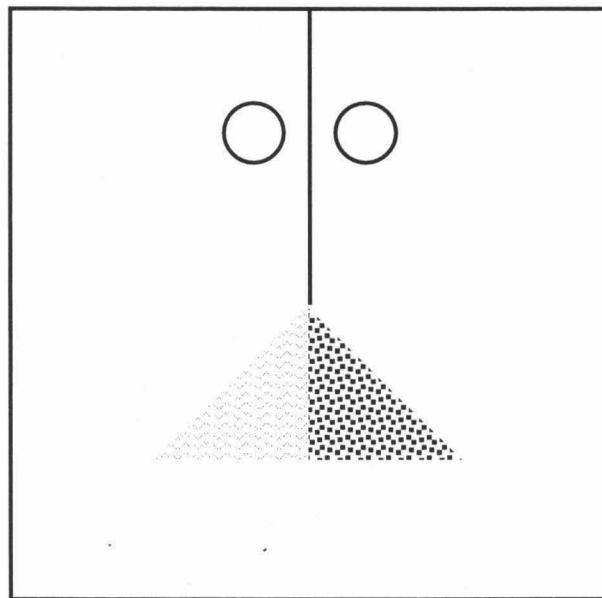


Figure 3.6.7 Schematic description of the damage or process region ahead of the global crack. An approach analogous to Irwin's correction for plasticity may be possible. The real damage seems to favor the development of just one of the two right triangles due to instabilities inherent in the damage progression.

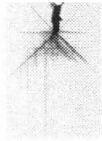
An examination of the x-ray images of all the tests shows that qualitatively there is no difference in the damage region between the different sizes of panels or between the two different layups, with the exception of what has already been said of the outer layer delamination of the Parallel panels.

One of the tests of a Large Perpendicular panel provides an interesting result. In that case the damage region grew in the fashion that we have described previously (Figure 3.6.7) but only up to a certain width (0.8" to 1") and from that point on, it appeared to stop extending in the direction lateral to the global crack and only advanced with the global crack extension retaining essentially the same width (Figure 3.6.8).

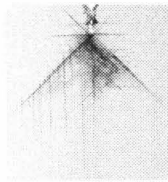
5094.3 lb



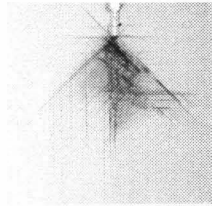
5731.1 lb



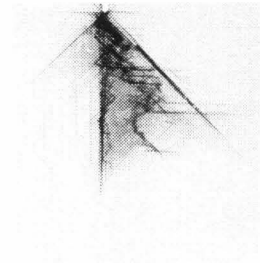
6367.8 lb



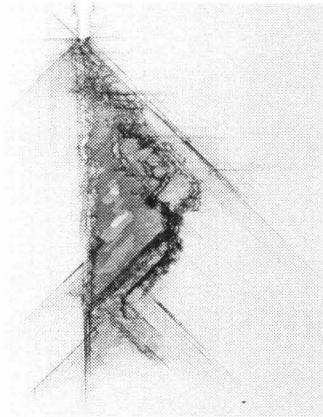
6845.4 lb



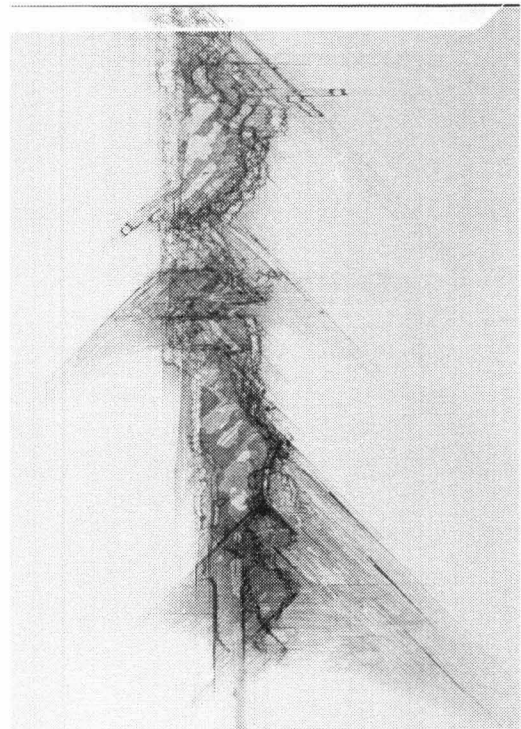
7323.0 lb



7959.8 lb



7163.8 lb



6527.0 lb

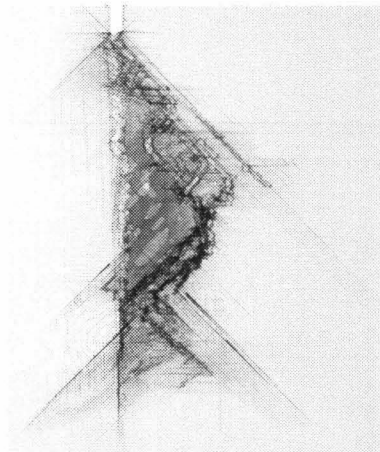
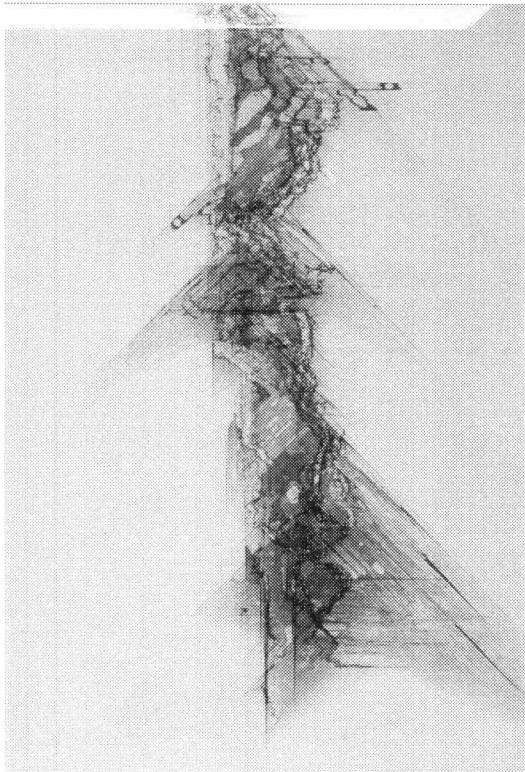


Figure 3.6.8 Continuous growth in a Large Perpendicular panel. Observe how the damage region first grows until it reaches a certain width ($\sim 0.8''$ from the center of the panel) which remains essentially constant as measured lateral to the latter, trailing the advancing global crack but does not expand horizontally.

3979.9 lb



4298.3 lb

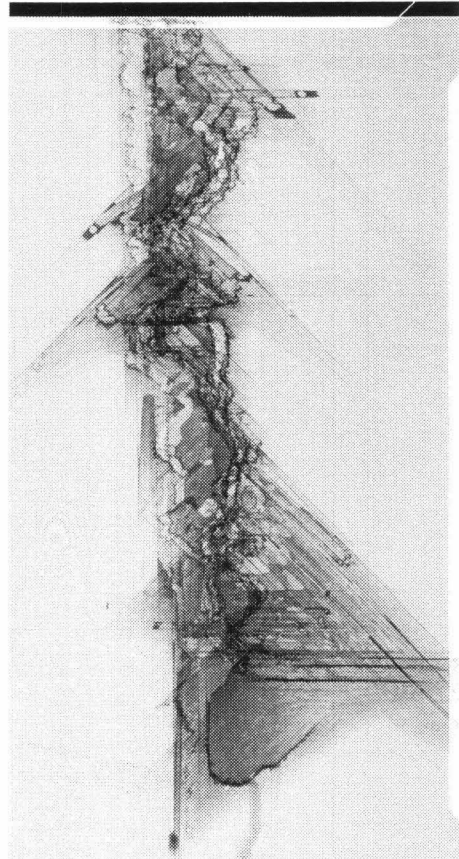


Figure 3.6.8 *Continued*

This result is interesting because it indicates a finite damage extent that is at least insensitive to, if not independent of, the crack size. Whether this idea can be sustained for still larger panels, and, specifically for full sized (e.g. fuselage) structures needs further evaluation. However, so much is clear that if a bound on the damage zone exists independently of the size of the structure, then the energy consumption by the failure process is correspondingly limited also; an unstable fracture process is thus more easily generated than for a situation in which the energy expenditure increases in some proportion to the crack size. Figure 3.6.8 corresponds to one of the Large Perpendicular panels in which one might expect to be able to observe this phenomenon. At the same time, it must be stated that this well defined and bounded wake was not observed in the other test (c.f. Large Perpendicular panels in Appendix C). Clearly, further tests need to be performed to confirm or deny this concept more unambiguously.

3-7 DAMAGE AREA CONCEPT

The results of the previous section show that the bulk of the damage is contained in a roughly triangular region bounded by the ply-cracks extending in the 0° and one of the $\pm 45^\circ$. In the current section, the extension of this “process” region is measured as a function of the pin displacement.

The length of lamina cracks along the 0° line and along the $\pm 45^\circ$ orientation were measured. Because of the triangular shape of the “damage region,” its area can be readily calculated. Its magnitude was then plotted against the displacement of the loading pins

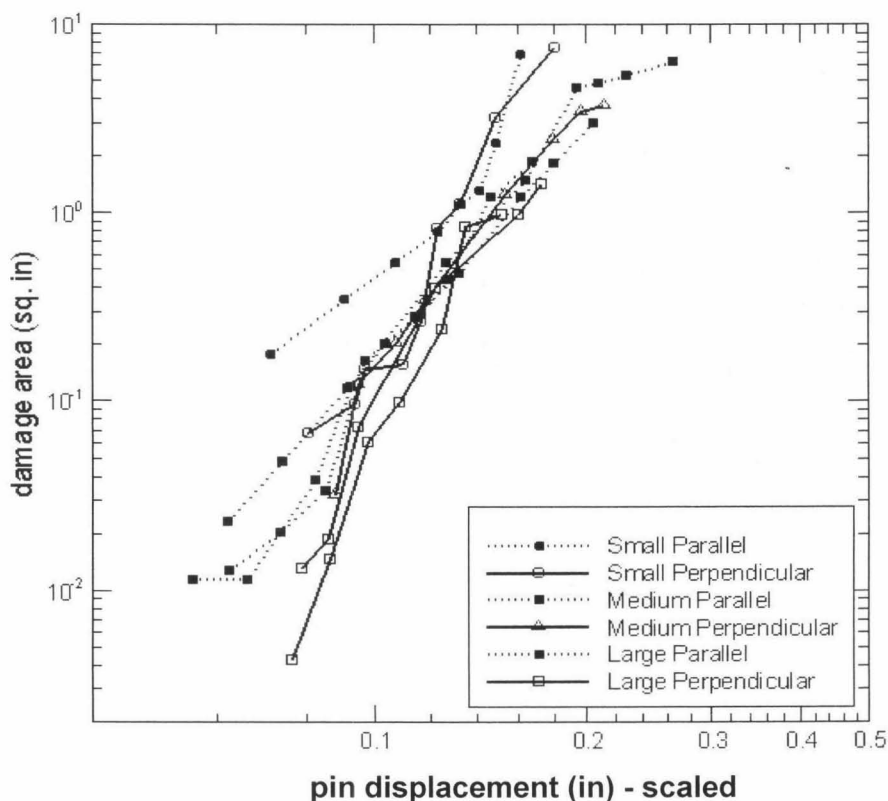


Figure 3.7.1 Log-log plot of measured damaged area as a function of pin displacement for all panels using the triangle method

scaled for panel size with respect to the medium sized panels: the displacement values of the Large panels were divided by the square root of 1.5, while those of the Small panels

were multiplied by the square root of 2, which will be recalled to be the geometric size proportion. The results for all the panels are collected in Figure 3.7.1.

An alternative method of estimating the “process region” area consists on digitizing the x-ray images of the internal damage; with the aid of the computer program for image processing Photoshop, the darker regions in the images—representing areas of damage—which have a certain value of light intensity (gray number) are replaced by black pixels. The images manipulated in this way are then loaded into the computer program Matlab where the amount of black pixels is counted. Since the density of the image is known, this number provides the extension of this “process region.” The results of this analysis are shown in Fig. 3.7.2, which shows a remarkable agreement with Fig. 3.7.1.

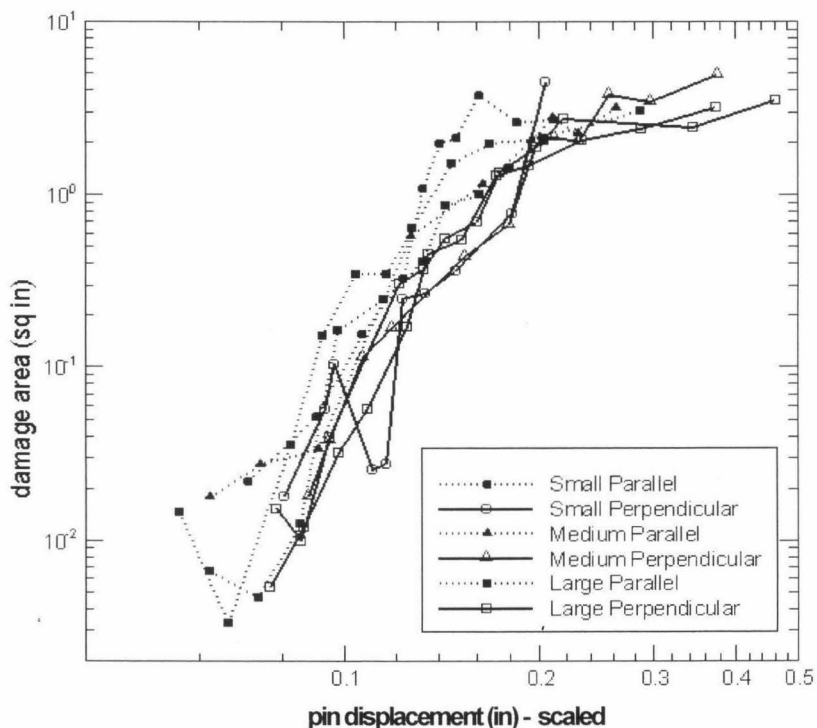


Figure 3.7.2 Log-log plot of measured damaged area as a function of pin displacement for all panels using the x-ray projection method.

Some “structure” is apparent in the growth of the damage area. First, it is evident that a power relation can be identified to connect the two variables. Second, as would have been expected, the growth of the Parallel panels’ damage is possibly somewhat faster than that of the Perpendicular ones. Then, two equations should be obtained; one for each layup. Its general form is thus:

$$A = C\delta^q \quad (3.7.1)$$

where A is the damage area, δ the loading pin displacement, and C and q , the fitting parameters, whose values have been calculated and appear in table 3.7.1.

Table 3.7.1 Calculation of Eq. 3.7.1. parameters for both area damage calculation methods

Layup	Triangle Method		Projection Method	
	C	q	C	q
Parallel	$7,892 \pm 6,283$	4.49 ± 0.55	$20,456 \pm 12,592$	5.13 ± 0.46
Perpendicular	$186,847 \pm 254,473$	5.07 ± 0.92	$37,003 \pm 49,678$	5.61 ± 0.63

The results of both methods are consistent with each other. The exponent is of around 5 and, because of the spread of the data, it is impossible to conclude anything regarding a difference between the Parallel and the Perpendicular panels. A larger number of tests would be needed to explore that issue.

In previous sections it was observed that the load-displacement curve for these panels, up to the initiation of fracture, was linear (Figure 3.6.1). Therefore, the complicated analysis of the panels once damage has begun, could be substituted by the linear model of the undamaged panel with a “superposed” model of the failure

progression containing the information of the advance or growth of the “process” area, provided by Equation 3.7.1 and the new constitutive law for the material in it, still to be developed.

Failure Initiation Criterion Based on Damage Area Investigation

The coupling of the damage area growth curves with the measured load-displacement curves can be used as a failure initiation criterion (Fig. 3.7.3 and Table 3.7.2)

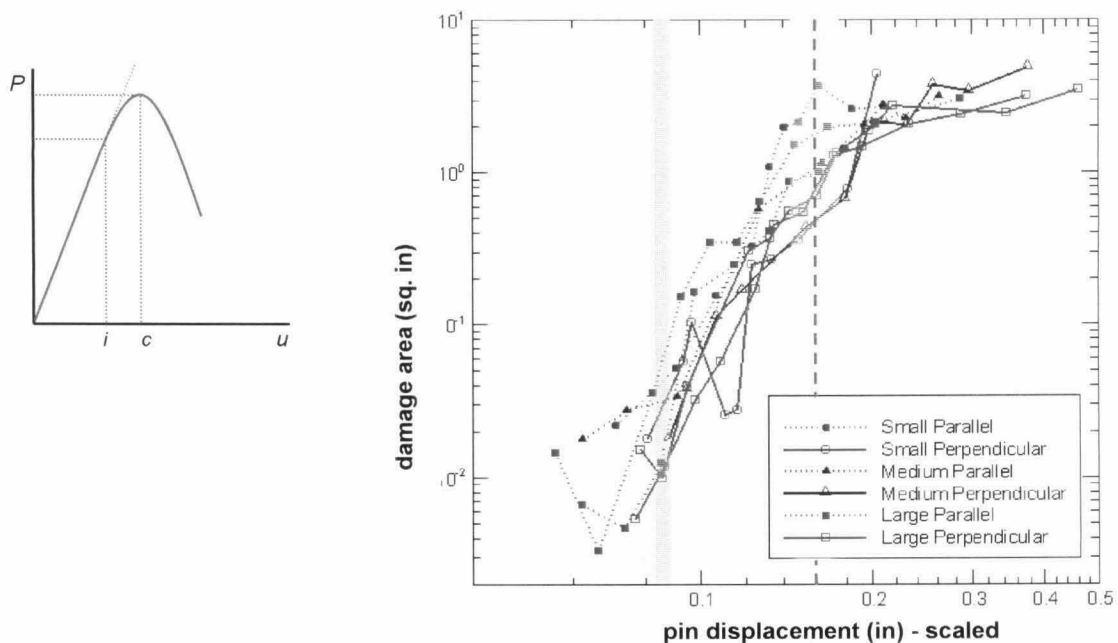


Fig. 3.7.3 On the left, a schematic of the load-displacement response of the panels. Point *i* corresponds to the moment when the first damage appears and the specimen stops behaving linearly. Point *c* identifies the peak load reached after which it can be considered that the panel has lost cohesion and, therefore, the crack has propagated. Points *i* and *c* are shown on the pin displacement-damage area plot on the right. With this information, an equivalent value of the J integral from the analysis of the unbroken panels can be provided as a criterion of failure initiation and crack propagation.

The load-displacement response of the unbroken panels is linear, as it has already been discussed, until the first ply cracks appear. From that moment on (point *i* in Fig.

3.7.3), the material accumulates damage until a critical point, c , is reached, after which the panel loses cohesion. These two moments are of great relevance for structural design. One can calculate their corresponding damage areas. In a sense, they can be considered as characteristic “flaw” sizes or, alternatively, from the analysis of the unbroken panels one can calculate an equivalent value of the J integral at those instances. That information can be used as the critical stress intensity factor for these materials. A summary of the results of these calculations are contained in Table 3.7.2.

Table 3.7.2 Values for pin displacement, opening load (both scaled) and equivalent damage area and J integral for damage initiation and moment of loss of cohesion for all the panels (refer to Fig. 3.7.3).

	u^* (in)	P^* (lb)	J (ft lb)	A (in ²)
Initiation	0.087 ± 0.007	$4,460 \pm 500$	91 ± 17	0.039 ± 0.026
Critical	0.16 ± 0.02	$6,480 \pm 400$	308 ± 83	1.27 ± 1.04

3-8 SURFACE DEFORMATIONS—INTERNAL DAMAGE (DIC—X-RADIOGRAPHY)

In closing this chapter on the damage assessment near the tip of a growing global crack, we examine the applicability or efficacy of using the measurement of the surface deformations or strain fields for the assessment of the internal state of the laminate.

When discussing the failure initiation process, it was observed in previous sections that cracks had developed in the interior of the material in all the cases before any damage or change was apparent to the unaided eye. It was also mentioned how troublesome this was in view of the fact that it is a common practice to resort to visual inspection of composite material structures in the field.

The DIC technique would seem to be an ideal candidate due to its relative simplicity and low cost. In what follows, we examine its application limits for this type of analysis. Measurements of the surface deformations using the DIC method were made each time an x-ray image of the interior damage was taken. The information of the two sources was blended into plots like that shown in Figure 3.8.1, the full set of which is collected in Appendix D.

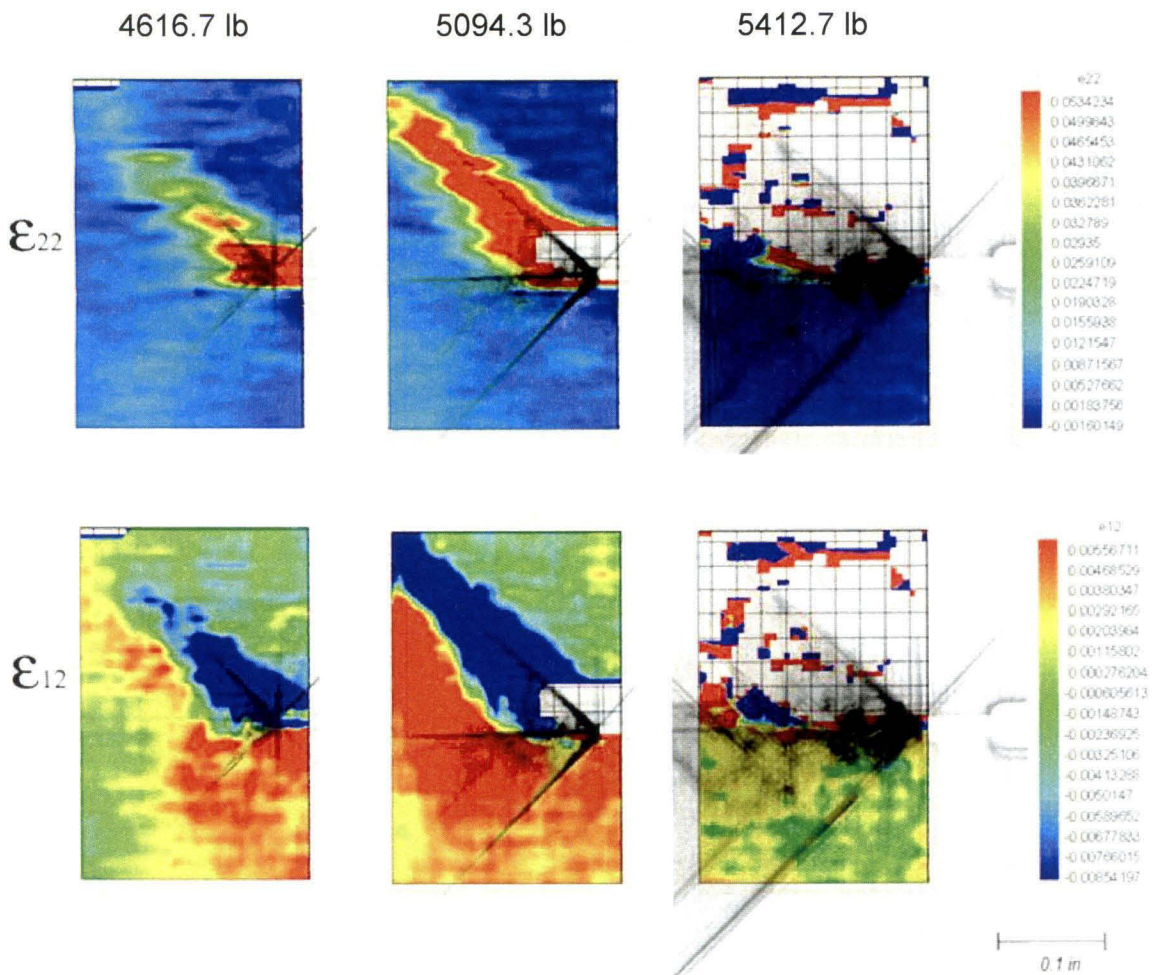


Figure 3.8.1 Strain fields of the outer layer calculated via digital image correlation and superposed on the x-ray image of the internal damage for one of the Medium Perpendicular panels at three different load levels. The center and right plots show regions (in white) where convergence of the method was not achieved.

These images summarize very well all the merits and limitations of the DIC method. It is obvious that the surface strains reveal the existence of one of the ply-cracks at 45°, where high strain gradients appear. This is encouraging but, at the same time, it is also evident that there exist other lamina-cracks that do not manifest themselves in the strain field. This could be due to any—or the combination—of the two following reasons:

- i. The strain field produced by the first crack is larger than that produced by the others so it “overshadows” it.
- ii. There are four $[\pm 45^\circ]_2$ layers in the laminate distributed through the thickness. If one of them lies just below the surface ply in view, the latter should be immediately influenced to show corresponding (inhomogeneous) strains. On the other hand, if the ply-crack occurs in a layer farthest away from the viewer, its effect on the strain field of the surface of observation would not be large enough to be detected by the DIC method.

Another feature apparent in Figure 3.8.1 is that, after a certain load level, the DIC method does not converge. This is merely indicative of the fact that even before this load level was achieved, the surface ply had already cracked, and delamination had started which was visually identifiable (Figure 3.8.2).

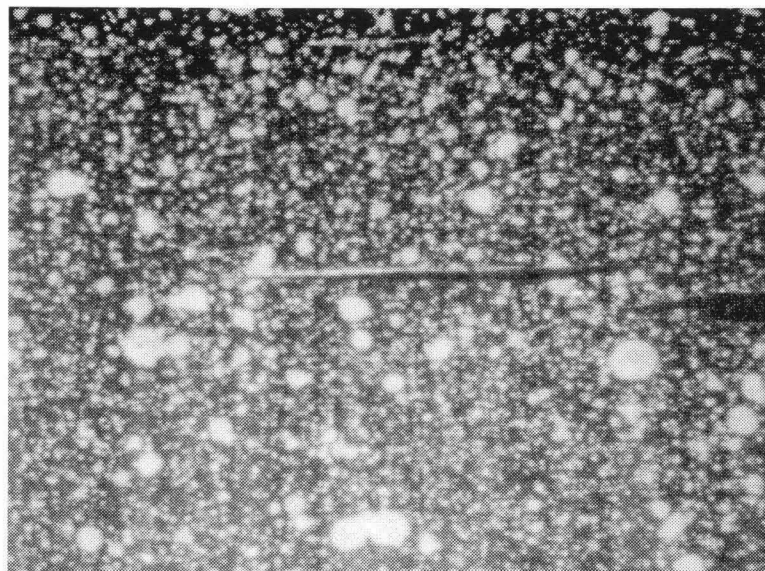


Figure 3.8.2 A photograph of the region around the crack tip (to the right, in the center) corresponding to the strain field and x-ray of damage at 5,412.7 lb in Figure 3.8.1. Notice the crack has extended in the surface layer. The surface displays the white paint splatter pattern employed for the DIC.

Having examined the surface and damage response of the Perpendicular panels, we turn to the behavior of the Parallel ones. In the latter specimens the external layers are damaged earlier than in their Perpendicular counterparts, as can be seen in Figure 3.8.3, which depicts results for one of the Small Parallel panels. The region of nonconvergence is larger because of the delamination of the outer 90° plies.

Thus, the DIC method has proved to be useful up to the initiation of the damage propagation. However, once the first cracks form, it can reveal their existence only if they are located close to the surface on which the digital photographs are recorded. The cracks farther from the surface cannot be identified by DIC. Therefore, in thick laminates, DIC would not be of much use but could be in thinner ones. Also, the “depth of perception” of this method could be increased if the DIC analysis was performed on both surfaces instead of only on one. Further experiments should be performed to quantify that “depth” and thus to better bound the limits of applicability of this technique.

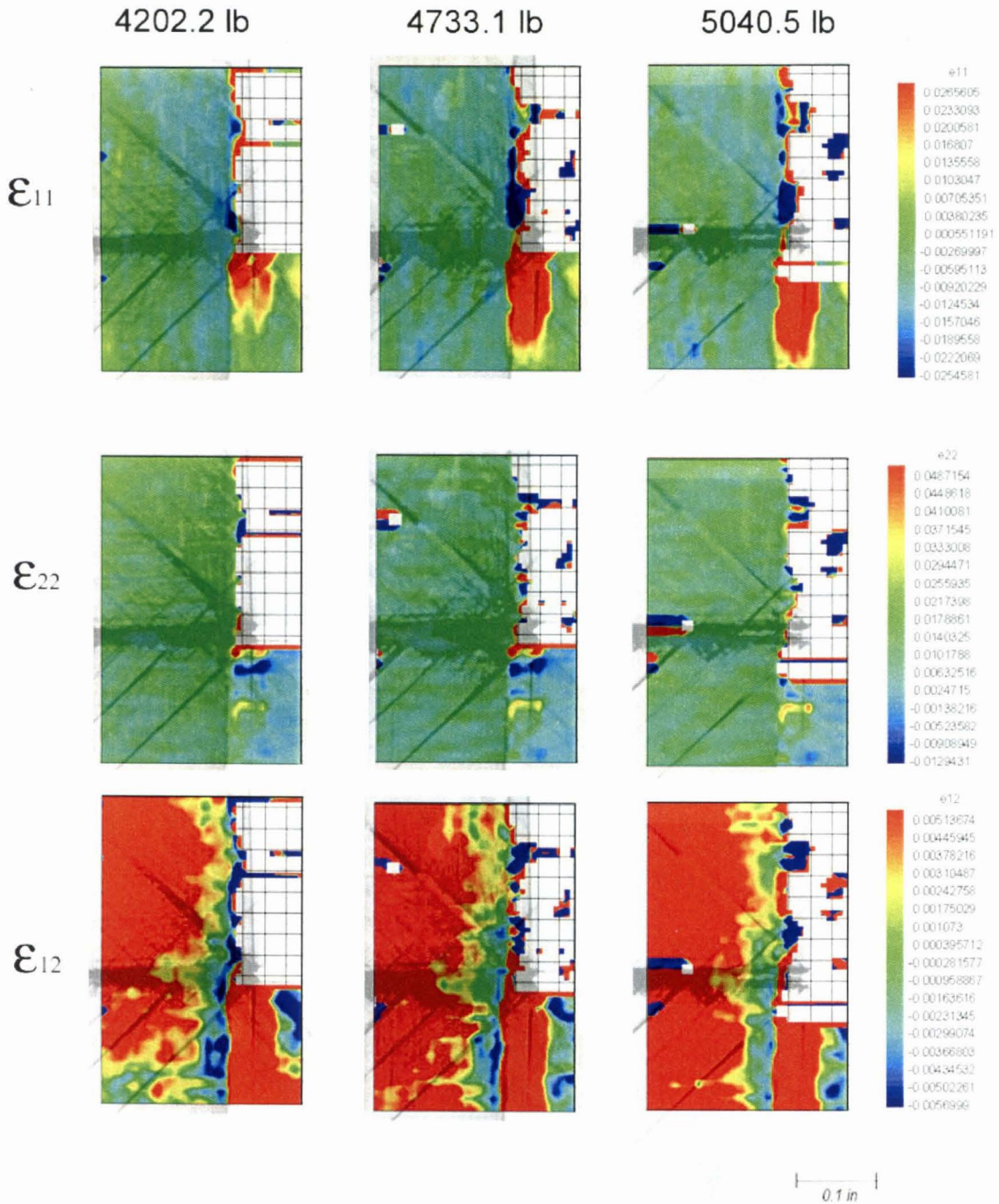


Figure 3.8.3 Plots of the strain field of the surface ply superposed on the x-ray images of internal damage of a Small Parallel panel. The calculations of the DIC method encounter more difficulty in converging because of more extensive and earlier delamination of the surface ply.

CONCLUSIONS AND RECOMMENDATIONS

A broad study of the failure process of laminated composite flat panels in the presence of a crack or stress concentrator was conducted, including experiments and numerical analyses. In the linear domain, for the load-displacement behavior, good correlation was found between them. A survey of the failure criteria currently available was presented and some of their problems and limitations were discussed. Most of these criteria are strength based, which render them more complicated to use from an engineering perspective because a precise prediction of the state of stress at every point of the laminate has to be provided. Besides, the great majority of these criteria have been developed for unidirectional composites, hardly encountered in real world applications. Therefore, for laminates, one is left with some recursive procedures like that illustrated in Section 1-5 that can only be as good as the ply failure criterion employed as a basis. Another problem adhering to many of these criteria is that they lack a solid physical grounding and are basically “curve fitting” procedures of, sometimes, totally unrelated failure mechanisms like fiber cracking under tension and ply delamination.

For these reasons we attempted to explore a failure initiation criterion based on ultimate lamina strains rather than strengths because, up to point of failure initiation, the panel can be well analyzed by using classical lamination theory, as long as the strains and deformations are uniform throughout the thickness of the plate. With the thin plate

approximation one can determine the strains and use them as input to a strain-based failure criterion. Two "popular" criteria were examined and compared with the experimental results, namely the maximum strain and the Tsai-Hill criteria. These two criteria have been incorporated in a number of finite element analysis commercial programs and are used in industry for design with composites.

The analysis of the initiation of damage in the panels showed the inadequacy of both criteria. The problem with the maximum strain criterion is that it does not take into account the interaction of the different strain components. The experiments showed that the failure starts with the formation of new cracks in various laminae along the fiber directions, so that the tensile or compressive strains along the fiber direction for each ply did not play a (significant) role (contrary to what the Tsai-Hill criterion implies) and neither do the out-of-plane strains. But there is definitely an interaction of the shear and the fiber-transverse strains. We discovered that the first damage appears roughly around 50% of the peak load achieved in the test.

The influence of the layup in the shape of the fracture propagation was observed, noticing that for Perpendicular panels ply-cracks appeared with a star shape in all the possible orientation of the layers of the laminate whereas for the Parallel panels no cracks were formed in the $\pm 135^\circ$ layers. The strain analysis showed that in this particular layup the transverse strain component was compressive along those rays while in all the other cases it was tensile coupled with shear. More work is needed to determine whether there is a simple relation between the two strain components that can be used as a failure criterion for fracture initiation. Another area for further research is to determine whether these first cracks develop in the matrix or in the interface fiber-matrix. Some SEM

photographs obtained from a delaminated panel seem to indicate that the delamination occurs at the interfaces. Some tests, in which the panels are destroyed, as soon as the first damage appears, to examine the nature of those cracks would solve this question.

The convenience of the utilization of complementary experimental techniques to study a complex phenomenon like the failure of a composite material was attempted through coupling the surface measurement technique of digital image correlation with the nondestructive Evaluation method of enhanced x-radiography. The applicability and ease of use of the digital image correlation method for the measurement of the laminate strains up to fracture initiation was demonstrated. Loss of linearity was coupled with the onset of surface delamination and thus no surface measurement technique—by definition—will be applicable. It was once more corroborated that internal damage can very well exist in a composite material that appears completely healthy to the unaided eye.

The DIC method can also be used to identify internal damage in a laminate but only under specific conditions and with some limitations that still need to be explored further. These conditions are basically that the damage has to occur in a layer close to the surface of measurement (if DIC is performed on both surfaces, this problem is slightly mitigated) and thus the applicability of this method would be constrained to thin laminates. Again, the DIC method can only be used as a damage initiation identifier and not to study the strains in the structure once the failure propagates—with some limited exceptions—because, in general, convergence is not achieved once the outer layer delaminates. In particular, it was observed that the panels with the outer layer perpendicular to the crack tip suffered “runaway” delaminations of the complete exterior layer (i.e., the delamination reached the edge of the panel, no matter how big the

specimen was), a phenomenon that was not present in the other (orthogonal) layup. This result is significant and should be taken into account if the structure is to be reinforced with “ribs” or stiffeners. On the other hand, more experiments are needed to determine whether this delamination is due to buckling of the layer because it is not constrained on the free surface. If this is the case, then the integrity of the stiffener would not be as compromised.

It was shown that the time dependence inherent to viscoelastic materials (and the matrix is one) is not an issue for tests in at room temperatures and for a range of test times on the order of one hour. More research has to be conducted to assess this effect for structures that will be in service for years or decades. The loading rate showed no significant influence on the effective elastic properties (Young’s moduli and Poisson’s ratio), at least in the range of rates from 0.002 in/s to 0.2 in/s; the values measured were essentially the same.

The experiments showed that the fracture process can be scaled with the size of the specimens, i.e., the load-displacement curves could be reduced to a single set using as a scaling factor the square root of the quotient of the two linear sizes of the two panels. This factor has to be applied to both the displacement and the load. This result is important because it says that the results obtained from small coupons can be applied to component size elements*.

The x-ray inspection of the panels, in all cases, showed that although the damage appeared initially as distinct lamina-cracks in all the ply orientations (not in the $\pm 135^\circ$

* It was also learned that the wedge angle used to open the crack has an influence in the load-displacement curves because a wider wedge produces more compression on the panel, effectively making it a stiffer structure.

rays for the Parallel panels), it appeared to grow in a region bound by the $\pm 45^\circ$ plies. While such damage is expected to be symmetrical, the observations did not usually show this and the damage grew faster on one side of the global crack thus creating an effective “damage” or “process” area that has the shape of a triangle formed by the line of the global crack and the 45° line on that side of it and with its vertex at the original crack tip location. A mathematical relation of the size of the “process” region as a function of the displacement of the loading pins (and thus of the opening load) was deduced. It can be coupled with a constitutive law for the damaged material (with some degraded properties from the original) to be used in engineering design. In this way an approach analogous to Irwin’s correction for the plastic zone may be feasible for design purposes.

Finally, damage initiation and “crack” propagation criteria based on the damage area measurements and in the numerical calculation of equivalent values of the J integral, which can be considered analogous to the critical stress intensity factor.

REVIEW OF FAILURE CRITERIA

Hankinson Criterion

The study of strength theory in composite materials started in the beginning of the twentieth century. In 1921, Hankinson proposed the first well-known one-dimensional empirical formula for the off-axis uniaxial compressive strength of wood. Hankinson's formula expresses the compressive strength of wood in a direction inclined at an angle ϕ to the grain as

$$X'_{\phi} = \frac{X' Y'}{X' \sin^2 \phi + Y' \cos^2 \phi}, \quad (\text{A.1})$$

where X' and Y' have been defined in Equation (A.1). He noted that this formula applies both to the fiber stress at elastic limit in compression, and also to the ultimate strength in compression. Investigators have shown that this formula is quite accurate for several different species of wood.

Malmeister Criterion

Malmeister (1966) suggested a general form of strength criterion in the following:

$$p_{\alpha} \sigma_{\alpha} + p_{\alpha\beta} \sigma_{\alpha} \sigma_{\beta} + p_{\alpha\beta\gamma} \sigma_{\alpha} \sigma_{\beta} \sigma_{\gamma} + \dots = I, \quad (\text{A.2})$$

where p_{α} , $p_{\alpha\beta}$ and $p_{\alpha\beta\gamma}$ are strength tensors of the second, fourth and sixth rank, respectively. In strain space, Equation (A.2) becomes

$$e_{\alpha} \varepsilon_{\alpha} + e_{\alpha\beta} \varepsilon_{\alpha} \varepsilon_{\beta} + e_{\alpha\beta\gamma} \varepsilon_{\alpha} \varepsilon_{\beta} \varepsilon_{\gamma} + \dots = I, \quad (\text{A.3})$$

where all the terms with e are tensors of the ultimate strain surface.

Gol'denblat-Kopnov Criterion

Gol'denblat and Kopnov (1966) assumed that the strength of fiber-reinforced composites can be predicted by the following equation:

$$(a_{ik}\sigma_{ik})^\alpha + (a_{pqmn}\sigma_{pq}\sigma_{mn})^\beta + (a_{rspqmn}\sigma_{rs}\sigma_{pq}\sigma_{mn})^\gamma + \dots = 1, \quad (\text{A.4})$$

where a_{ik} , a_{pqmn} and a_{rspqmn} are strength tensors of the second, fourth and sixth order, respectively. The strength tensors in Equation (A.4) satisfy the following symmetry conditions:

$$a_{ik} = a_{ki} \quad a_{pqmn} = a_{qpnm} \quad a_{pqmn} = a_{pqnm} \quad a_{pqmn} = a_{mnpq} \quad (\text{A.5})$$

As the simplest criterion of this type they choose $\alpha = 1$, $\beta = 1/2$ and $\gamma = -\infty$ such that

$$a_{ik}\sigma_{ik} + (a_{pqmn}\sigma_{pq}\sigma_{mn})^{1/2} + \dots = 1 \quad (\text{A.6})$$

Ashkenazi Criterion

Ashkenazi (1966) has proposed a series of methods for the strength prediction of orthotropic materials. In one of his later works, he proposed the following criterion:

$$\begin{aligned} A_{11}\sigma_1^2 + A_{22}\sigma_2^2 + A_{33}\sigma_3^2 + 2A_{12}\sigma_1\sigma_2 + 2A_{23}\sigma_3\sigma_2 \\ + 2A_{31}\sigma_1\sigma_3 + 4A_{55}\sigma_5^2 + 4A_{44}\sigma_4^2 + 4A_{66}\sigma_6^2 = 1, \end{aligned} \quad (\text{A.7})$$

where σ_4 , σ_5 and σ_6 denote τ_{23} , τ_{31} , and τ_{12} , respectively. In the case of a plane stress state Equation (A.9) can be written as

$$\frac{\sigma_1^2}{X^2} + \frac{\sigma_2^2}{Y^2} + \frac{\tau_{12}^2}{S^2} + \left(\frac{4}{V^2} - \frac{1}{X^2} - \frac{1}{Y^2} - \frac{1}{S^2} \right) \sigma_1\sigma_2 = 1, \quad (\text{A.8})$$

where X , Y and S are the tensile strength of a 0° laminate, the tensile strength of a 90° laminate and the shear strength of a 0° laminate, respectively. Note that Equation (A.8)

only contains quadratic terms. The tensile strengths are assumed the same as the compressive strengths if this equation is used to predict the strength envelope of the four stress quadrants in a single step.

Hoffman Criterion

Hoffman (1967) realized the difference in tensile and compressive strengths for orthotropic composites. He modified Hill's criterion, Equation (1.5.4), by adding linear terms as shown in the following:

$$C_1(\sigma_2 - \sigma_3)^2 + C_2(\sigma_3 - \sigma_1)^2 + C_3(\sigma_1 - \sigma_2)^2 + C_4\sigma_1 + C_5\sigma_2 + C_6\sigma_3 + C_7\sigma_4^2 + C_8\sigma_5^2 + C_9\sigma_6^2 = 1, \quad (\text{A.9})$$

where C_1 through C_9 are strength parameters that have to be determined experimentally.

Under plane stress condition, $\sigma_4 = \sigma_5 = \sigma_6 = 0$, this criterion simplifies to

$$\frac{\sigma_1^2 - \sigma_1\sigma_2}{XX'} + \frac{\sigma_2^2}{YY'} + \frac{X'-X}{XX'}\sigma_1 + \frac{Y'-Y}{YY'}\sigma_2 + \frac{\tau_{12}^2}{S^2} = 1, \quad (\text{A.10})$$

where the strength parameters are summarized in the following:

X = longitudinal tensile strength of a unidirectional laminate

X' = longitudinal compressive strength of a unidirectional laminate

Y = transverse tensile strength of a unidirectional laminate

Y' = transverse compressive strength of a unidirectional laminate

S = shear strength of a unidirectional laminate

Tsai-Wu Criterion

Tsai and Wu (1967) assumed that the strength criterion of fiber-reinforced composites takes the form:

$$F_i \sigma_i + F_{ij} \sigma_i \sigma_j = 1, \quad (\text{A.11})$$

where F_i and F_{ij} are strength parameters that can be determined by simple uniaxial tests, except the interaction term F_{ij} , $i \neq j$. More discussions are given in the following under plane stress state. Applying σ_1 and $-\sigma_1$ individually, and substituting into the above equation we obtain

$$F_1 = \frac{1}{X} - \frac{1}{X'} \quad F_{11} = \frac{1}{XX'} \quad (\text{A.12})$$

Similarly, from applying σ_2 and $-\sigma_2$ we obtain

$$F_2 = \frac{1}{Y} - \frac{1}{Y'} \quad F_{22} = \frac{1}{YY'} \quad (\text{A.13})$$

The shear strength in principal material axes is independent of shear stress sign, thus

$$F_6 = 0 \quad F_{66} = \frac{1}{S^2} \quad (\text{A.14})$$

The stress interaction term has to be solved using a specimen that fails under combined stress state. This term is normalized and given below:

$$F_{12}^* = \frac{F_{12}}{\sqrt{F_{11}F_{22}}} \quad (\text{A.15})$$

There are many methods that can solve this interaction term. Tsai and Wu suggested six methods. In order to assure that the strength surface be closed in an ellipsoidal shape, the following relation for the stress interaction terms must be imposed

$$F_{ii}F_{jj} - F_{ij}^2 \geq 0, \quad (\text{A.16})$$

where repeated indices are not summations and $i, j = 1, \dots, 6$. This equation has been found to be a realistic condition for many composite materials. Tsai and Hahn (1980) further showed graphically that the strength envelopes for most composite materials can be bounded by

$$-1/2 \leq F_{12}^* \leq 0 \quad (\text{A.17})$$

It can be shown that when $F_{12}^* = -0.5$ this criterion reduces to Mises yield criterion. In strain space Equation (A.11) can be written as

$$G_i \varepsilon_i + G_{ij} \varepsilon_i \varepsilon_j = 1, \quad (\text{A.18})$$

where

$$\begin{aligned} G_i &= Q_{ij} F_j \\ G_{ij} &= Q_{ik} Q_{js} F_{ks} \end{aligned} \quad (\text{A.19})$$

and Q_{ij} is plane stress modulus.

This criterion can be improved to fit data better by adding a cubic term to Equation (A.11), i.e.,

$$F_i \sigma_i + F_{ij} \sigma_i \sigma_j + F_{ijk} \sigma_i \sigma_j \sigma_k = 1, \quad (\text{A.20})$$

where F_{ijk} represents sixth-order strength parameters. Wu (1974) and Tennyson et al. (1978) showed that Equation (A.20) brings in four additional constants: F_{112} , F_{221} , F_{166} and F_{266} . These four additional constants are certainly not easy to measure. Therefore, although adding a cubic term to the quadratic failure criterion is a sound mathematical approach, it probably will not be widely used by most engineers.

Hashin Criterion

Hashin (1980) developed a failure criterion from the consideration of stress invariants. The criterion is in a quadratic form. He emphasized that the choice of quadratics is based on curve fitting considerations rather than physical reasoning.

Tensile Matrix Mode [$\sigma_1 > 0$]

$$\left(\frac{\sigma_1}{X}\right)^2 + \frac{1}{S_0^2}(\sigma_5^2 + \sigma_6^2) = 1 \quad (\text{A.21})$$

Compressive Fiber Mode [$\sigma_1 < 0$]

$$\sigma_1 = -X' \quad (\text{A.22})$$

Tensile Matrix Mode [$(\sigma_2 + \sigma_3) > 0$]

$$\left(\frac{1}{Y^2}\right)(\sigma_2 + \sigma_3)^2 + \frac{1}{S_4^2}(\sigma_4^2 - \sigma_2\sigma_3) + \frac{1}{S_6^2}(\sigma_5^2 - \sigma_6^2) = 1 \quad (\text{A.23})$$

Compressive Matrix Mode [$(\sigma_2 + \sigma_3) < 0$]

$$\begin{aligned} \frac{1}{Y'} \left[\left(\frac{Y'}{2S_4} \right)^2 - 1 \right] (\sigma_2 + \sigma_3) + \frac{1}{4S_4^2} (\sigma_2 + \sigma_3)^2 \\ + \frac{1}{S_4^2} (\sigma_4^2 - \sigma_2\sigma_3) + \frac{1}{S_6^2} (\sigma_5^2 - \sigma_6^2) = 1 \end{aligned} \quad (\text{A.24})$$

where the indices are $1 \equiv 11$, $2 \equiv 22$, $3 \equiv 33$, $4 \equiv 23$, $5 \equiv 31$ and $6 \equiv 12$, as before. The parameters S_4 and S_6 ($= S_5$) are shear strengths that have to be determined experimentally. For plane stress condition, all the terms with indices 3, 4, and 5 vanish. Hashin's criterion assumes that there is no stress interaction between σ_1 and σ_2 stress components, as well as σ_1 and σ_3 terms. Therefore, it reduces to the maximum stress criterion in the $\sigma_1 - \sigma_2$ space. The interaction coefficients for σ_2 and σ_3 stress components are different for tensile matrix mode and compressive matrix mode. However, they are given as basic strength parameters (on-axis), and thus no additional tests are needed to determine these interaction coefficients.

The most general form among all the classical failure criteria is given by Equation (A.4). The Tsai-Wu criterion [Equation (A.11)] also represents a general form in which all the

power coefficients are set equal to unity. This criterion has a very sound mathematical foundation. Consequently, it has been used and further studied by many engineers and researchers. The main concern about this criterion is the evaluation of the stress interaction terms. In fact, this problem is the same for all the classical failure criteria—that the stress interaction terms have to be determined by experiment. Many investigators in advanced composites have reported that the stress interaction terms are very sensitive to the test methods used. In off-axis tension tests, this interaction term also varies considerably for different fiber orientations. For paperboards, Rowland et al. (1984) found that large variations in F_{12} have relatively little effect on strength prediction in quadrants 2, 3, and 4. On the other hand, a little variation in F_{12} produces relatively large changes in predicted strength in quadrant 1. For wood materials, Liu (1984) suggested that F_{12} of the Tsai Wu criterion may be determined from Hankinson's formula. What he did is to express the Tsai-Wu criterion in the off-axis direction and compare it to the Hankinson's formula. In so doing, Liu obtained

$$F_{12} = \frac{1}{2} \left(\frac{1}{XY'} + \frac{1}{X'Y} - \frac{1}{S^2} \right) \quad (\text{A.25})$$

Hill's types of failure criteria have the advantage that they only require basic strength parameters as input data. The stress interaction terms are expressed as a function of the basic strength parameters. The major drawback occurs at high shear stress levels. When the in-plane shear stress approaches or exceeds the pure shear strength, the strength envelope shrinks toward the origin of the stress axes. The prediction deviates significantly from the experimental data.

When a failure criterion contains a linear and a quadratic term (such as Tsai-Wu and Hoffman criteria), the entire strength envelope can be predicted using a single equation.

If it only contains a quadratic term [such as Ashkenazi, Tsai-Hill and Chamis (1969) criteria], then this strength equation with different values of strength parameters has to be used for each quadrant. Otherwise, the compressive strengths would have to be the same as the tensile strengths. The four-step procedures may result in a strength envelope that is not smooth.

The accuracy of a strength criterion can be improved by at least two methods. The first is to use higher-order terms such as the addition of cubic terms for the Tsai Wu criterion. However, much added work is needed to solve the additional coefficients. The second method is to use a different value of stress interaction term for each quadrant. This approach has been taken by several investigators including Chamis (*op. cit.*) and Rowland et al. (*op. cit.*). It is a simple yet efficient method, although it may be difficult to prove or disprove its physical meaning.

Tan-Cheng Criterion

Although Hankinson's formula is a one-dimensional criterion, the fact that it has been widely used in the wood industry has aroused interest among researchers who attempted to derive that formula from a general strength theory. Recently, Tan and Cheng (1993) assumed that the off-axis strength of composites can be predicted using the following cosine series:

$$X_{\phi}^i = \left(\sum_{n=0,2,4,\dots} C_n \cos n\phi \right)^{-1}, \quad (\text{A.26})$$

where superscript i is either blank (tension) or ' (compression). The number of coefficients (C_n) used for the series depends on the number of uniaxial characterization tests performed. For instance, if $\phi = 0^\circ$, 90° and 45° off-axis laminates are characterized

under compression load for the basic strength parameters, we obtain the following solution by substituting the data into Equation (A.23):

$$X_{\phi}^i = \left[\frac{X' \sin^2 \phi + Y' \cos^2 \phi}{X' Y'} + \frac{1}{2} \left(\frac{1}{V'} - \frac{X'+Y'}{2X' Y'} \right) (1 - \cos 4\phi) \right]^{-1}, \quad (\text{A.27})$$

where V' denotes the compressive strength of a 45° off-axis laminate. Note that the first term inside the bracket is the Hankinson's formula. The Hankinson's formula can be obtained by using the first two terms of the series in Equation (A.26). Tan and Cheng's criterion in a two-dimensional space is given in the following scalar invariant form:

$$\left(\frac{\sigma_x}{X_{\phi}^i} \right)^2 + \left(\frac{\sigma_y}{Y_{\phi}^i} \right)^2 - \left[\sum_{n=0,2,4,\dots} a_n \cos n(|\phi| - 45) \right] \left(\frac{\sigma_x}{X_{\phi}^i} \right) \left(\frac{\sigma_y}{Y_{\phi}^i} \right) = 1, \quad (\text{A.28})$$

where Y_{ϕ}^i can be related to X_{ϕ}^i by

$$Y_{\phi}^i = X_{90-\phi}^i \quad i = \text{blank or ' } \quad (\text{A.29})$$

In a three-dimensional space, this criterion becomes

$$\begin{aligned} & \left(\frac{\sigma_x}{X_{\phi}^i} \right)^2 + \left(\frac{\sigma_y}{Y_{\theta}^i} \right)^2 + \left(\frac{\sigma_z}{Z_{\beta}^i} \right)^2 - \left[\sum_{m,n=0,2,4,\dots} \sum a_{mn} \cos n\phi_1 \cos m\theta_2 \right] \left(\frac{\sigma_x}{X_{\phi}^i} \right) \left(\frac{\sigma_y}{Y_{\theta}^i} \right) \\ & - \left[\sum_{m,n=0,2,4,\dots} \sum b_{mn} \cos n\phi_1 \cos m\beta_3 \right] \left(\frac{\sigma_x}{X_{\phi}^i} \right) \left(\frac{\sigma_z}{Z_{\beta}^i} \right) \\ & - \left[\sum_{m,n=0,2,4,\dots} \sum c_{mn} \cos n\theta_2 \cos m\beta_3 \right] \left(\frac{\sigma_y}{Y_{\theta}^i} \right) \left(\frac{\sigma_z}{Z_{\beta}^i} \right) = 1, \end{aligned} \quad (\text{A.30})$$

where θ and β denote the off-axis angles with respect to the y - and z -axes, respectively.

The parameters Y_{ϕ}^i and Z_{β}^i are uniaxial strengths in the y - and z -axes, respectively.

This criterion has much operational flexibility. It has good fit to data and does not need shear strength properties. Good correlation between theory and experimental data for bones were obtained and given in Reference (Tan and Cheng, 1993)

Tan Criterion

Based on the objective that a failure criterion can be applied easily to any composite materials with good fit, Tan (1990) developed another failure criterion. He assumed a general strength function,

$$X_{\phi}^i = \left(A_0 - \sum_{n=1,2,3,\dots}^m A_n \sin^2 n\phi \right)^{-1} \quad (\text{A.31})$$

where A_n , $n = 0, 1, \dots, m$, are strength coefficients to be determined with experimental data. Any uniaxial tests with on-axis or off-axis laminates can be treated as basic strength data. With the development of Sun-Berreth's off-axis specimen (1988), off-axis strength of unidirectional composites can be characterized easily and accurately. The unidirectional strength data, input to this strength function, can be treated as strength boundary conditions. The parameters X , X' , Y , and Y' are regarded as the fundamental strength parameters. If we only use the first two coefficients in Equation (A.31) and set $A_n = 0$ for $n \geq 2$, we will obtain the Hankinson's formula. If one additional strength data of $\phi = 30^\circ$ laminate, U^i is considered, the coefficients can be obtained in

$$A_0 = \frac{1}{X^i} \quad (\text{A.32a})$$

$$A_1 = \frac{1}{X^i} - \frac{1}{Y^i} \quad (\text{A.32b})$$

$$A_2 = \frac{1}{3} \left(\frac{3}{X^i} + \frac{1}{Y^i} - \frac{4}{U^i} \right) \quad (\text{A.32c})$$

where superscript i is either blank (tension) or ' (compression). Equation (A.31) with A_i given in Equation (A.32) can be rewritten as

$$X'_\phi = \left[\frac{X^i \sin^2 \phi + Y^i \cos^2 \phi}{X^i Y^i} - \frac{1}{3} \left(\frac{3}{X^i} + \frac{1}{Y^i} - \frac{4}{U^i} \right) \sin^2 2\phi \right]^{-1} \quad (\text{A.33})$$

If four strength parameters are utilized, for instance U^i and W^i (strengths of a $\theta = 30^\circ$ and a $\phi = 60^\circ$ laminates, respectively), in addition to X^i and Y^i , the following results are obtained

$$A_0 = \frac{1}{X^i} \quad (\text{A.34a})$$

$$A_1 = \frac{2}{3} \left(\frac{1}{X^i} - \frac{1}{Y^i} + \frac{1}{U^i} - \frac{1}{W^i} \right) \quad (\text{A.34b})$$

$$A_2 = \frac{2}{3} \left(\frac{3}{X^i} + \frac{1}{Y^i} - \frac{1}{U^i} - \frac{1}{W^i} \right) \quad (\text{A.34c})$$

$$A_3 = \frac{1}{3} \left(\frac{1}{X^i} - \frac{1}{Y^i} - \frac{2}{U^i} + \frac{2}{W^i} \right) \quad (\text{A.34d})$$

If N strength data are used, N coefficients can be solved from N equations. A general strength theory is now developed using the x - y - z system. This criterion assumes that a strength surface must be closed in an ellipsoidal space. If any stress vector is equal to or greater than the strength surface envelope, the material would fail. Mathematically, the failure surface is described by the following quadratic equation:

$$F_i \sigma_i + F_{ij} \sigma_i \sigma_j = 1 \quad i = x, y, z, \quad (\text{A.35})$$

which can be written more explicitly as

$$\begin{aligned} F_x \sigma_x + F_y \sigma_y + F_z \sigma_z + F_{xx} \sigma_x^2 + F_{yy} \sigma_y^2 + F_{zz} \sigma_z^2 \\ + 2F_{xy} \sigma_x \sigma_y + 2F_{xz} \sigma_x \sigma_z + 2F_{yz} \sigma_y \sigma_z = 1, \end{aligned} \quad (\text{A.36})$$

where the strength coefficients, F_i and F_{ij} can be expressed as functions of the uniaxial strength parameters. The accuracy of this general theory depends on the number of strength parameters used to characterize the fundamental strength function, Equation (A.31). If a uniaxial tensile stress, σ_x , is applied to a ϕ -degree laminate, and the failure strength is X_ϕ then Equation (A.36) can be solved by substituting $\sigma_x = X_\phi$:

$$F_{xx} X_\phi^2 + F_x X_\phi = 1 \quad (\text{A.37})$$

If compressive stress is applied for the same laminate, then Equation (A.34) can be solved by substituting $\sigma_x = -X_\phi'$,

$$F_{xx} X_\phi'^2 - F_x X_\phi' = 1 \quad (\text{A.38})$$

Solving Equations (A.37) and (A.38) yields

$$F_x = \frac{1}{X_\phi} - \frac{1}{X_\phi'} \quad F_{xx} = \frac{1}{X_\phi X_\phi'} \quad (\text{A.39})$$

Note that the coefficients F_x and F_{xx} of a laminate with any fiber orientation can be calculated using X_ϕ and X_ϕ' given by Equation (A.31). The coefficients F_y , F_{yy} , F_z , and F_{zz} can be solved following the same procedure and the results are

$$F_y = \frac{1}{Y_\phi} - \frac{1}{Y_\phi'} \quad F_{yy} = \frac{1}{Y_\phi Y_\phi'} \quad (\text{A.40})$$

and

$$F_z = \frac{1}{Z_\phi} - \frac{1}{Z_\phi'} \quad F_{zz} = \frac{1}{Z_\phi Z_\phi'} \quad (\text{A.41})$$

where Y_ϕ^i and Z_ϕ^i , $i = \text{blank or '}$, are the respective uniaxial strengths in the y - and z -directions. Since fibers are on the x - y plane, Y_ϕ^i can be related to X_ϕ^i by:

$$Y_\phi^i = X_{90-\phi}^i \quad (\text{A.42})$$

Substituting Equation (A.42) into Equation (A.31) yields

$$Y_{\phi}^i = \left(A_0 - \sum_{n=1,2,3,\dots}^m A_n \sin^2 n(90 - \phi) \right)^{-1} \quad (\text{A.43})$$

$$= \left(A_0 - A_1 \cos^2 \phi - A_2 \sin^2 2\phi - A_3 \cos^2 3\phi - A_4 \sin^2 4\phi \dots \right)^{-1}$$

The strengths in the z -axis can be expressed in a form similar to Equation (A.31):

$$Z_{\phi}^i = \left(B_0 - \sum_{n=1,2,3,\dots}^m B_n \sin^2 n\phi \right)^{-1}, \quad (\text{A.44})$$

where the strength coefficients can be solved from the following conditions:

$$Z_{\phi}^i = Y^i \text{ at } \phi = 0^{\circ}$$

$$Z_{\phi}^i = Z^i \text{ at } \phi = 90^{\circ}, \quad (\text{A.45})$$

and Y^i has been defined before and Z^i ($i = \text{blank or } \prime$) denote the tensile and compressive strengths transverse to the fibers direction with fibers going out-of-plane.

The stress interaction terms, F_{xy} , F_{xz} and F_{yz} , in Equation (A.36) are assumed, in a general form, as

$$F_{xy} = - \left(C_0 - \sum_{n=1,2,3,\dots}^m C_n \sin^2 n(|\phi| - 45) \right) \sqrt{F_{xx} F_{yy}} \quad (\text{A.46a})$$

$$F_{xz} = - \left(D_0 - \sum_{n=1,2,3,\dots}^m D_n \sin^2 n\phi \right) \sqrt{F_{xx} F_{zz}} \quad (\text{A.46b})$$

$$F_{yz} = - \left(E_0 - \sum_{n=1,2,3,\dots}^m E_n \sin^2 n\phi \right) \sqrt{F_{yy} F_{zz}} \quad (\text{A.46c})$$

From the consideration of biaxial strength symmetry (x - y plane) with respect to $\phi = 45^{\circ}$, the term inside the bracket, $|\phi| - 45$, is assumed. The coefficients (C_n , D_n , E_n , $n = 0, 1, 2, \dots$) can be determined by substituting biaxial strength data into Equation (A.36).

For instance, the coefficients of F_{xy} are obtained by substituting ϕ_x and ϕ_y into Equation (A.36),

$$C_0 - \sum_{n=1,2,3,\dots}^m C_n \sin^2 n(|\phi| - 45) = \frac{F_x \sigma_x + F_y \sigma_y + F_{xx} \sigma_x^2 + F_{yy} \sigma_y^2 - 1}{2\sigma_x \sigma_y \sqrt{F_{xx} F_{yy}}} \quad (\text{A.47})$$

The coefficients of F_{xz} , and F_{yz} can be determined by substituting respective biaxial strengths, σ_x with σ_z and σ_y with σ_z , into Equation (A.36). For highly orthotropic materials, more than one set of biaxial strength data may be needed to solve the coefficients C_n , D_n , and E_n . However, it is expected that only the first terms, C_0 , D_0 , and E_0 are needed for most materials. When C_0 , D_0 , and E_0 are equal to 0.5 and $C_n = D_n = E_n = 0$ for $n \geq 1$, Equation (A.36) is a generalization of the Mises yield criterion.

In the case that shear stresses exist, the tensor transformation rule can be applied to rotate the laminate stresses into principal stresses. When the fibers of a laminate do not lie on any plane of the principal stress axes, the fibers are defined as three-dimensional oriented fibers with respect to the principal stress axes. The fundamental strength function given in the x -direction, Equation (A.36), can be converted to y - and z -direction if the angles between the fibers and the y - and z -axis are known. A complete derivation for this problem is given by Tan (1990).

Plane Stress Problem

Plane stress problem is of particular practical importance. Two-dimensional strength criterion can be obtained from Equation (A.36) as

$$F_x \sigma_x + F_y \sigma_y + F_{xx} \sigma_x^2 + F_{yy} \sigma_y^2 + 2F_{xy} \sigma_x \sigma_y = 1 \quad (\text{A.48})$$

Assuming that σ_x and σ_y are applied in a ratio of a to b , then they can be written as

$$\sigma_x = a \sigma \quad \sigma_y = b \sigma \quad (\text{A.49})$$

By substituting Equation (A.48) into Equation (A.49) and solving for σ , we obtain

$$\sigma = \frac{-B + \sqrt{B^2 + 4A}}{2A}, \quad (\text{A.50})$$

where

$$\begin{aligned} A &= \frac{a^2}{X_\phi X'_\phi} + \frac{b^2}{Y_\phi Y'_\phi} + 2F_{xy} ab \\ B &= a \left(\frac{1}{X_\phi} - \frac{1}{X'_\phi} \right) + b \left(\frac{1}{Y_\phi} - \frac{1}{Y'_\phi} \right) \end{aligned} \quad (\text{A.51})$$

The term F_{xy} has been given in Equation (A.51a); X'_i and Y'_i ($i = \text{blank or } \prime$) have been given in Equations (A.31) and (A.43), respectively. Substitution of Equation (A.50) into Equation (A.49) gives the allowable stresses σ_x and σ_y .

Other Criteria

Christensen (1988) developed a three-dimensional failure criterion from the consideration of tensor transformation. Most recently, Feng (1991) also developed a three-dimensional failure criterion in terms of strain invariants. These are interesting theoretical works. However, the agreement of these theories with experimental data cannot be judged without sufficient comparisons.

Failure Criteria in the Presence of Stress Gradient

Many models have been developed to predict the notched strength of laminated composites. Most of these models are developed for tensile loading. A laminated

composite containing a cutout normally goes through a very complicated damage process before it reaches the ultimate failure. Therefore, all the failure models contain a number of approximations and assumptions to make the problem solvable. If we trace these models to their original principles, some failure criteria could be identified. These may be classified as the failure criteria in the presence of stress gradient. A brief description is given in the following for those criteria which are widely accepted.

Fracture Mechanics Criterion

Wu (1968) found that under certain conditions the techniques of isotropic fracture mechanics can be directly applied to composite materials. These conditions are:

- 1) The orientation of the flaw with respect to the principal axis of symmetry must be fixed.
- 2) The stress intensity factors defined for the anisotropic cases must be consistent with the isotropic case in stress distribution and in crack displacement modes.
- 3) The critical orientation coincides with one of the principal directions of elastic symmetry.

It has been shown that unidirectional materials satisfy these restrictive conditions. However, advanced composites in use today are at least bidirectional. This suggests that fracture mechanics are not suitable for use in multidirectional laminates since they do not satisfy the restrictive conditions stated above. In addition, unlike isotropic materials, the failure mechanisms of multidirectional laminates are very complicated. They involve many

microcracks around the cutout, with different crack densities at different locations. This mechanism also varies from ply to ply. Furthermore, delamination could occur between two adjacent plies. Strictly speaking, fracture mechanics may only be applicable to unidirectional laminates.

Waddoups-Eisenmann-Kaminski Criterion

Waddoups et al. (1971) considered a laminate containing either a hole or a crack. In the first case, they used the relationship between the energy release rate G_I and the stress intensity factor K_I developed by Irwin (1948):

$$G_I = \frac{(1 - \nu)\pi}{2G} K_I^2 = \frac{(1 - \nu^2)\pi}{E} K_I^2 \quad (\text{A.52})$$

based on a plane strain Mode I crack. They assume that regions of intense energy of length, a , are developed at the edges of the hole in a direction transverse to the loading direction. From our viewpoint, regions of intense energy do exist because of the stress concentrations. They further assume that the characteristic length, a , is small. For isotropic and homogeneous material, the problem of symmetrical cracks emanating from a circular hole of radius R has been solved by Bowie (1956). Also from the work of Paris and Sih (1965)

$$K_I = \bar{\sigma} \sqrt{\pi a} f(a/R) \quad (\text{A.53})$$

where $\bar{\sigma}$ and R denote the respective remote applied stress and the hole radius. Combining equations (A.52) and (A.53) and assuming that changes in a are negligibly small compared to changes in r or $f(a/R)$, we obtain

$$\sqrt{G_I} \left(\pi \sqrt{\frac{a(1-\nu^2)}{E}} \right)^{-1} = \bar{\sigma} f(a/R) \cong \text{const} \quad (\text{A.54})$$

At failure, the notched strength of the composite can be obtained by substituting the applied stress $\bar{\sigma}$ by σ_N^∞ in equation (A.53) and the result is

$$\sigma_N^\infty = \frac{K_{IC}}{\sqrt{\pi a} f(a/R)} \quad (\text{A.55})$$

The strength of a specimen with no hole can be obtained from equation (A.55) by letting R approach 0,

$$\sigma_0 = \sigma_N^\infty \Big|_{a/R \rightarrow \infty} = \frac{K_{IC}}{\sqrt{\pi a} (1.00)} \quad (\text{A.56})$$

Combining Equations (A.55) and (A.56) yields the following notched strength ratio:

$$\frac{\sigma_N^\infty}{\sigma_0} = \frac{1}{f(a/R)} \quad (\text{A.57})$$

This approach has also been applied to composites containing a straight crack. The stress intensity factor of an isotropic material containing a crack of length $2c$ is given by Griffith (1920):

$$K_I = \bar{\sigma} \sqrt{\pi c} \quad (\text{A.58})$$

Again, intense energy regions are assumed to exist at the crack tips. This approach is similar to Irwin's (*op. cit.*) plastic zone correction in metals. At failure, the critical stress intensity factor is

$$K_{IC} = \sigma_N^\infty \sqrt{\pi(c+a)}, \quad (\text{A.59})$$

where a and $(c + a)$ are the crack tip damage zone and the effective crack length, respectively. For unnotched specimens, the unnotched strengths can be obtained from Equation (A.59):

$$K_{IC} = \sigma_0 \sqrt{\pi a} \quad (\text{A.60})$$

One can see from this equation that a can be regarded as the half crack length of an *inherent flaw*. Combining Equations (A.59) and (A.60) results in

$$\frac{\sigma_N^\infty}{\sigma_0} = \sqrt{\frac{a}{c + a}} \quad (\text{A.61})$$

This criterion involves two unknowns: the unnotched strength and the length of the intense energy region (or characteristic length). These unknowns have to be determined empirically using experimental data. The criterion is valid for unidirectional laminates.

Mar-Lin Approach

Mar and Lin (*op. cit.*) assume that the notched strength of an orthotropic plate has a form similar to Equation (A.58). However, they replace the K_{IC} by H_C (composite fracture toughness) and the power term $1/2$ by n . They noted that the exponent n is “the order of the singularity of a crack with its tip at the interface of two different materials.” The two different materials refer to fiber and matrix. The coefficients of H_C and n are determined by plotting the data on a log-log scale. Good correlation was obtained between the experimental data and the prediction.

Stress Failure Criteria

Whitney and Nuismer (1974) developed a point stress and an average stress criterion for the notched strength prediction of laminated composites under uniaxial tension. These two stress criteria use the stress field to predict the notched strength without resorting to the classical concepts of linear elastic fracture mechanics. The development of these stress failure criteria is based on the observation of the stress fields around a hole with two different sizes. The stress distribution of an isotropic plate containing a circular hole (1979) is given in the following

$$\frac{\sigma_y}{\bar{\sigma}} = 1 + \frac{1}{2} \left(\frac{R}{x} \right)^2 + \frac{3}{2} \left(\frac{R}{x} \right)^4, \quad (\text{A.62})$$

where $\bar{\sigma}$ is the applied stress parallel to the y -axis at infinity and R denotes the hole radius. If the normalized stress is plotted as a function of the distance ahead of the hole ($x - R$), the stress concentration is much more localized for the smaller size hole. From these stress distributions Whitney and Nuismer proposed the following stress failure criteria.

Point Stress Criterion

Point stress failure criterion assumes that failure occurs when the stress, σ_y , over some distance, d_0 , away from the opening is equal to or greater than the strength of the unnotched laminate:

$$\sigma_y(x,0) \Big|_{x=R+d_0} = \sigma_0 \quad (\text{A.63})$$

Because the stress concentration factors at the point $(d_0, 0)$ are different for different hole sizes, this approach apparently can predict the hole size effect on the notched strength.

For infinite orthotropic plates containing a circular hole, the approximate solution of

stress distribution (Konish and Whitney, 1975) along the axis perpendicular to the loading direction is:

$$\sigma_y(x,0) = \frac{\bar{\sigma}}{2} \left\{ 2 + \left(\frac{R}{x}\right)^2 + 3\left(\frac{R}{x}\right)^4 - (K_T^\infty - 3) \left[5\left(\frac{R}{x}\right)^6 - 7\left(\frac{R}{x}\right)^8 \right] \right\}$$

$$x > R, \quad (\text{A.64})$$

where

$$K_T^\infty = 1 + \sqrt{\frac{2}{A_{22}} \left[\sqrt{A_{11}A_{22}} - A_{12} + \frac{A_{11}A_{22} - A_{12}^2}{2A_{66}} \right]}, \quad (\text{A.65})$$

and K_T^∞ denotes the stress concentration factor at the edge of the hole; A_{ij} , $i, j = 1, 2, 6$, are the components of the in-plane stiffness matrix with 1 and 2 parallel and transverse to the loading directions, respectively. Equation (A.65) can be written in terms of engineering constants as

$$K_T^\infty = 1 + \sqrt{2 \left[\sqrt{\frac{E_y}{E_x}} - \nu_{xy} \right] + \frac{E_y}{G_{xy}}}, \quad (\text{A.66})$$

where E_y and E_x are the laminate stiffnesses in the respective y - (loading) and x -direction; the variables ν_{xy} and G_{xy} are the Poisson's ratio and shear modulus, respectively. In the case of orthotropic plates containing a hole, Nuismer and Whitney (1975) obtained their point stress criterion by substituting Equation (A.64) into Equation (A.63) and the result is

$$\frac{\sigma_N^\infty}{\sigma_0} = \frac{2}{2 + \xi_1^2 + 3\xi_1^4 - (K_T^\infty - 3)(5\xi_1^6 + 7\xi_1^8)}, \quad (\text{A.67})$$

where

$$\xi_1 = \frac{R}{R + d_0} \quad (\text{A.68})$$

In the case of infinite orthotropic plate containing a straight crack, an exact elasticity solution is given by Lekhnitskii (1968):

$$\sigma_y = \frac{K_1 x}{\sqrt{\pi c(x^2 - c^2)}} = \frac{\bar{\sigma} x}{\sqrt{x^2 - c^2}} \quad (\text{A.69})$$

where c is the half length of the crack. Substituting Equation (A.69) into Equation (A.63) yields

$$\frac{\sigma_N^\infty}{\sigma_0} = \sqrt{1 - \xi_3^2}, \quad (\text{A.70})$$

where

$$\xi_3 = \frac{c}{c + d_0} \quad (\text{A.71})$$

Average Stress Criterion

A larger volume of material is subjected to high stress in the case of the plate containing the larger hole. Therefore, instead of considering the stress at a point, this criterion considers the average stress over a characteristic length. In other words, this criterion assumes that failure occurs when the average stress, $\bar{\sigma}_y$, over some distance, a_0 , away from the opening is equal to or greater than the strength of the unnotched laminate:

$$\frac{1}{a_0} \int_R^{R+a_0} \sigma_y(x,0) dx = \sigma_0 \quad (\text{A.72})$$

In the case of orthotropic plates containing a hole, the solution is obtained by substituting Equation (A.64) into Equation (A.72):

$$\frac{\sigma_N^\infty}{\sigma_0} = \frac{2(1 - \xi_2)}{2 - \xi_2^2 + 3\xi_2^4 - (K_T^\infty - 3)(\xi_2^6 - \xi_2^8)}, \quad (\text{A.73})$$

where

$$\xi_2 = \frac{R}{R + a_0} \quad (\text{A.74})$$

For orthotropic plates containing a crack, the solution is obtained by substituting Equation (A.69) into Equation (A.72) and is given in the following

$$\frac{\sigma_N^\infty}{\sigma_0} = \sqrt{\frac{1 - \xi_4}{1 + \xi_4}} \quad (\text{A.75})$$

where

$$\xi_4 = \frac{c}{c + a_0} \quad (\text{A.76})$$

The point stress criterion and the average stress criterion both contain two unknowns, i.e., the unnotched strength, σ_0 , and the characteristic length, d_0 or a_0 . These unknowns have to be determined experimentally. The procedure is to first obtain a set of unnotched and notched strengths from experiment. Then we substitute these data into either Equation (A.67) or Equation (A.73) in the case of a circular hole and solve for d_0 or a_0 . Assuming d_0 (or a_0) is a constant, the notched strength for a plate with a hole (or crack) with any other size can be predicted.

The use of the characteristic length can be explained as the inelastic, nonlinear material behavior and the imperfection of the hole so that the theoretical value of the maximum stress concentration may not be reached just before the laminate fails. These two criteria have drawn significant attention and have been widely used. They are very useful for structural designs under simple loading conditions.

However, many engineers use these criteria to predict the notched strength of multidirectional laminates. Under this circumstance, all the microdamage around the cutout is not taken into account. Although the effects of the microdamage may be absorbed in the characteristic length, the details of the failure mechanisms cannot be analyzed with this simplified approach. For this application, they should be regarded as point stress model and average stress model rather than failure criteria.

Point Strain and Average Strain Criteria

The failure criteria can also be predicted in terms of strains. The point strain failure criterion assumes that failure occurs when the strain, ε_y , over some distance, d_0 , away from the opening is equal to or greater than the strength of the unnotched laminate:

$$\varepsilon_y(x,0) \Big|_{x=R+d_0} = \varepsilon_0 \quad (\text{A.77})$$

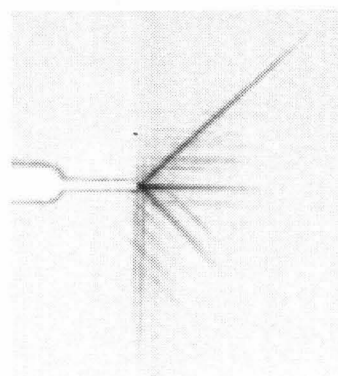
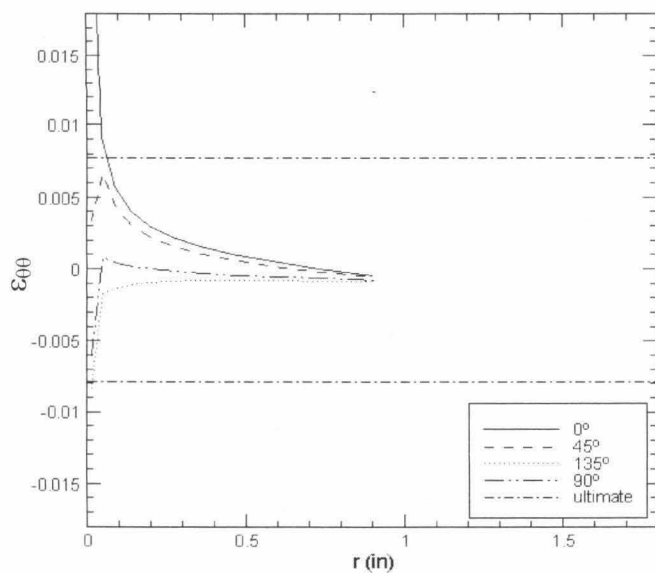
The average strain failure criterion assumes that failure is not due to the strain at a point. Instead, failure is caused by the strain over a volume of materials. In other words, average strain criterion assumes that failure occurs when the average strain, ε_y , over some distance, a_0 , away from the opening is equal to or greater than the strength of the unnotched laminate:

$$\frac{1}{a_0} \int_R^{R+a_0} \varepsilon_y(x,0) dx = \varepsilon_0 \quad (\text{A.78})$$

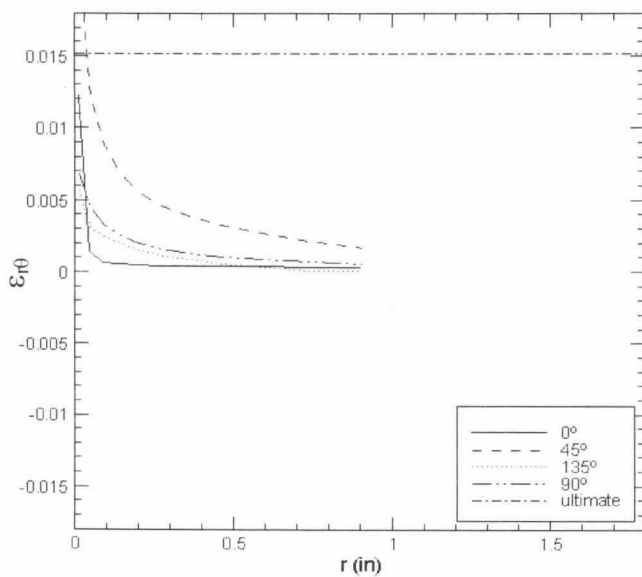
Some Additional Considerations

In the cases where stress gradients exist, very few failure criteria have been developed for composite materials. Strictly speaking, the criterion of Waddoups Eisenmann-Kaminski, the Whitney-Nuismer's point stress, and the average stress criteria as well as the point strain and the average strain criteria are only valid for unidirectional composites. These criteria have been widely used to predict the notched strength of laminated composites with very good results. They should be considered as models rather than failure criteria because they do not take into account the details of the complex failure mechanisms.

STRAIN DISTRIBUTIONS AT DAMAGE INITIATION

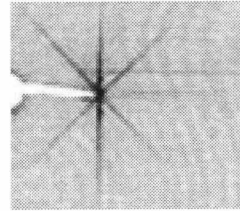
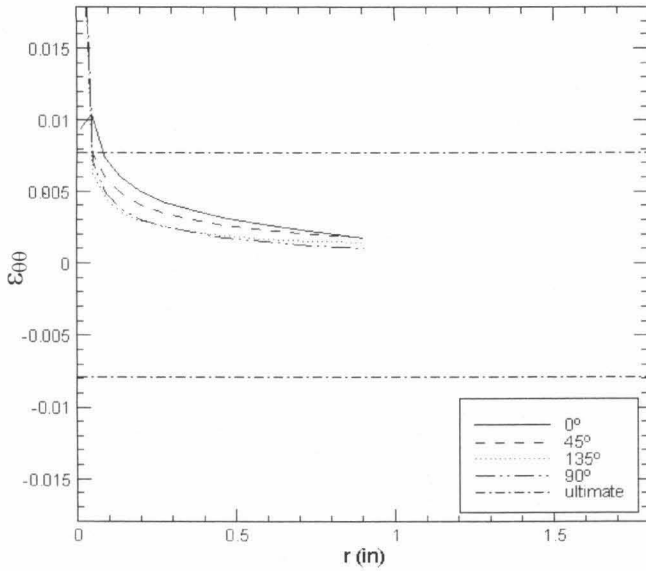
SMALL PANEL (6" × 6")**Parallel (Load = 2,810 lb)**

0.5"

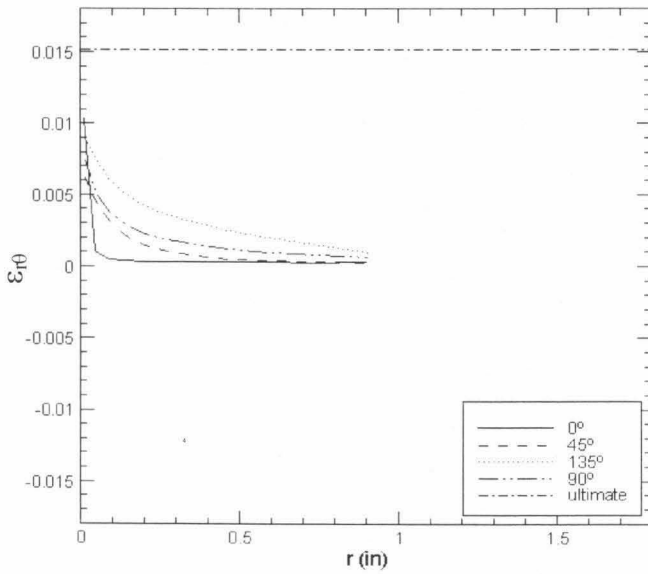


SMALL PANEL (6" × 6")

Perpendicular (Load = 2,794 lb)

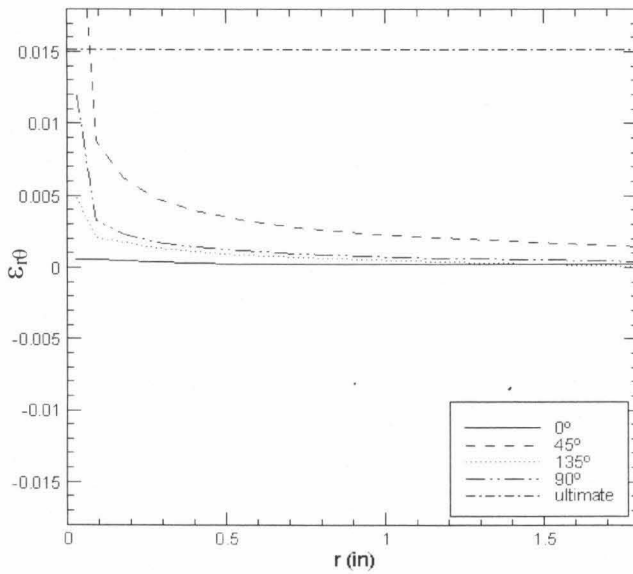
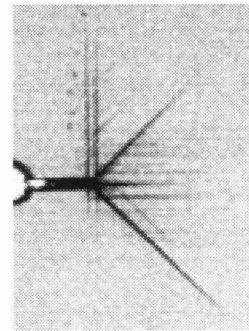
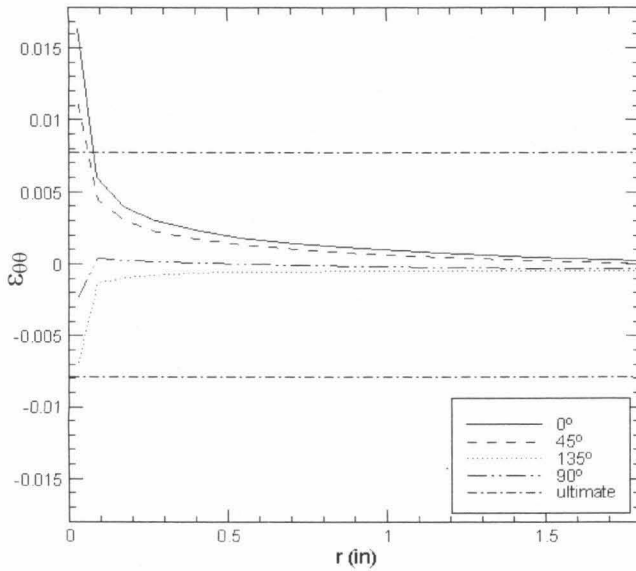


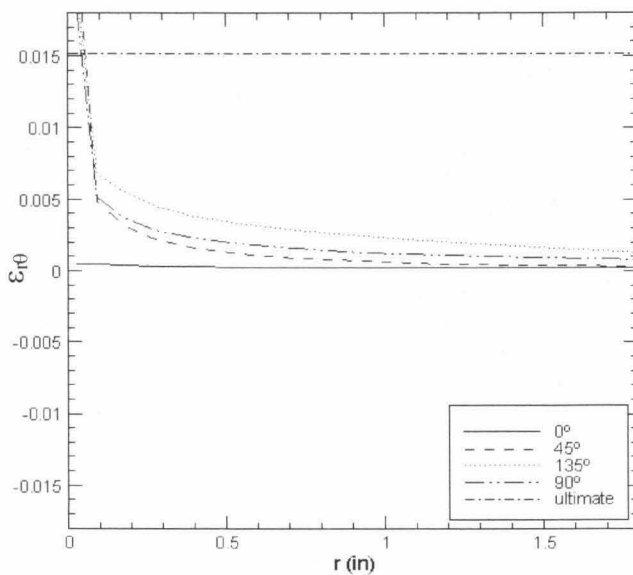
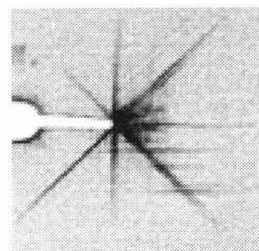
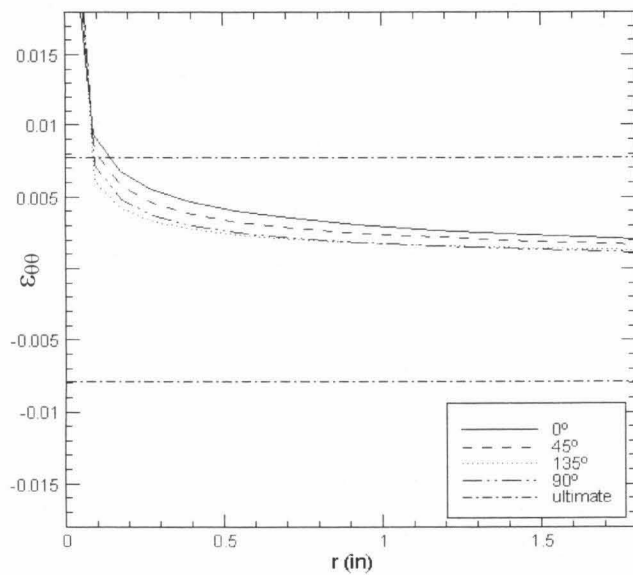
0.25"



MEDIUM PANEL (12" × 12")

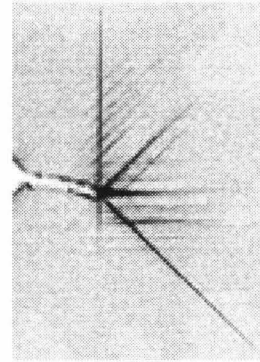
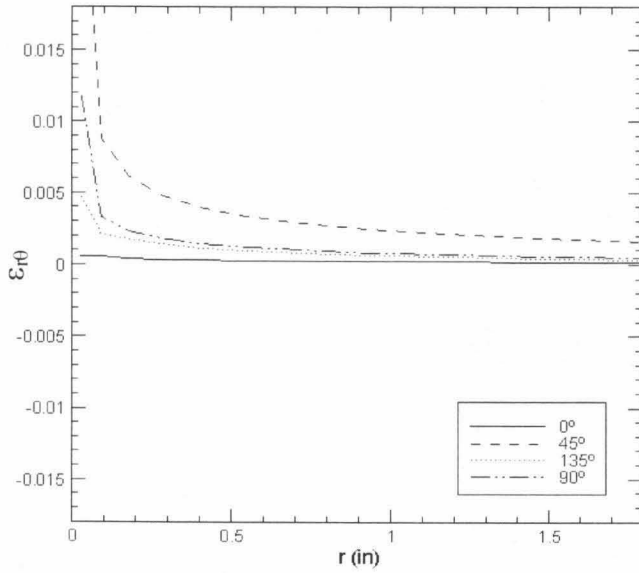
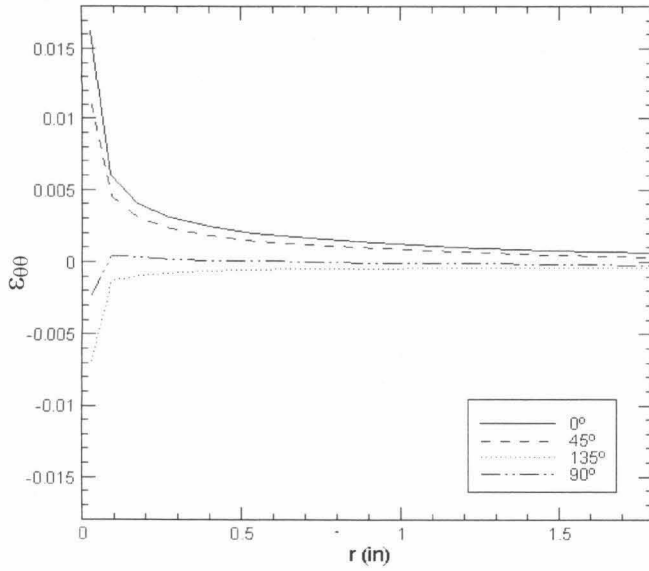
Parallel (Load = 2,852 lb)



MEDIUM PANEL (12" × 12")**Perpendicular (Load = 4,605 lb)**

LARGE PANEL (18" × 18")

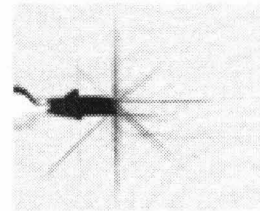
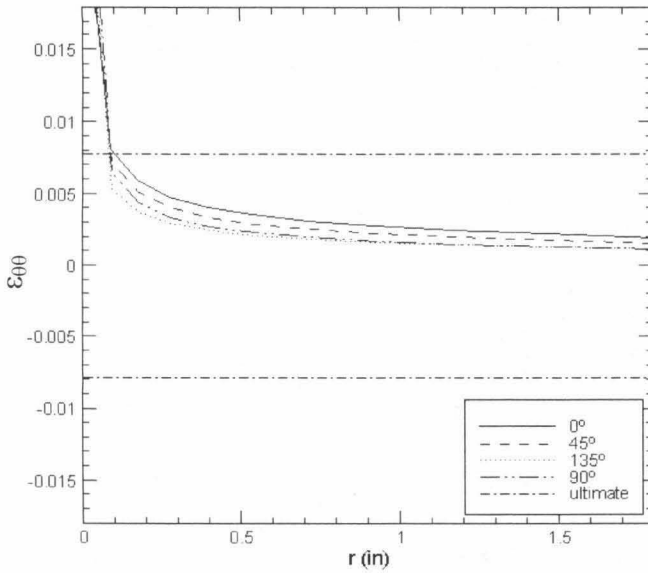
Parallel (Load = 3,502 lb)



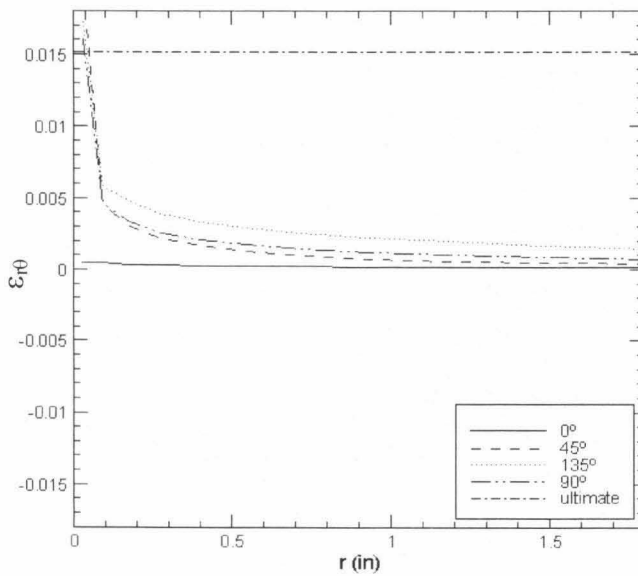
0.25"

LARGE PANEL (18" × 18")

Perpendicular (Load = 5,094 lb)



0.25"



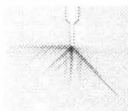
**X-RAY INSPECTION OF THE INTERNAL
DAMAGE PROGRESSION**

Panel Size: 6" x 6"

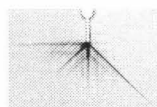
θ :Parallel

Test id. no.: 3

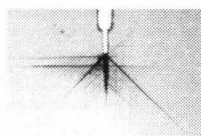
2564.6 lb



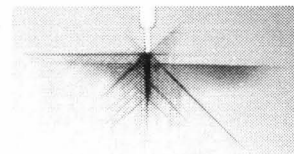
2810.8 lb



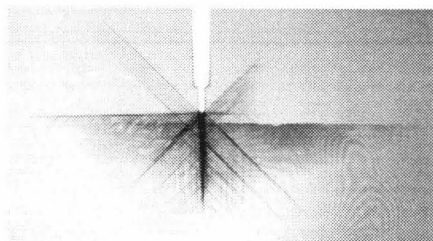
3643.44 lb



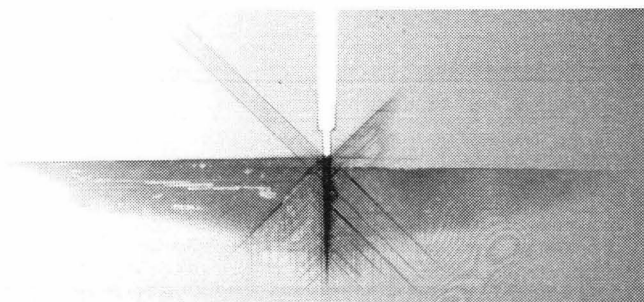
4202.2 lb



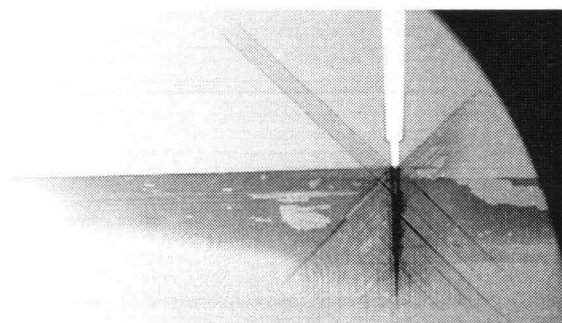
4733.1 lb



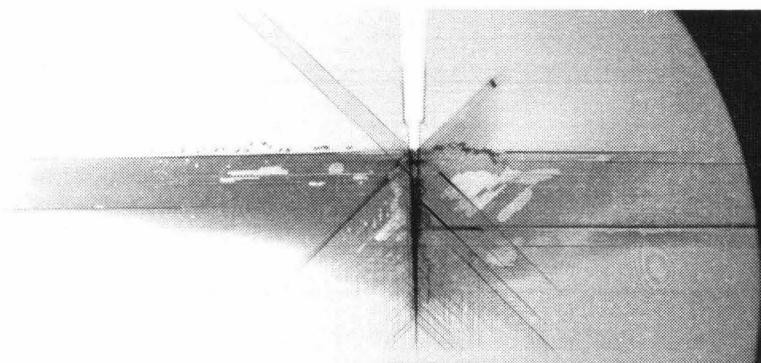
5040.5 lb



5163.4 lb



5319.9 lb



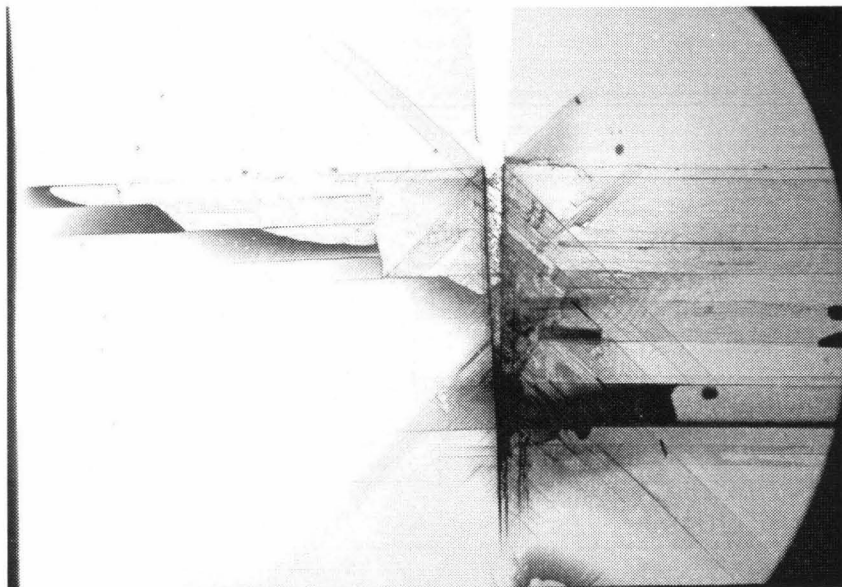
(True scale)

Panel Size: 6" x 6"

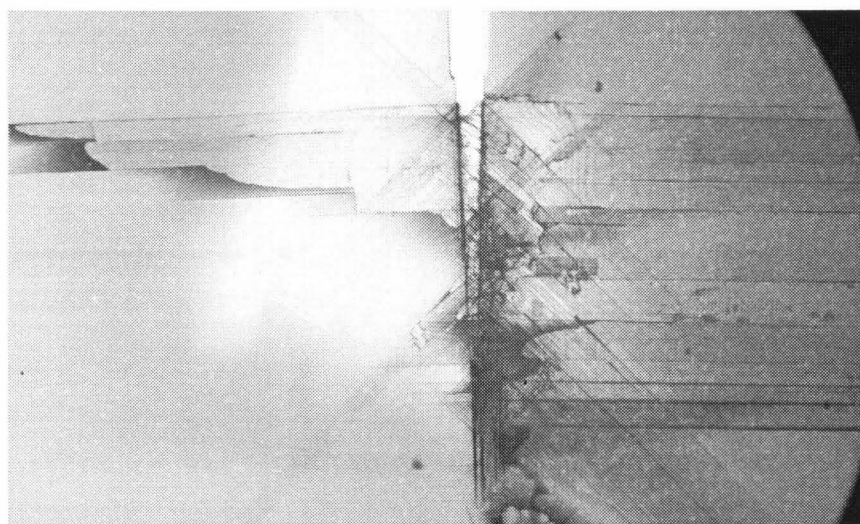
θ :Parallel

Test id. no.: 3

4677.2 lb



1430.5 lb



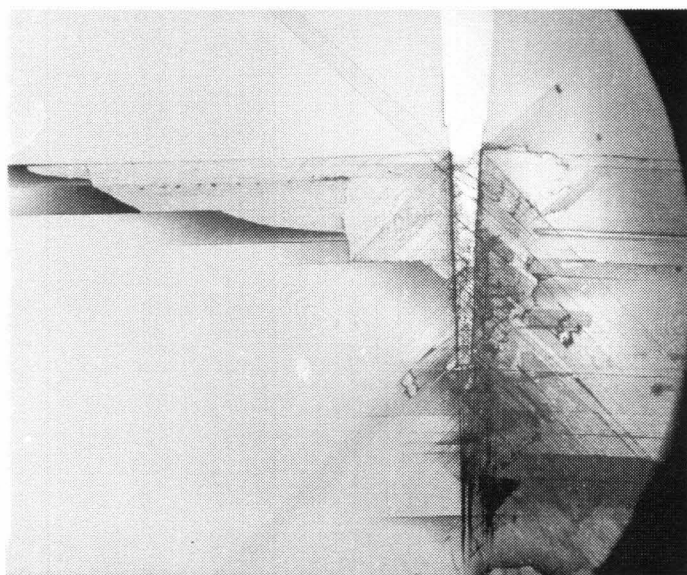
(True scale)

Panel Size: 6" x 6"

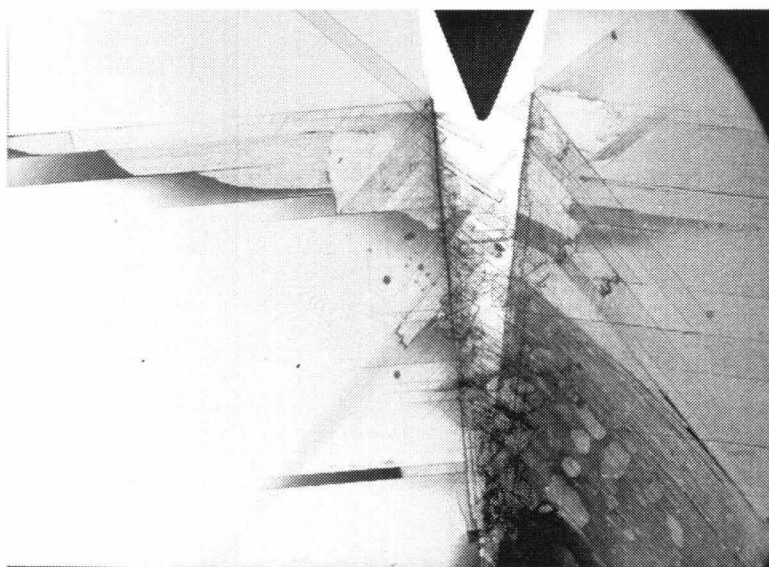
θ :Parallel

Test id. no.: 3

709.7 lb



~ 50 lb



(True scale)

Panel Size: 6" x 6"

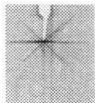
θ : Perpendicular

Test id. no.: 4

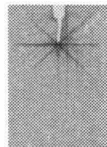
3408.7 lb



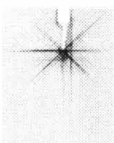
3878.1 lb



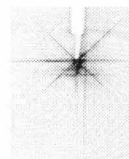
4045.8 lb



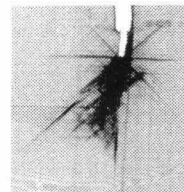
4565.5 lb



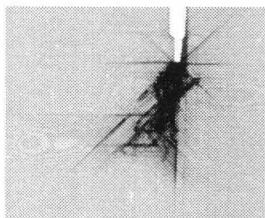
4889.6 lb



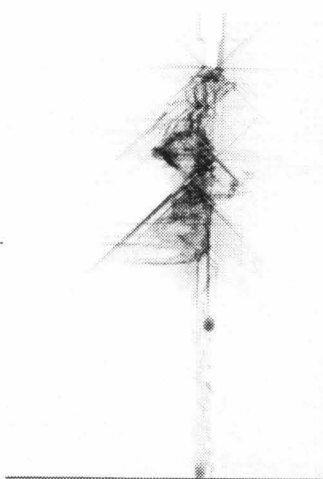
5074.0 lb



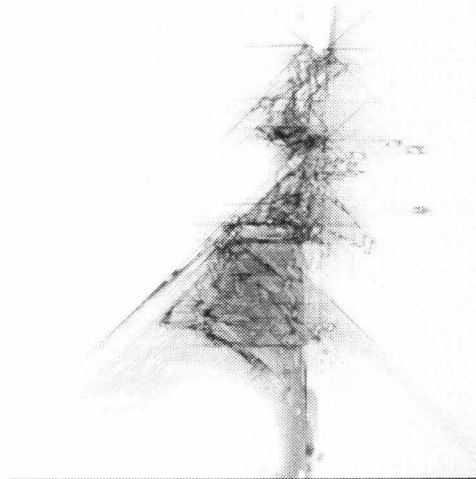
4772.2 lb



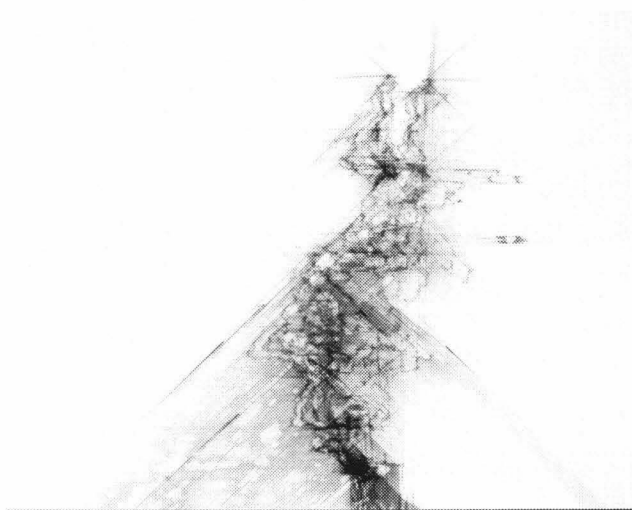
5135.5 lb



4241.4 lb



2386.1 lb



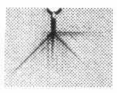
(True scale)

Panel Size: 12" x 12"

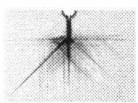
θ : Parallel

Test id. no.: 7

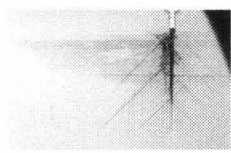
2865.5 lb



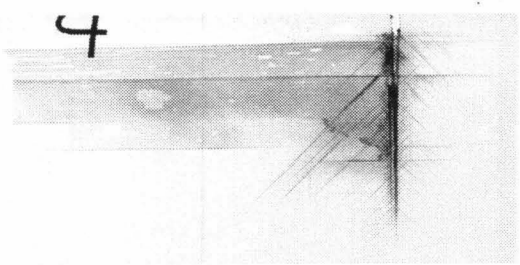
3502.3 lb



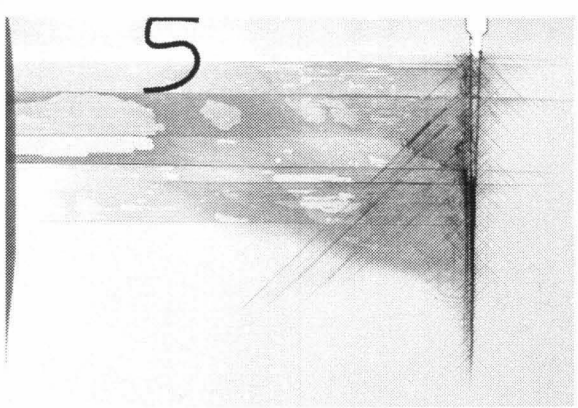
4139.1 lb



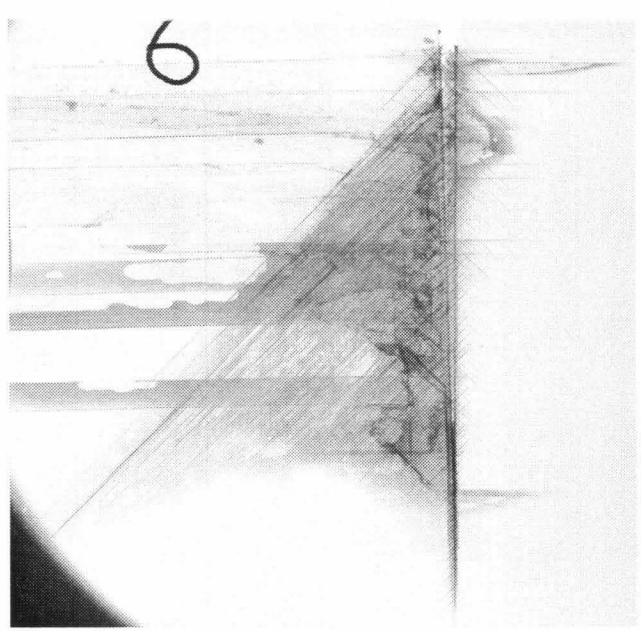
5412.7 lb



6208.6 lb



6845.4 lb

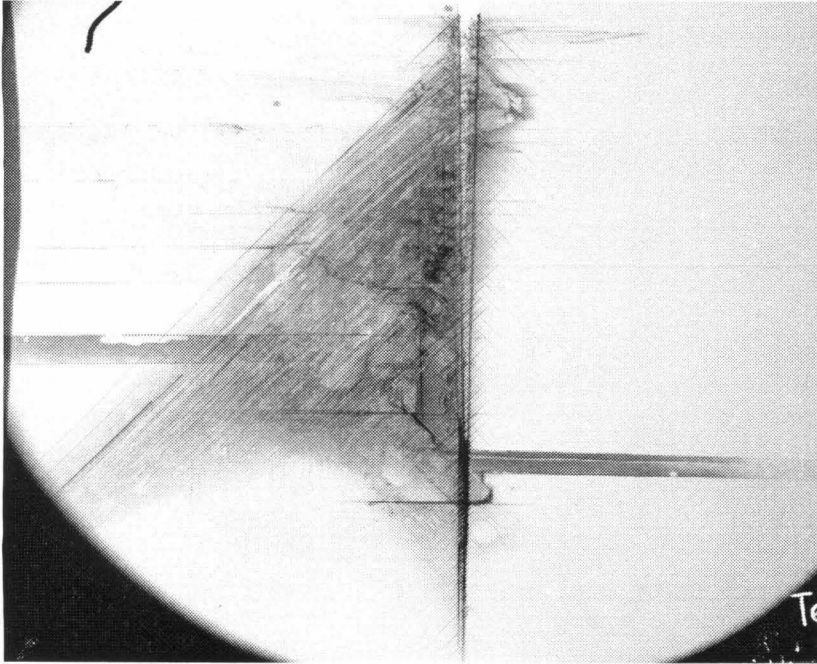


(True scale)

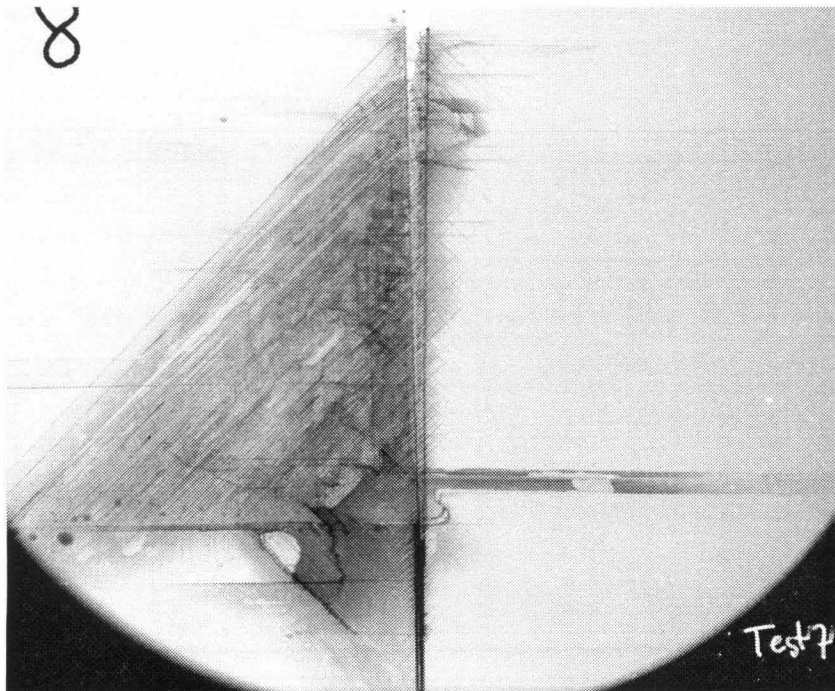
Panel Size: 12" x 12"

θ : Parallel

Test id. no.: 7



5094.3 lb



4616.7 lb

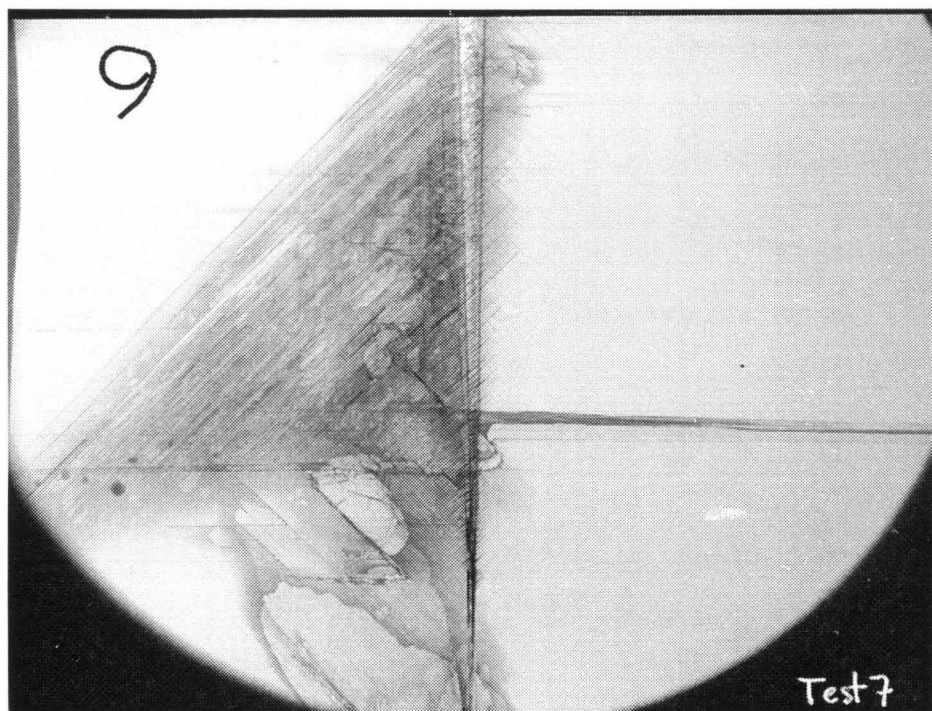
(True scale)

Panel Size: 12" x 12"

θ : Parallel

Test id. no.: 7

3979.9 lb



(True scale)

Panel Size: 12" x 12"

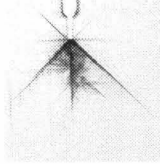
θ : Perpendicular

Test id. no.: 8

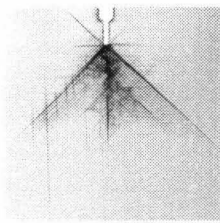
4616.7 lb



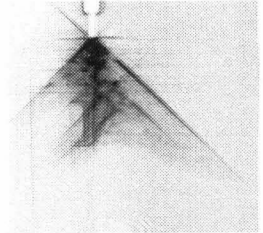
5094.3 lb



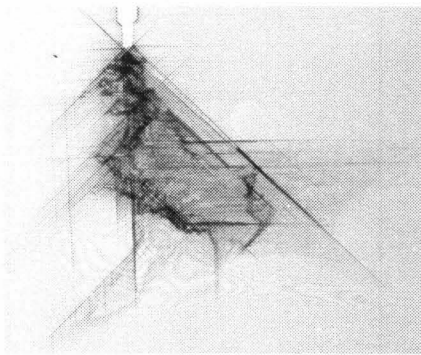
5412.7 lb



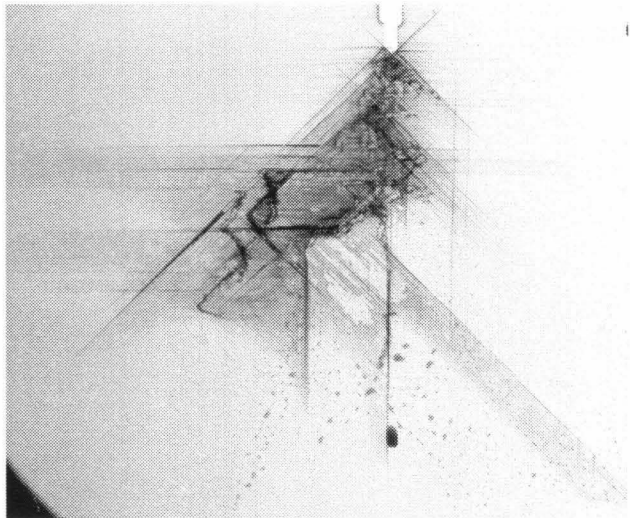
5731.1 lb



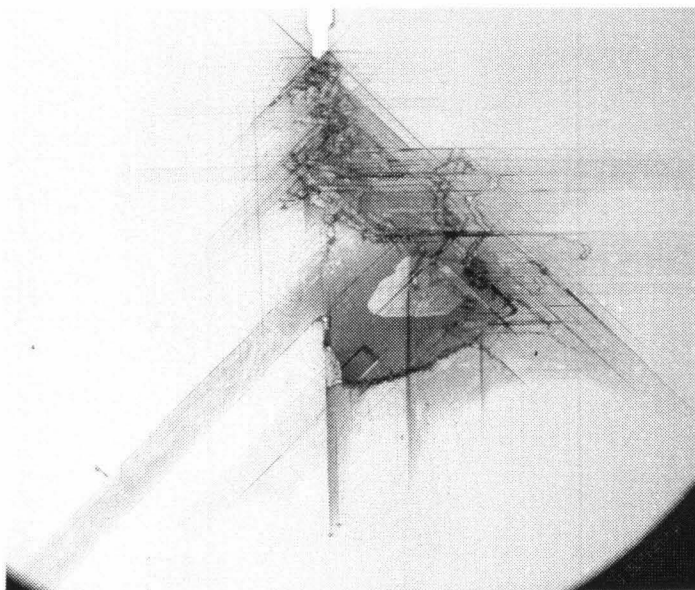
6845.4 lb



6686.2 lb



6686.2 lb



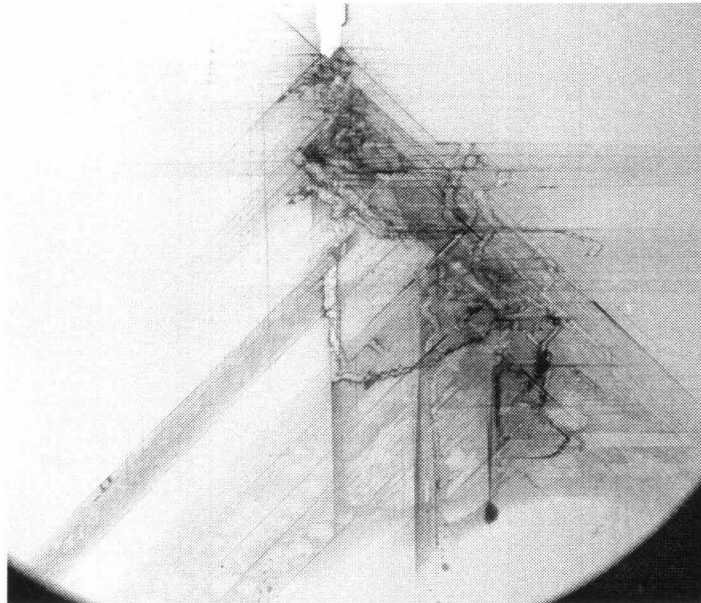
(True scale)

Panel Size: 12" x 12"

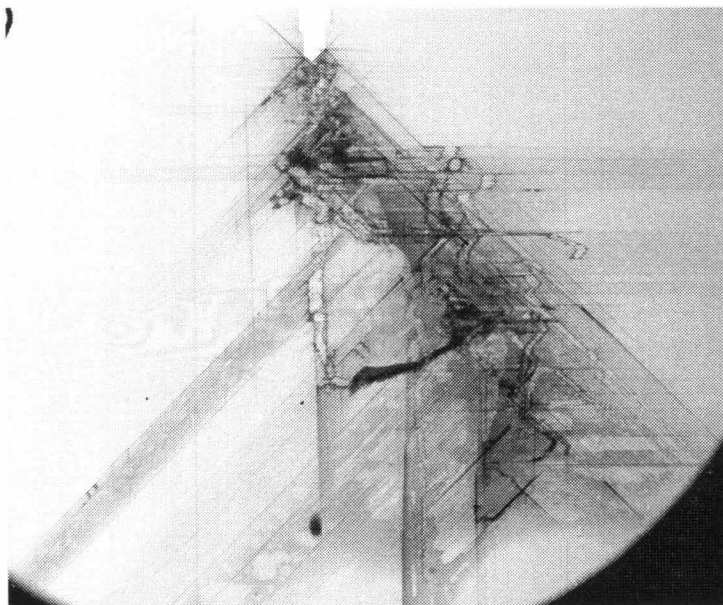
θ : Perpendicular

Test id. no.: 8

6367.8 lb



5571.9 lb



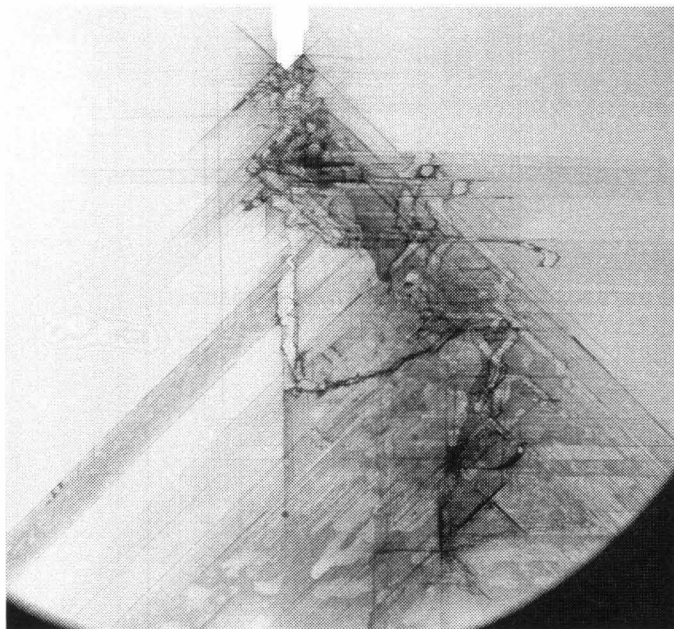
(True scale)

Panel Size: 12" x 12"

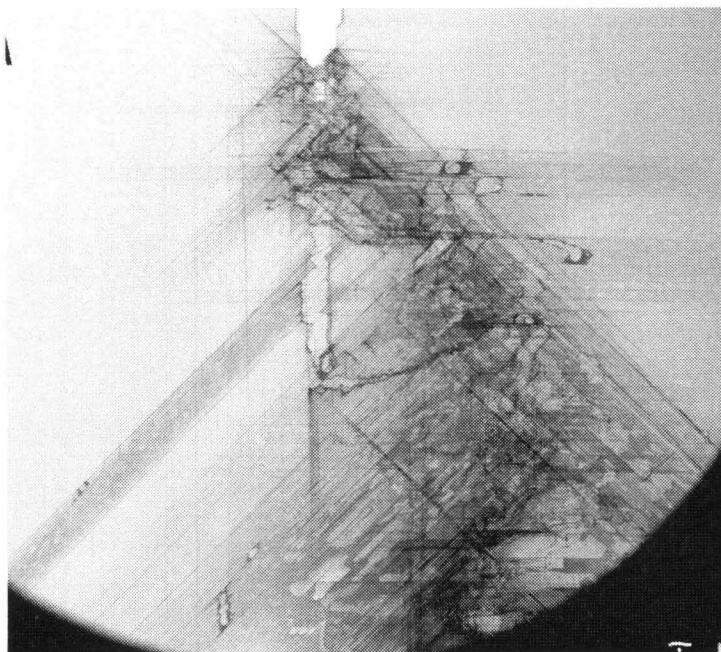
θ : Perpendicular

Test id. no.: 8

5731.1 lb



5412.7 lb



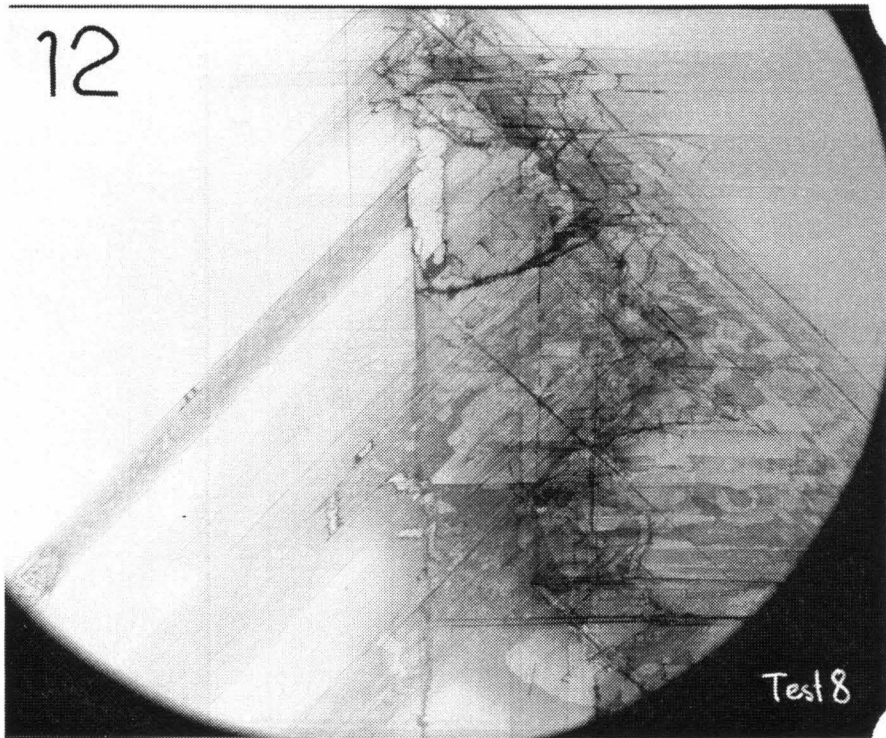
(True scale)

Panel Size: 12" x 12"

θ : Perpendicular

Test id. no.: 8

3343.1 lb



(True scale)

Panel Size: 18" x 18"

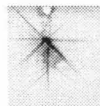
θ : Perpendicular

Test id. no.: 9

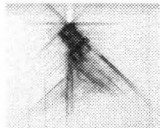
5253.5 lb



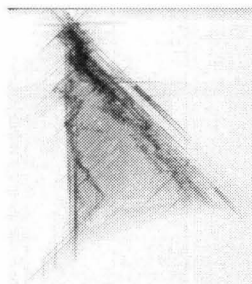
5731.1 lb



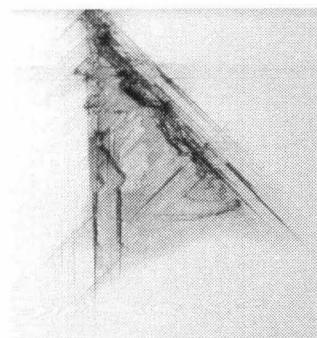
6208.7 lb



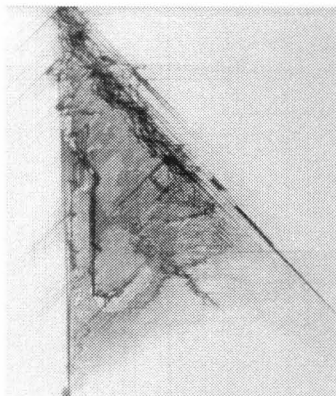
7482.2 lb



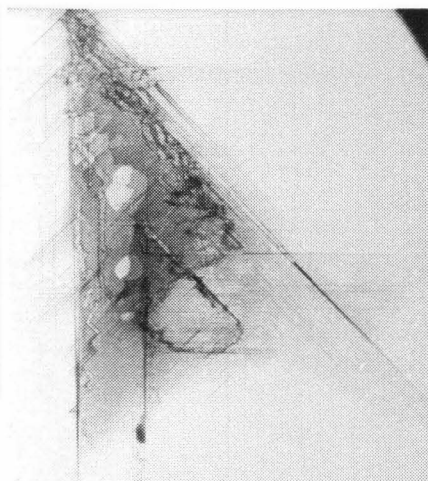
7323.0 lb



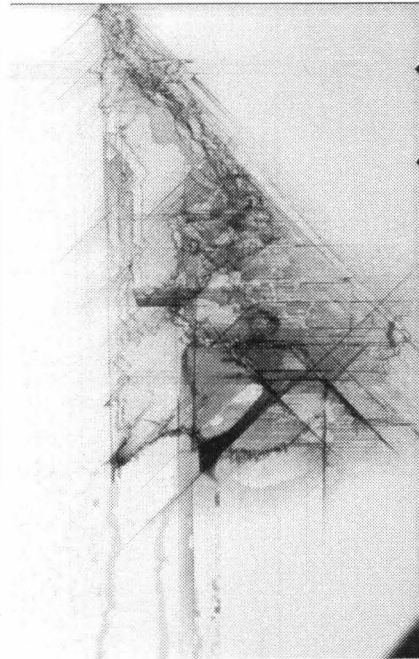
7641.4 lb



7800.6 lb



7163.8 lb



(True scale)

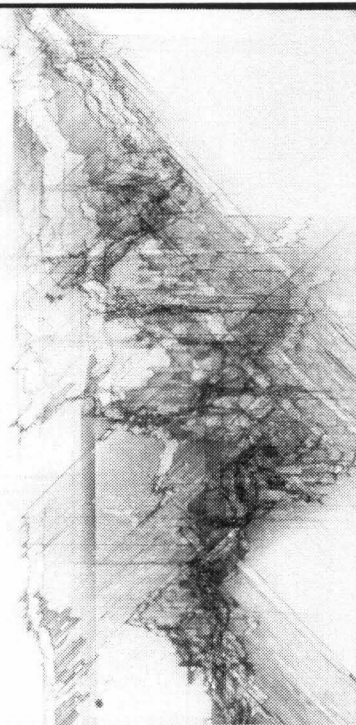
Panel Size: 18" x 18"

θ : Perpendicular

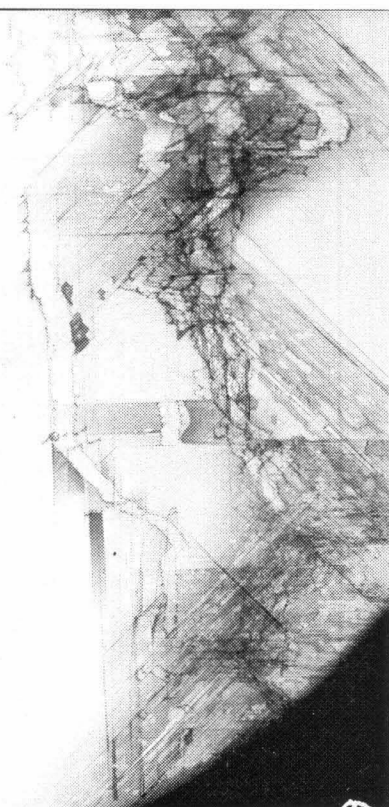
Test id. no.: 9



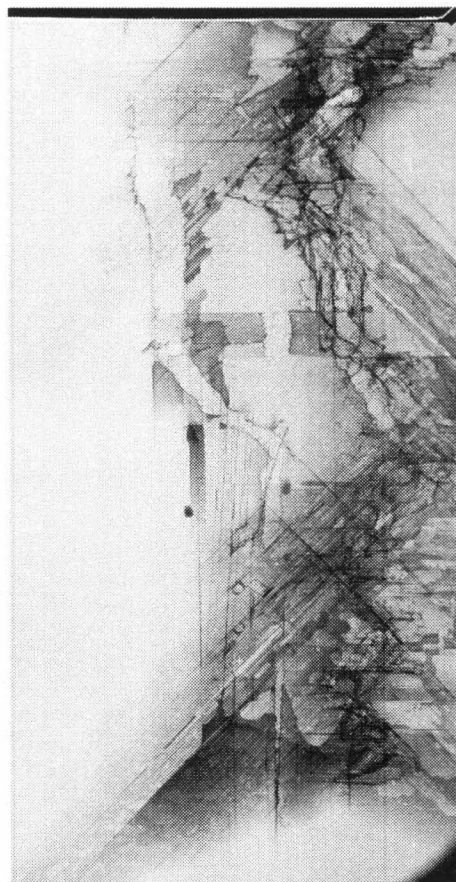
6049.5 lb



3979.9 lb



2547.1 lb



955.2 lb

(True scale)

There are no pages 154-156.

Panel Size: 18" x 18"

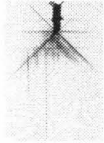
θ : Perpendicular

Test id. no.: 11

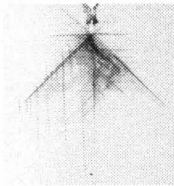
5094.3 lb



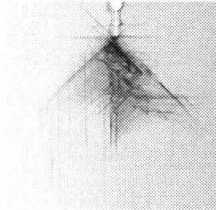
5731.1 lb



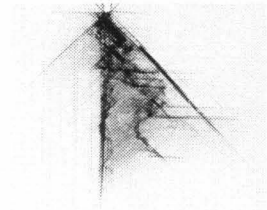
6367.8 lb



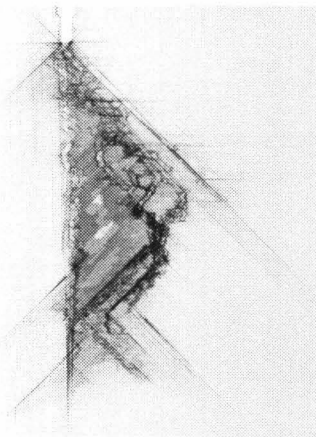
6845.4 lb



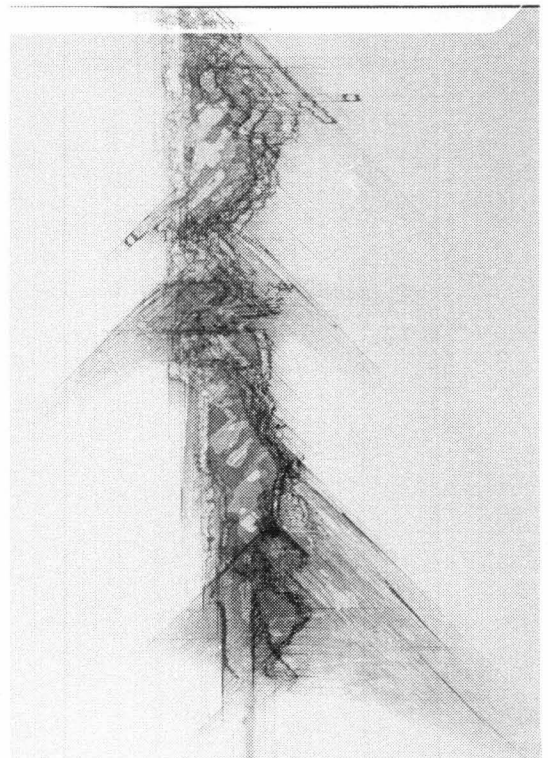
7323.0 lb



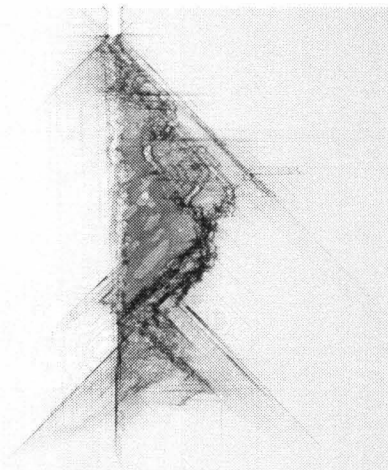
7959.8 lb



7163.8 lb



6527.0 lb



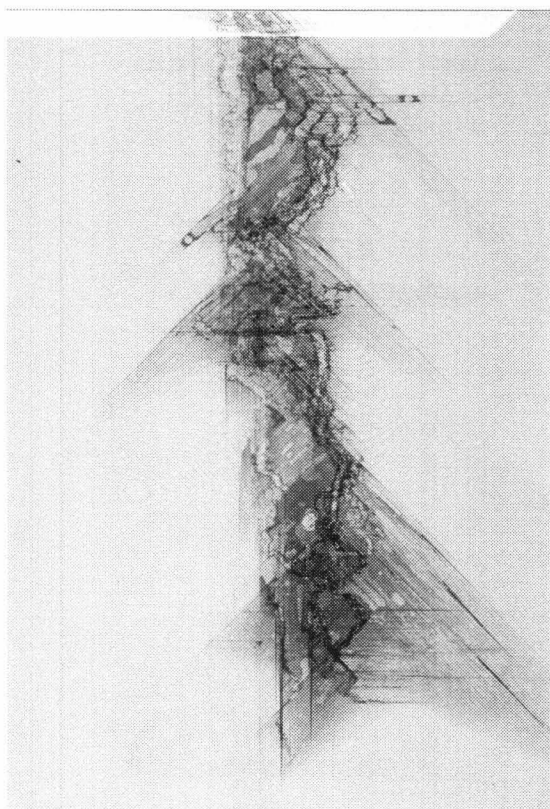
(True scale)

Panel Size: 18" x 18"

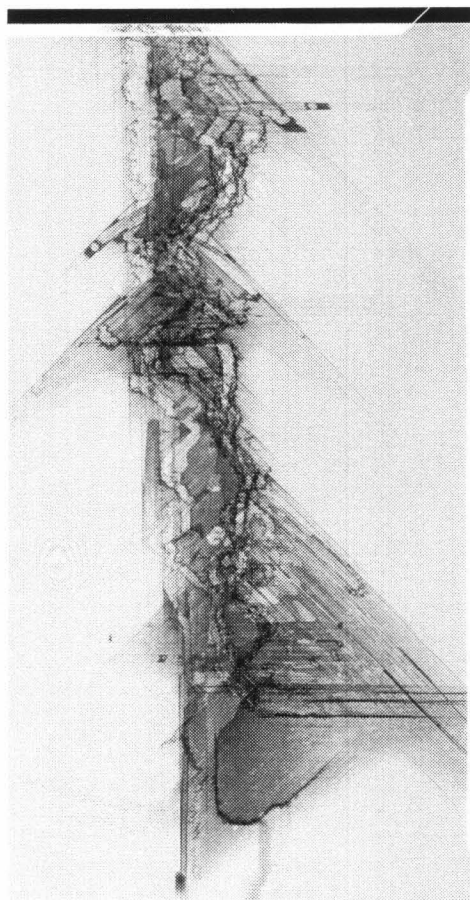
θ : Perpendicular

Test id. no.: 11

3979.9 lb



4298.3 lb



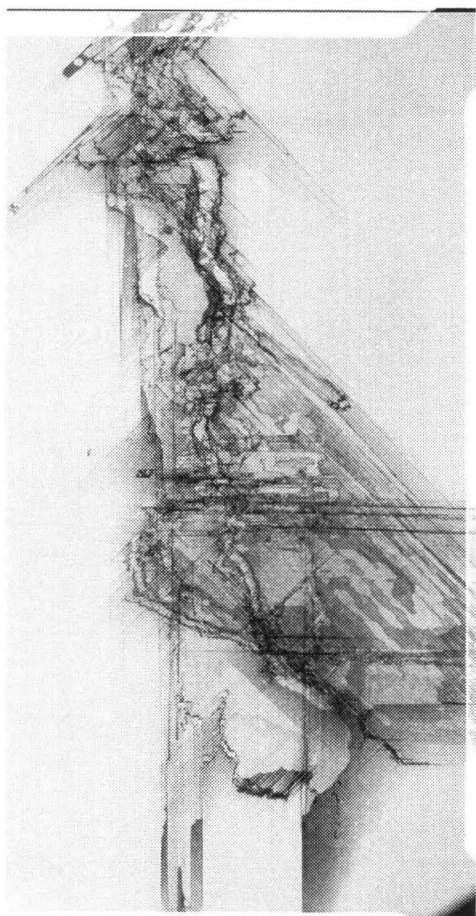
(True scale)

Panel Size: 18" x 18"

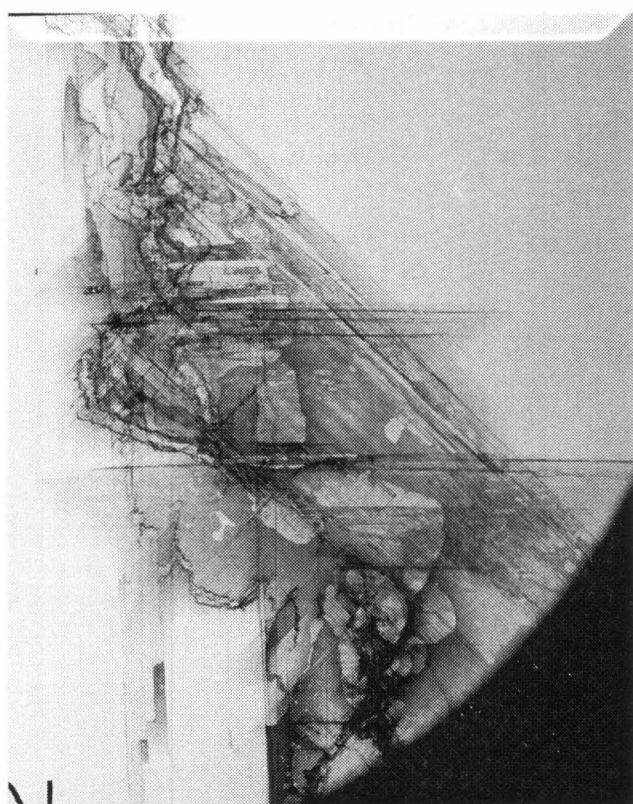
θ : Perpendicular

Test id. no.: 11

4616.7 lb



3343.1 lb



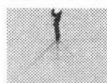
(True scale)

Panel Size: 18" x 18"

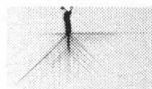
θ : Parallel

Test id. no.: 12

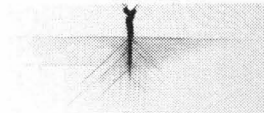
3820.7 lb



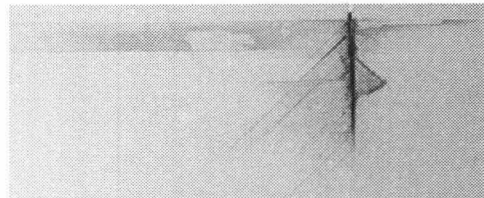
4457.5 lb



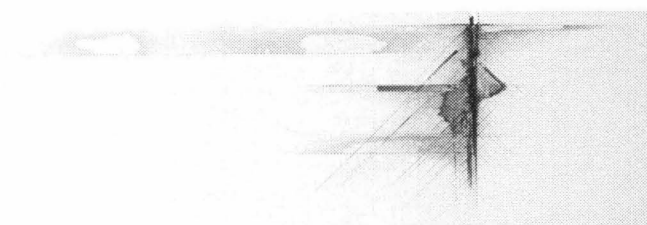
5094.3 lb



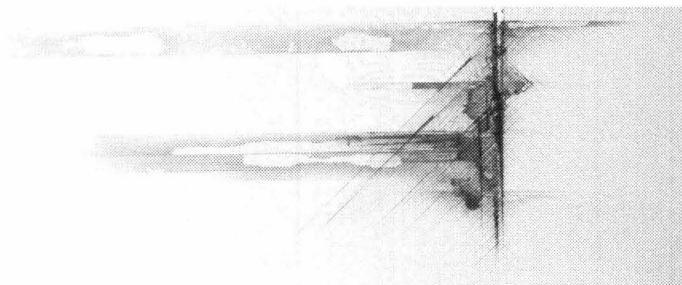
5731.1 lb



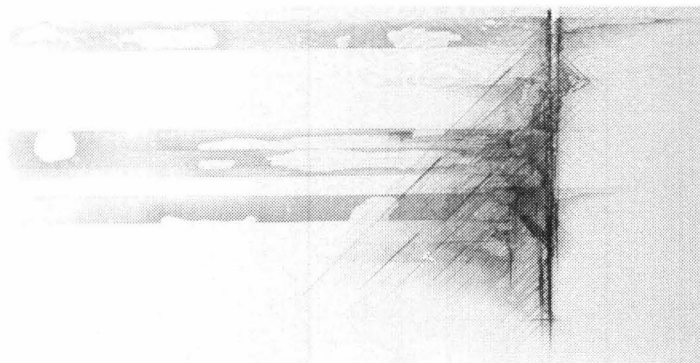
6367.8 lb



7163.8 lb



7323.0 lb



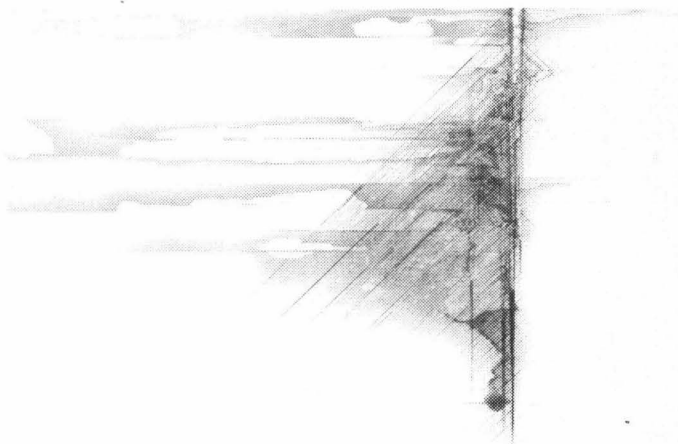
(True scale)

Panel Size: 18" x 18"

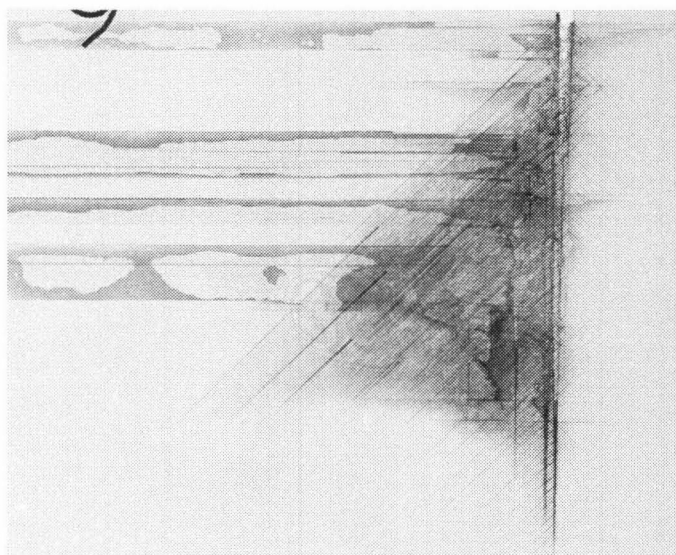
θ : Parallel

Test id. no.: 12

7482.2 lb



7800.6 lb



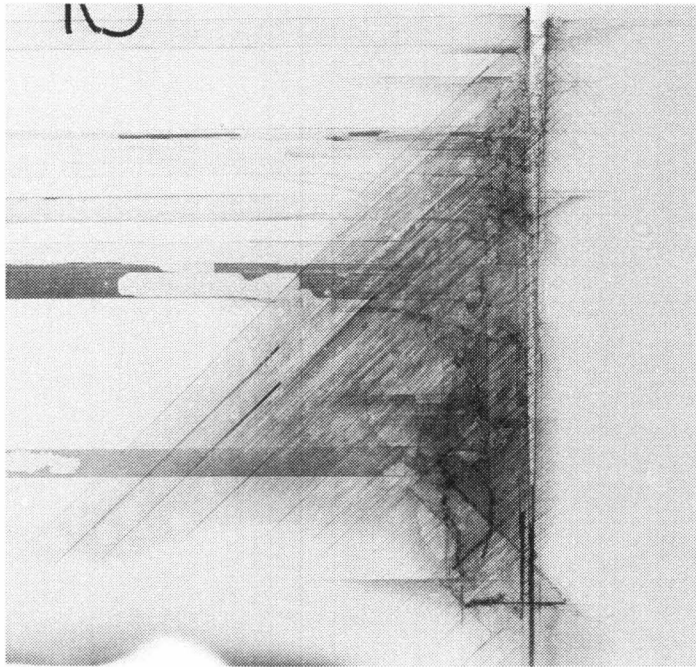
(True scale)

Panel Size: 18" x 18"

θ : Parallel

Test id. no.: 12

7959.8 lb



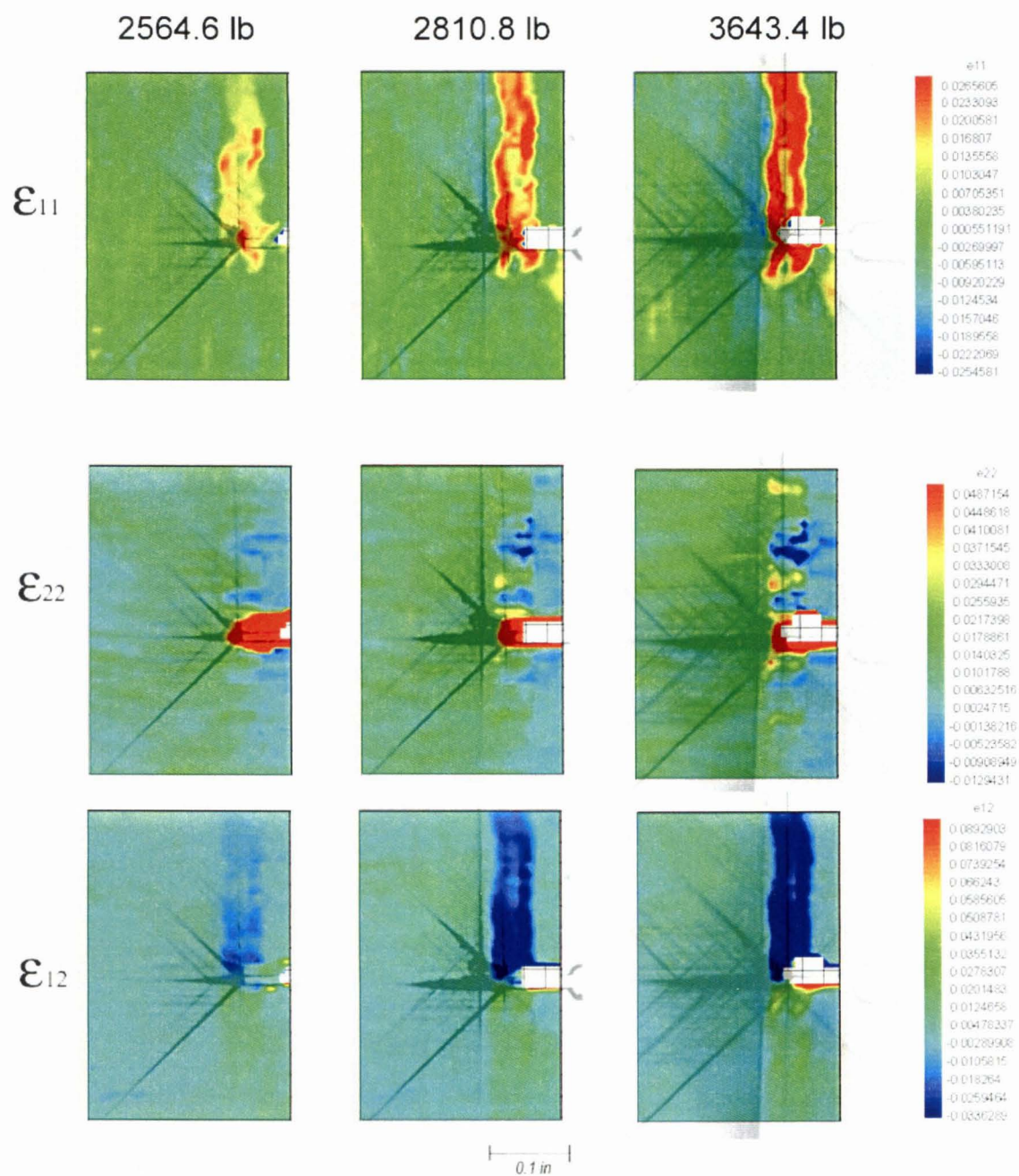
(True scale)

SURFACE STRAIN FIELDS ON X-RAY IMAGES OF
INTERNAL DAMAGE

Panel Size: 6" x 6"

 θ : Parallel

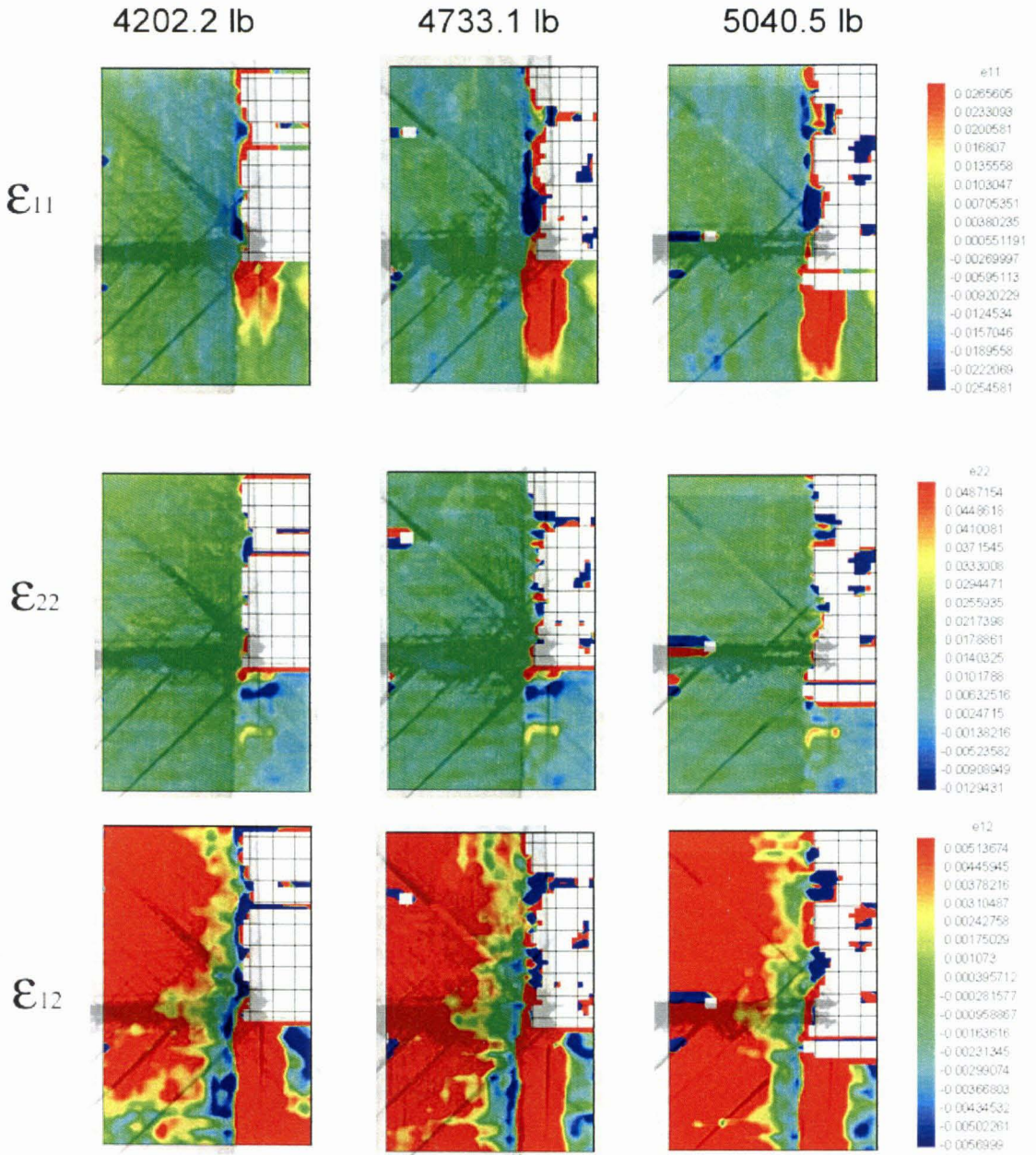
Test id. no.: 3



Panel Size: 6" x 6"

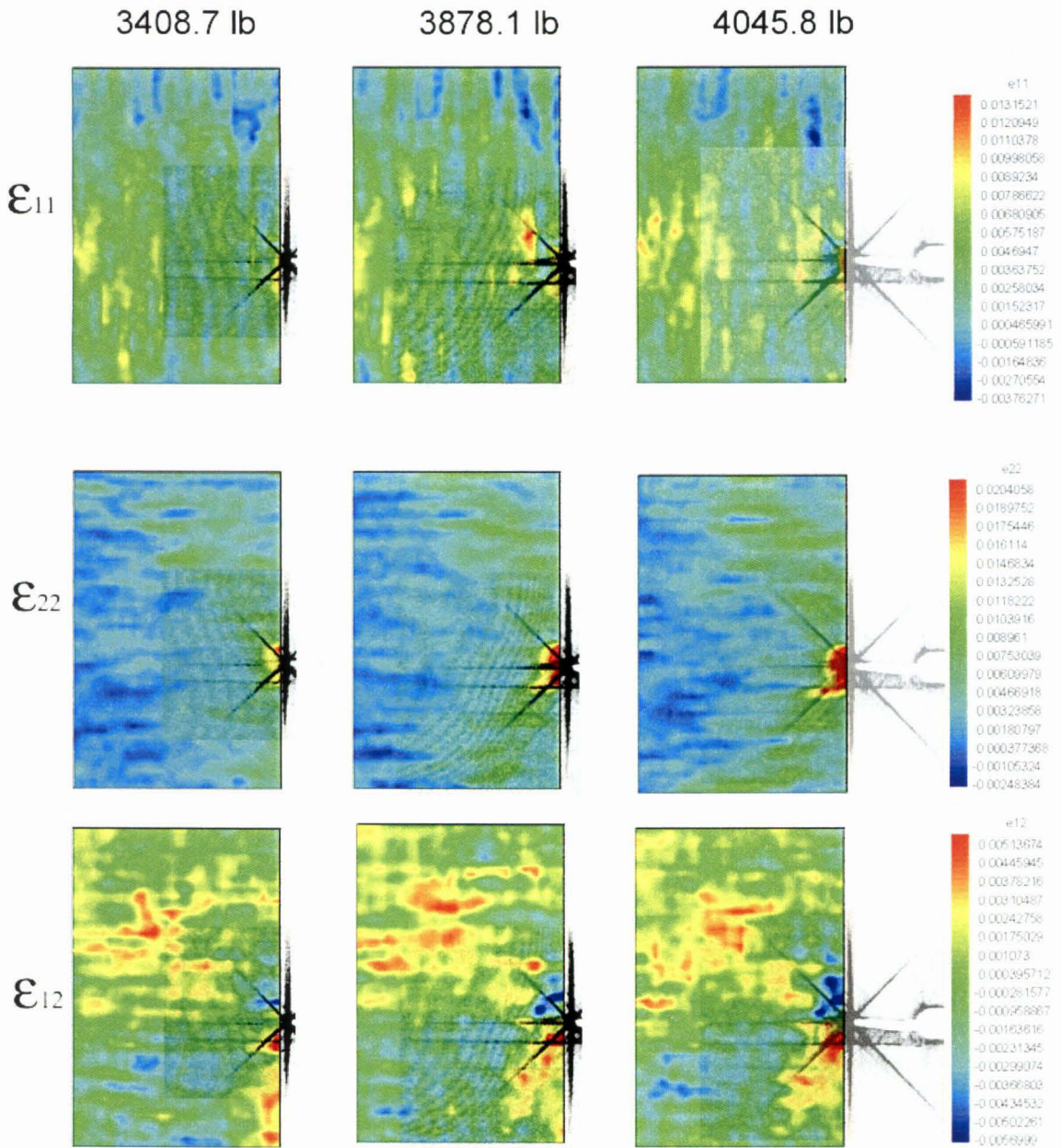
θ :Parallel

Test id. no.: 3



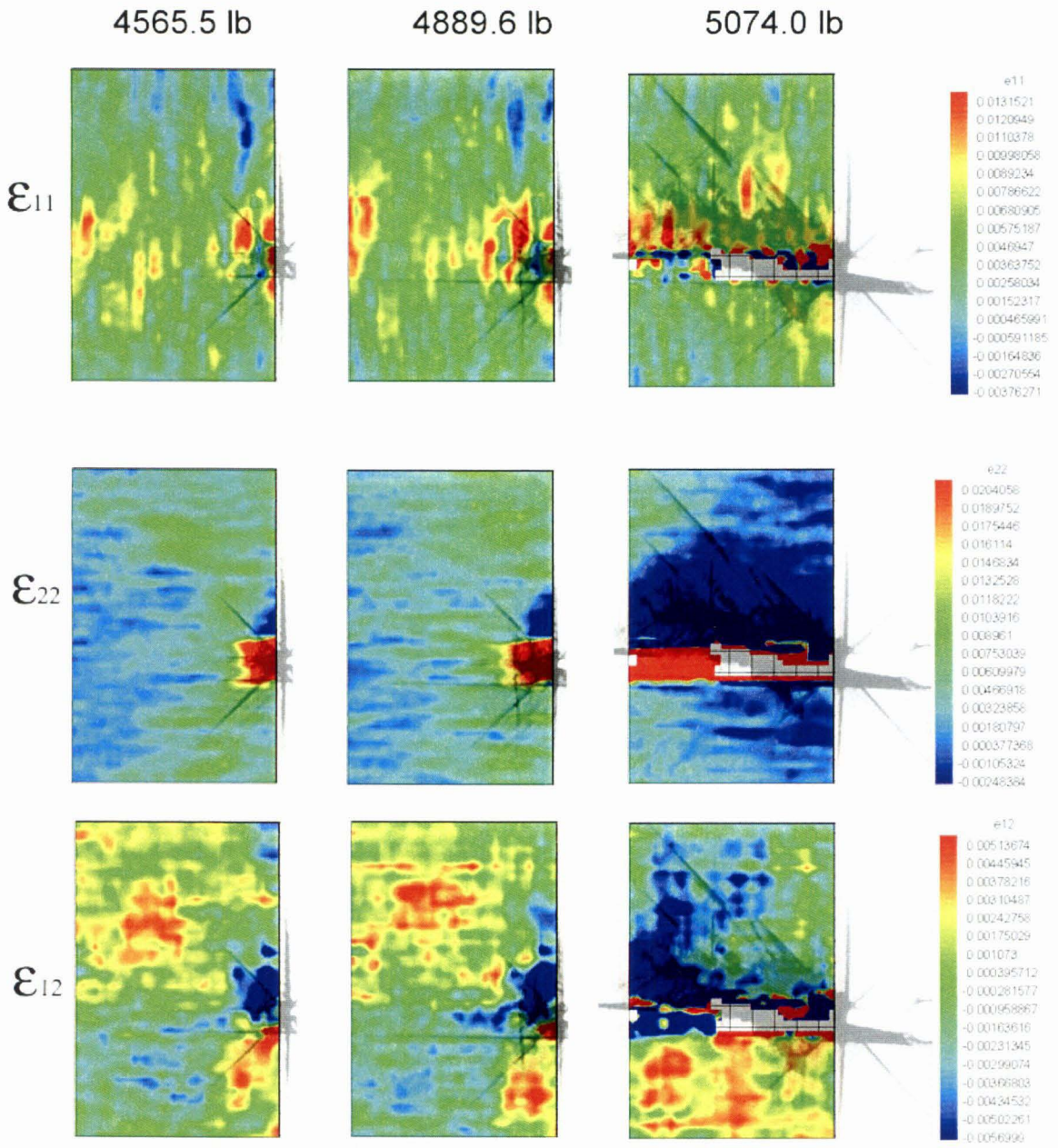
0.1 in

Panel Size: 6" x 6" θ : Perpendicular Test id. no.: 4



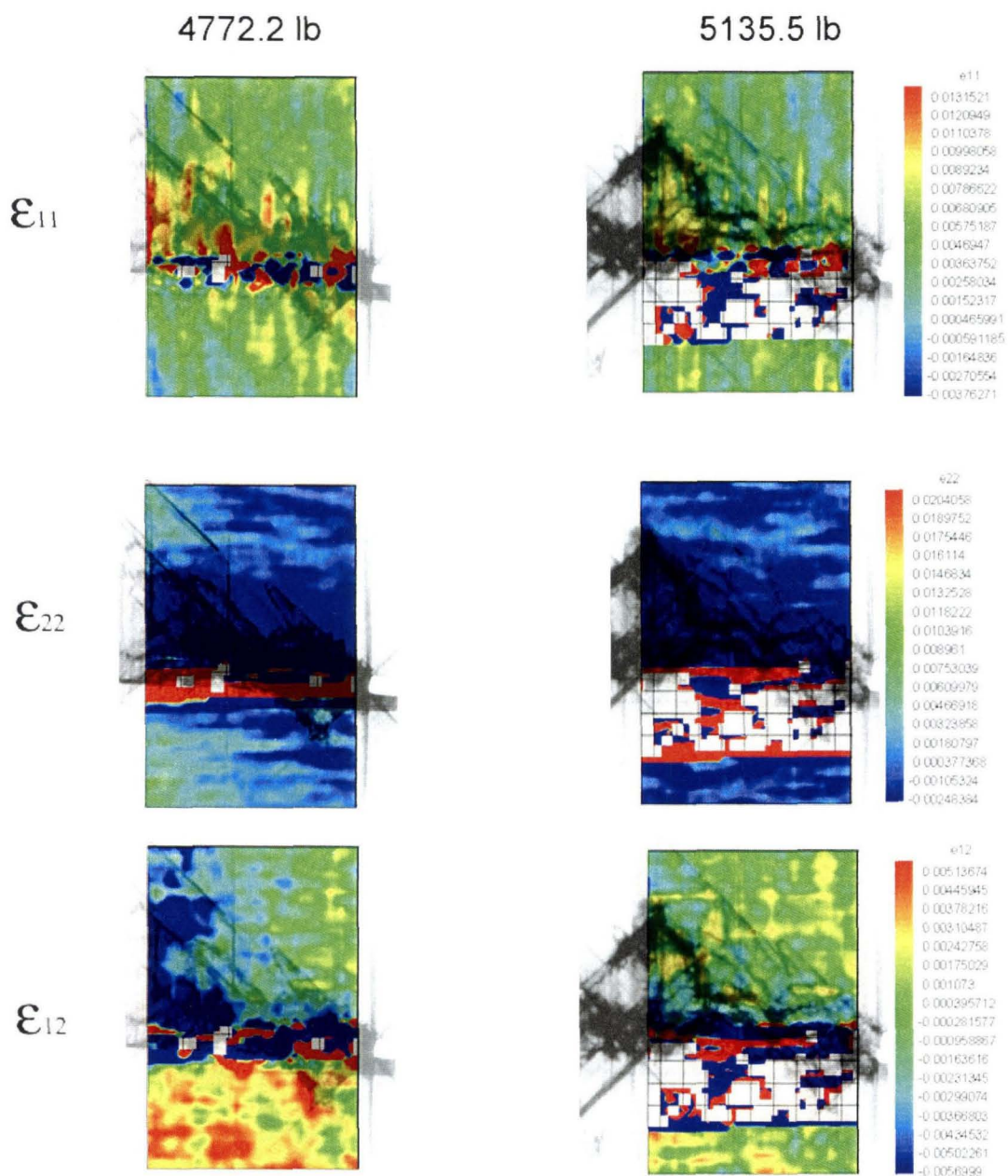
0.1 m

Panel Size: 6" x 6" θ :Perpendicular Test id. no.: 4



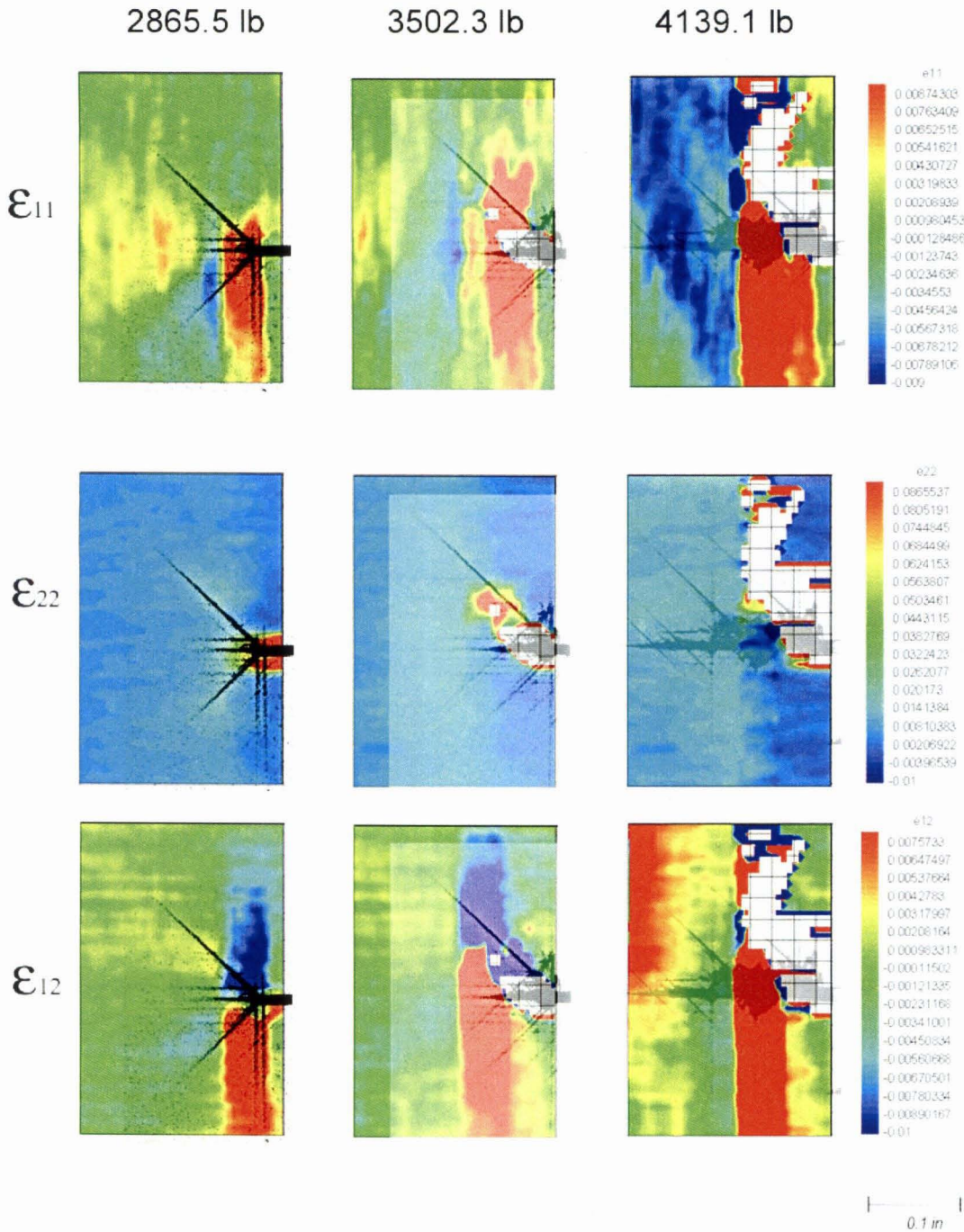
0.1 m

Panel Size: 6" x 6" θ : Perpendicular Test id. no.: 4



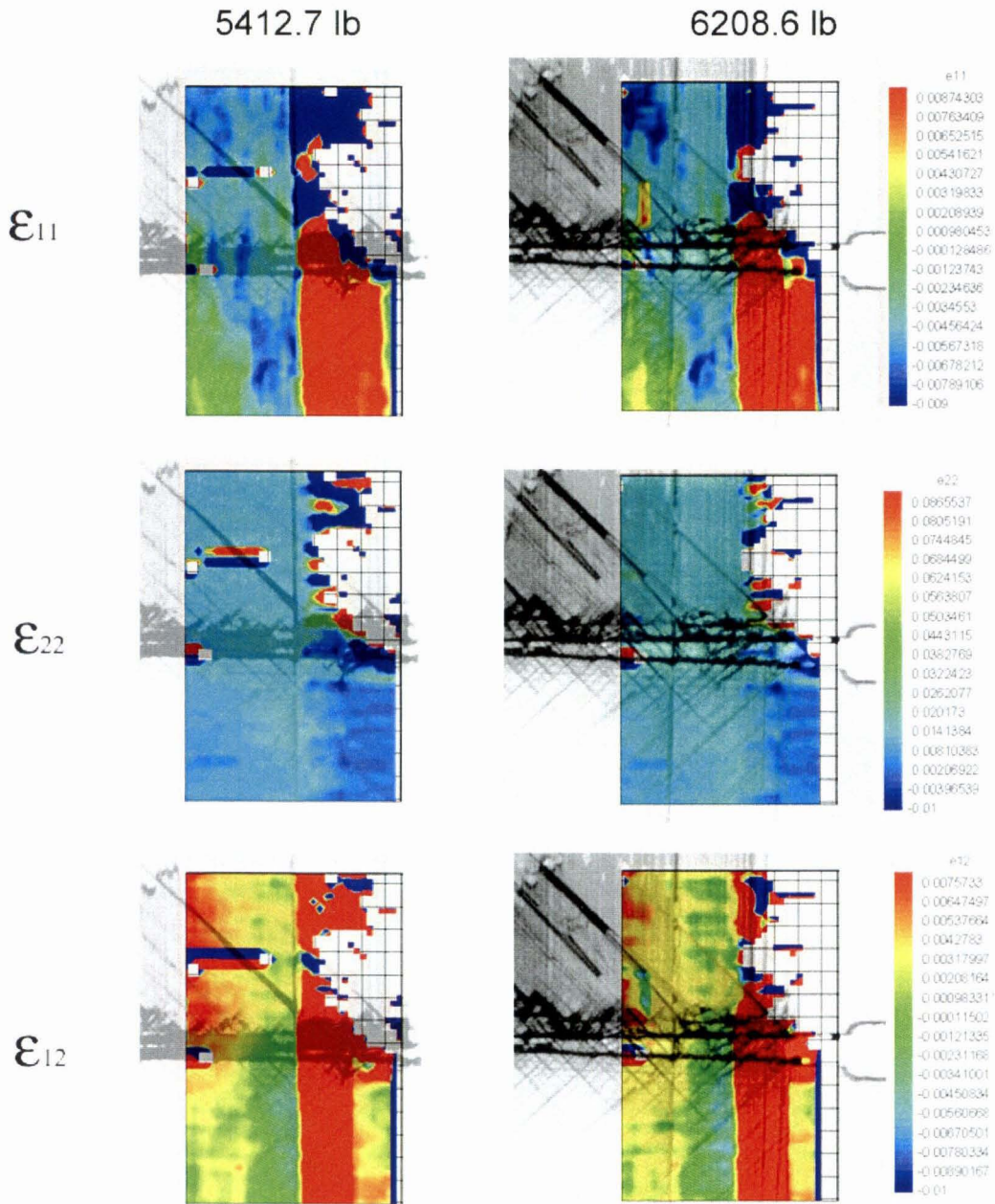
Panel Size: 12" x 12" θ :Parallel

Test id. no.: 7

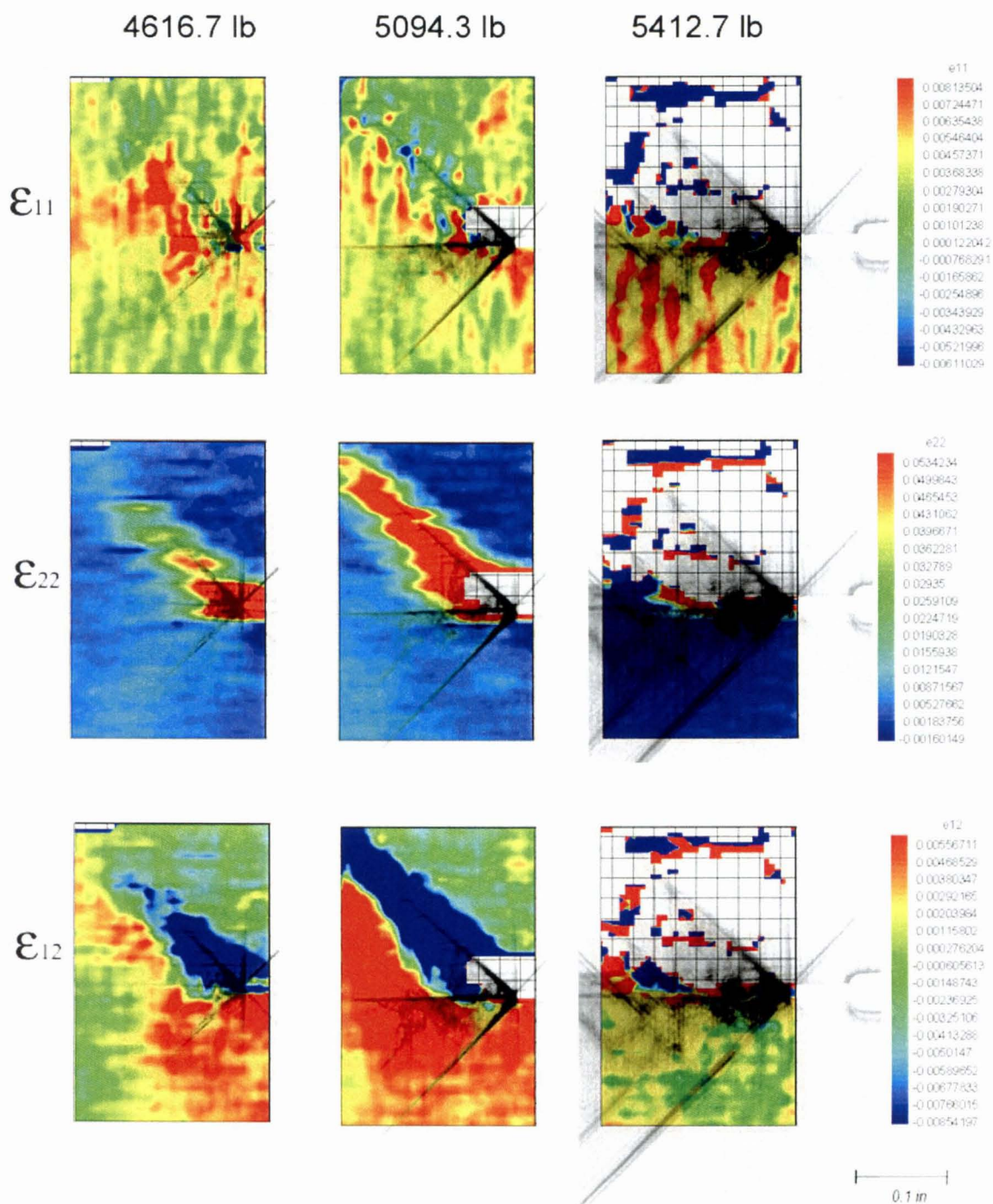


Panel Size: 12" x 12" θ :Parallel

Test id. no.: 7

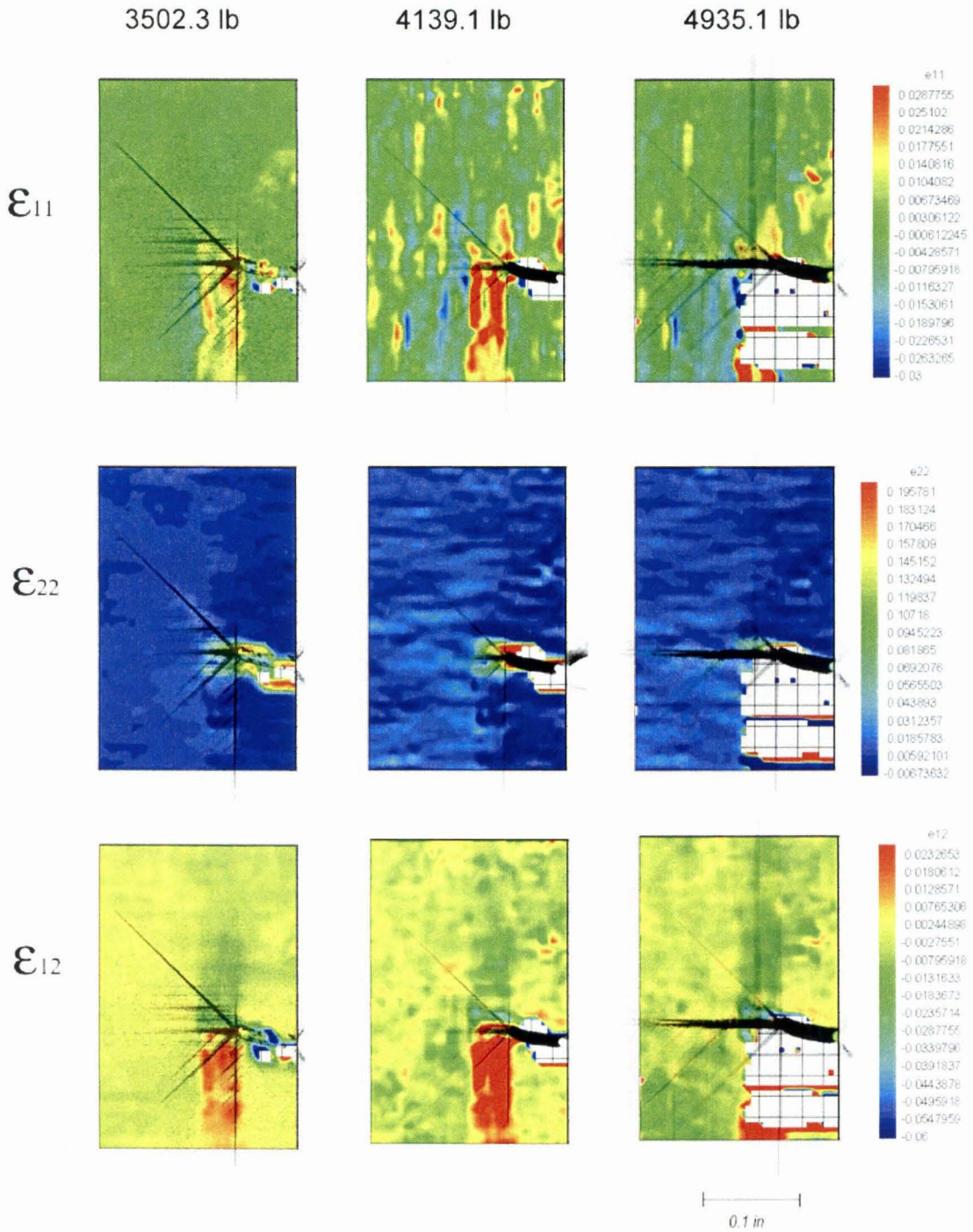


Panel Size: 12" x 12" θ :Perpendicular Test id. no.: 8



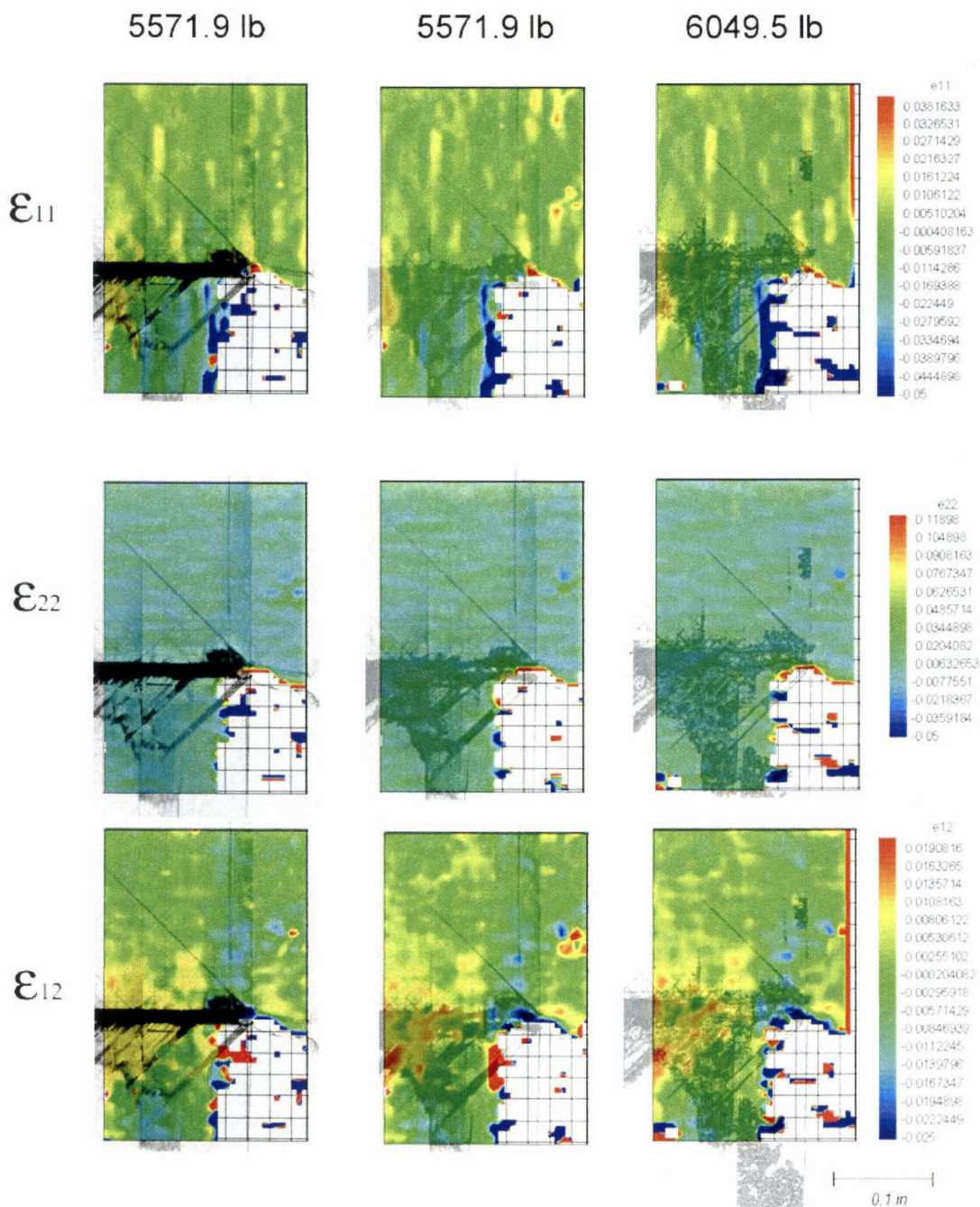
Panel Size: 18" x 18" θ :Parallel

Test id. no.: 10

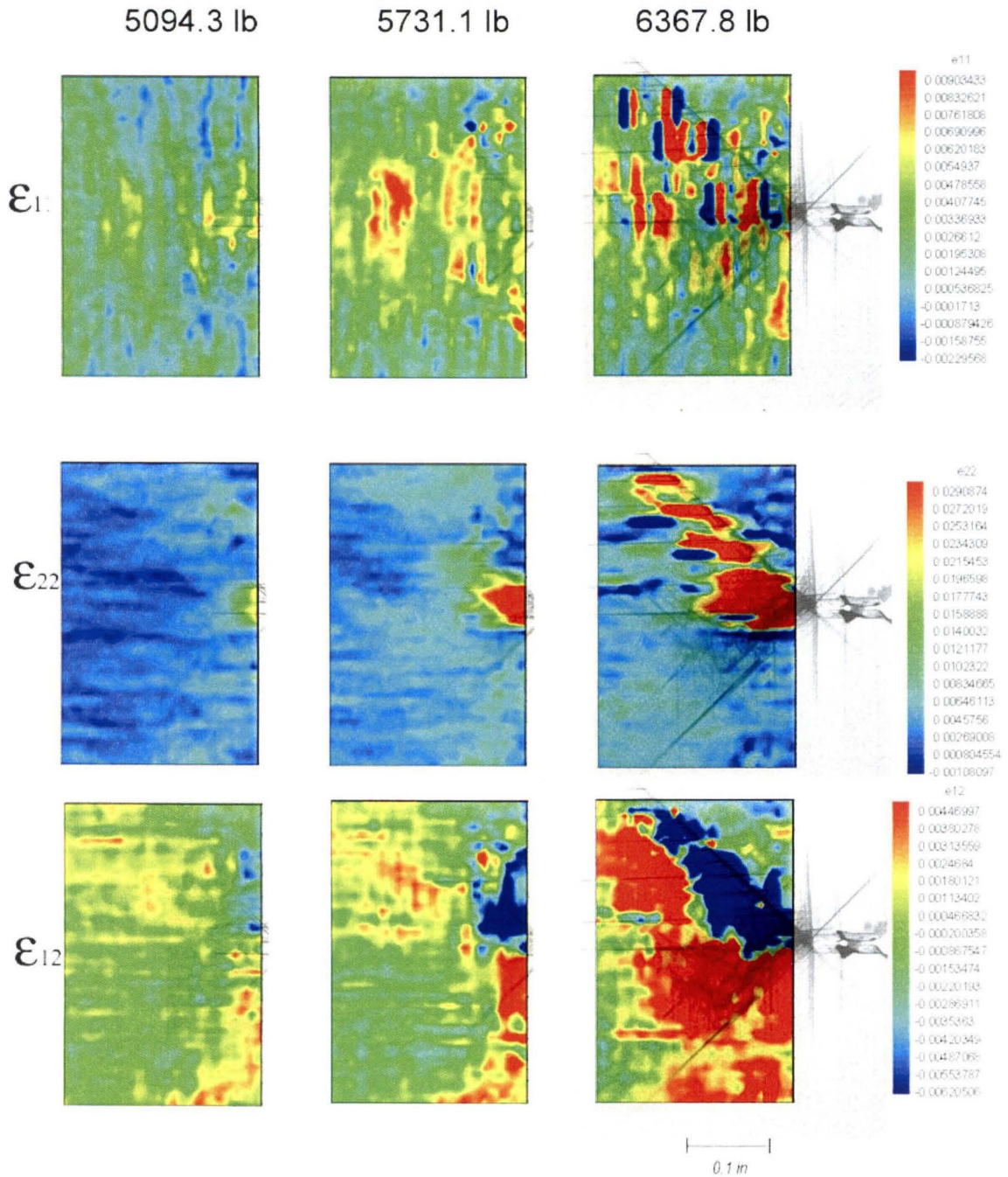


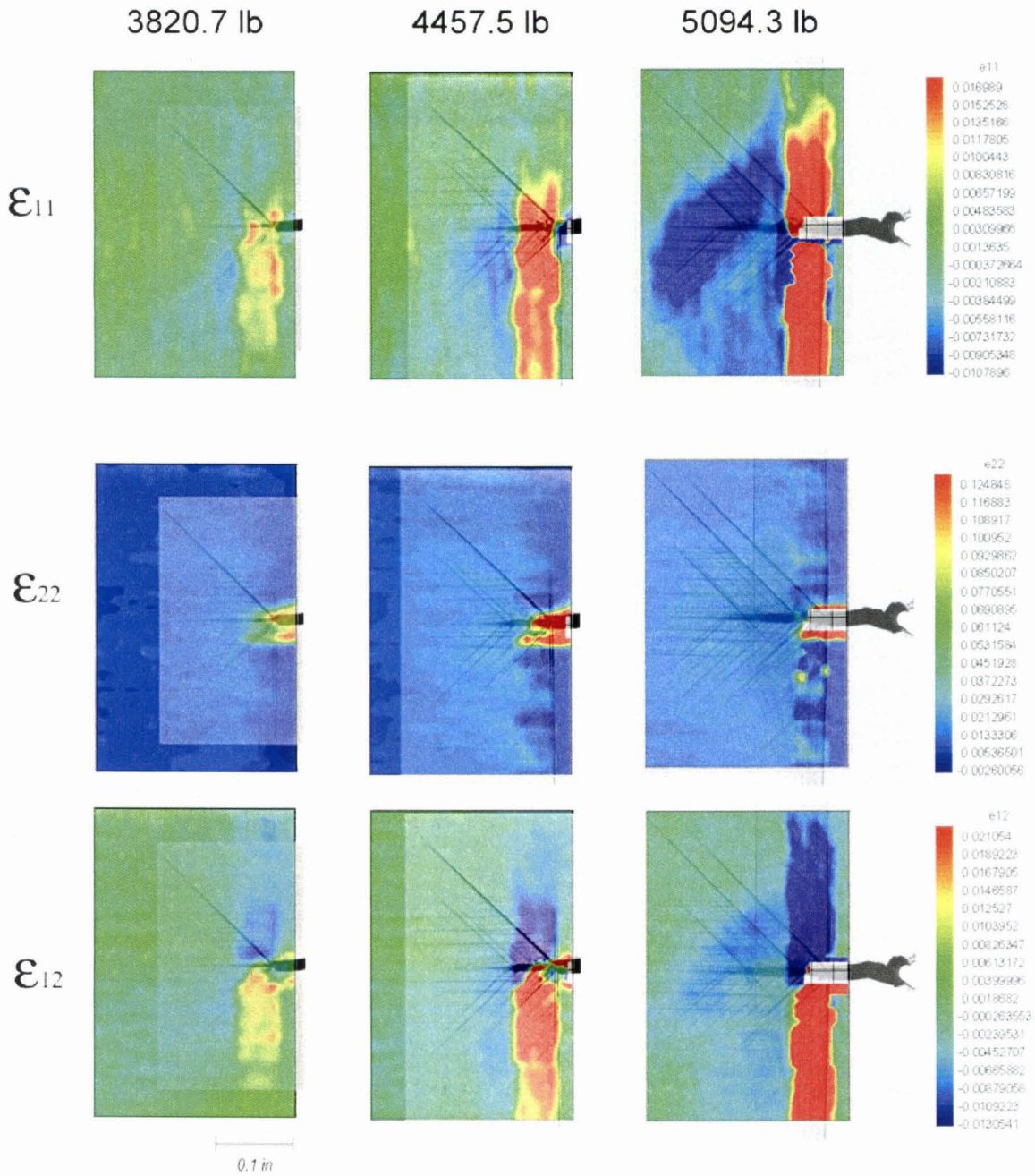
Panel Size: 18" x 18" θ :Parallel

Test id. no.: 10



Panel Size: 18" x 18" θ :Perpendicular Test id. no.: 11





BIBLIOGRAPHY

- Agarwal, B. D. and Broutman, L. J. "Analysis and Performance of Fiber Composites," John Wiley & Sons, Inc., 2nd ed. 1990.
- Ashkenazi, E. K. "Problems of the Anisotropic of Strength," *Mechanica Polymerov*, 1(2):79-92 (Polymer Mechanics, 1966, 1:60-70).
- Bowie O. L. "Analysis of an Infinite Plate Containing Radial Cracks Originating from the Boundary of an Internal Circular Hole," *J. of Mathematics and Physics*, 35:60-71. 1956.
- Bruck, H. A., *et al.* "Digital Image Correlation using Newton-Raphson method of partial differential correction," *Experimental Mechanics*, Vol. 29, No. 3, pp. 261-267. 1989.
- Bullock, R. E., *Journal of Composite Materials*, 8, pp 200-206, 1974.
- Chamis, C. C. "Failure Criteria for Filamentary Composites," in Composite Materials: Testing and Design, ASTM STP 460. *American Society for Testing and Materials*, pp. 336-351. 1969.
- Chang, F. H. *et al.* "Application of a Special X-Ray Nondestructive Testing Technique for Monitoring Damage Zone Growth in Composite Laminates," Composite Reliability, ASTM STP 580, *American Society for Testing and Materials*, pp. 176-190. 1975.
- Choi, S., and Shah, S.P. "Measurement of deformation on concrete subjected to compression using image correlation," *Experimental Mechanics* 37 (3), pp. 307-313. 1997.
- Christensen, R. M. "Tensor Transformations and Failure Criteria for the Analysis of Fiber Composite Materials," *J. of Composite Materials*, 22:874-897. 1988.
- Chu, T.C., Ranson, W.F., Sutton, M.A., and Peters, W.H. "Applications of digital image correlation techniques to experimental mechanics," *Experimental Mechanics* 25 (3), pp. 232-244. 1985.
- Clarke, A., Wisnom, M. R. and Potter, K. "Proceedings of Deformation and Fracture of Composites," pp. 29-37, Manchester. 1997.
- Crane, R. *et al.* "Radiographic Inspection of Composites," *Comprehensive Composite Materials*, Vol. 6, pp. 321-344, Elsevier. 2000.
- Crowther, M. F. and Starkey, M. S., *Composites Science and Technology*, 31, pp. 87-95. 1988.
- Cunningham, M. E., Schoultz, S. V. and Toth, J. M. "Recent Advances in the United States and Japan," ASTM STP 864, pp. 253-262. 1985.
- Feng, W. W. "A Failure Criterion for Composite Materials," *Journal of Composite Materials*, 25:88-100. 1991.
- Franke, E.A., Wenzel, D.J., and Davison, D.L. "Measurement of microdisplacements by machine vision photogrammetry (DISMAP)," *Review of Scientific Instruments* 62 (5), pp. 1270-1279. 1991.
- Gol'denblat, I. I. and Kopnov, V. A. "Strength of Glass-Reinforced Plastics in the Complex Stress State," *Mechanica Polymerov*, 1(2):70-78 (Polymer Mechanics, 1966, pp. 54-59).

- Griffith A. A. "The Phenomena of Rupture and Flow in Solids;" *Philosophical Transactions of the Royal Society of London, Series A*, 221:163-197. 1920.
- Hankinson, R. L. "Investigation of Crushing of Spruce at Varying Angles of Grain," Air Service Information Circular No. 259, *U.S. Air Service*. 1921.
- Harris, C. E. and Morris, D. H. "Fracture Behavior of Thick, Laminated Graphite/Epoxy Composites," NASA Contractor Report 3784. 1984.
- Hashin, Z. "Failure Criteria for Unidirectional Fiber Composites," *Journal of Applied Mechanics*, 47:329-334. 1980.
- Hoffman O. "The Brittle Strength of Orthotropic Materials," *Journal of Composite Materials*, 1:200-206.1967.
- Hojo, M., Sawada, Y. and Miyairi, H. *Composites*, 25, pp. 786-796. 1994.
- Irwin, G. R. "Fracture Dynamics," in *Fracture of Metals*, Cleveland, OH: A.S. M. 1948.
- Jackson, K. E., *AIAA Journal of*, 30, pp. 2099-2105. 1992.
- Jones, R. M. "Mechanics of Composite Materials," 2nd ed. Taylor & Francis, Inc. 1999.
- Jones, R. M. "Mechanics of Composite Materials," Scripta Book Company, Washington, D.C. 1975.
- Kies, J. A. "NRL Report No. 6034," *US Naval Research Laboratory*, Washington, D.C. 1964.
- Konish H. I. and Whitney, J. M. "Approximate Stresses in an Orthotropic Plate Containing a Circular Hole," *Journal of Composite Materials*, 9:157-166. 1975.
- Lekhnitskii, S. G. "Anisotropic Plates" (translated from the second Russian edition by S. W. Tsai and T. Cheron). New York, NY: Gordon and Breach, Science Publishers, Inc. 1968.
- Li, L., Li, X. and Tong, W. "Moiré interferometry and digital image correlation: a comparative study," *Proceedings of 1998 SEM Spring Conference* (June 1-3, 1998, Houston, Texas, USA).
- Liu, J. Y. "Evaluation of the Tensor Polynomial Strength Theory for Wood," *Journal of Composite Materials*, 18:216-226. 1984.
- Mallick, P. K. "Composites Engineering Handbook," Marcel Dekker Inc., New York. 1997.
- Malmeister, A. "Geometry of Theories of Strength;" *Mechanica Polymerov*, 2(4):519-534 (Polymer Mechanics, 1966, pp. 324-331)
- Mar, J. W., and Lin, K. Y. "Fracture Mechanics Correlation for Tensile Failure of Filamentary Composites with Holes," *Journal of Aircraft*, Vol. 14, No. 7, pp. 703-704. 1977.
- Mar, J. W., and Lin, K. Y. "Fracture of boron/Aluminum Composites with Discontinuities," *Journal of Composite Materials*, Vol. 11, pp. 405-421. 1977.
- Mar, J. W., and Lin, K. Y. "Finite element analysis of stress intensity factors for cracks at a bi-material interface," *International Journal of Fracture*, Vol. 12, No. 4, pp. 521-531. 1976.
- Nuismer, R. J. and Whitney, J. M. "Stress Fracture Criteria for Laminated Composites," *Journal of Composite Materials*, Vol. 8, No. 3, pp. 253-265. 1974.

- Nuismer, R. J. and Whitney, J. M. "Uniaxial Failure of Composite Laminates Containing Stress Concentrations," in *Fracture Mechanics of Composites*, ASTM S7P 593. American Society of Testing and Materials, pp. 117-142. 1975.
- O'Brien, T. K. "Damage in Composite Materials," ASTM, Vol. 775, pp. 140-167, Philadelphia, PA. 1982.
- O'Brien, T. K. and Salpekar, S. A. "Composite Materials: Testing and Design," ed. E. Camponeschi, ASTM, Vol. 1206, pp. 23-52. 1993.
- Paris, P. C. and Sih, G. C. "Stress Analysis of Cracks," in *Fracture Toughness Testing and its Applications*, ASTM STP 381. *American Society of Testing and Materials*, pp. 30-85. 1965.
- Pipes, R. B., and Pagano, N. J. "Interlaminar Stresses in Composite Laminates Under Uniaxial Extension," *Journal of Composite Materials*, Vol. 4, pp. 538-548. 1970.
- Rowland, R. E. *et al.* "Biaxial Strength of Paperboard Predicted by Hill Type Theories," *Journal of Strain Analysis*, 20(2):121-127. 1984.
- Shivakumar, K. N., Allen, H. G. and Avva, V. S. *AIAA Journal*, 32, pp. 1478-1484. 1994.
- Sun, C. T. and S. P. "A New End Tab Design for Off-Axis Tension Test of Composite Materials," *Journal Composite Materials*, 22:767-779. 1988.
- Sutton, M. A. *et al.* "Determination of Displacements Using an Improved Digital Correlation Method," *Image and Vision Computing*, Vol. 1, No. 3, pp. 133-139. 1983.
- Tada, H. *et al.* "The Stress Analysis of Cracks Handbook", 3rd ed., ASME Press, p. 63. 2000.
- Tan, S. C. "A New Approach of Three-Dimensional Strength Theory for Anisotropic Materials," *International Journal of Fracture*, 45:35-50. 1990.
- Tan, S. C. "Stress Concentrations in Laminated Composites," Technomic Publishing Co., Inc., Lancaster, PA. 1994.
- Tan, S. C. and Cheng, S. "Failure Criteria for Fibrous Anisotropic Materials," *Journal of Materials in Civil Engineering*, 5(2):198-211. 1993.
- Tennyson, R. C., Macdonald, D. and Nanyaro, A. P. "Evaluation of the Tensor Polynomial Failure Criterion for Composite Materials," *Journal of Composite Materials*, 12:63-75. 1978.
- Timoshenko, S. P. and Goodier, J. N. "*Theory of Elasticity*," Third Edition. New York, NY: McGraw-Hill, p. 92. 1979.
- Tong W. *et al.* "Error assessment for strain mapping by digital image correlation," *Experimental Techniques*, Vol. 22, No. 4, pp. 19-21. 1998.
- Tsai S. W. "Strength Theories of Filamentary Structures," in *Fundamental Aspects of Fiber Reinforced Plastic Composites*, R. T. Schwartz and H. S. Schwartz, eds., New York, NY: Wiley Interscience, pp. 3-11. 1968.
- Tsai, S. W. and Wu, E. M. "A General Theory of Strength for Anisotropic Materials," *Journal Composite Materials*, 5:58-80. 1971.
- Tsai, S. W. and Hahn, H. T. "Introduction to Composite Materials," Technomic Publishing Co., Inc., Lancaster, PA. 1980.

- Vendroux, G. and Knauss, W. G. "Deformation Measurements at the Sub-micron Size Scale: II. Refinements in the Algorithm for Digital Image Correlation," GALCIT Report 94-5, California Institute of Technology, Pasadena. 1994.
- Vendroux, G. and Knauss, W. G. "Submicron deformation field measurements: Part 2. Improved digital image correlation," *Experimental Mechanics* 38 (2), pp. 85-92. 1998.
- Waddoups, M. E., *et al.* "Macroscopic Fracture Mechanics of Advanced Composite Materials," *Journal of Composite Materials*, 5:446-454. 1971.
- Whitney, J. M. and Knight, M. *Experimental Mechanics*, 17, pp. 211-216. 1980.
- Whitney, J. M. and Nuismer, R. J. "Laminated Composites Containing Stress Concentrations," *Journal of Composite Materials*, 8:253-265. 1974.
- Wisnom, M. R. "Size Effects in Composites," *Comprehensive Composite Materials*, Vol. 5, Elsevier. 2000.
- Wisnom, M. R. and Atkinson, J. A. *Composite Structures*, 38, pp. 405-411. 1997.
- Wisnom, M. R. and Maheri, M. R. "Proceedings of the 2nd European Conference on Composites Testing and Standardisation," pp. 239-247, Hamburg. 1994.
- Wisnom, M. R., Atkinson, J. A. and Jones, M. I. *Composites Science and Technology*, 57, pp. 1303-1308. 1997.
- Wu, E. M. "Fracture Mechanics of Anisotropic Plates," Composite Materials Workshop. Lancaster, PA: Technomic Publishing Co., Inc. 1968.
- Wu, E. M. "Phenomenological Anisotropic Failure Criterion," in *Composite Materials*, 2, *Mechanics of Composite Materials*. Orlando, FL: Academic Press, pp. 353-431. 1974.